REPORT DOCUMENTATION PAGE

1. REPORT DATE *(DD-MM-YYYY)*	2. REPORT TYPE	3. DATES COVERED *(From - To)*
31-03-2012	Final Technical	03/01/09 to 12/31/11

4. TITLE AND SUBTITLE
(YIP-09) AVIAN NANOSTRUCTURED TISSUES AS MODELS FOR NEW DEFENSIVE COATINGS AND PHOTONIC CRYSTAL FIBERS

5a. CONTRACT NUMBER

5b. GRANT NUMBER
FA9550-09-1-0159

5c. PROGRAM ELEMENT NUMBER

6. AUTHOR(S)
Matthew D. Shawkey

5d. PROJECT NUMBER

5e. TASK NUMBER

5f. WORK UNIT NUMBER

7. PERFORMING ORGANIZATION NAME(S) AND ADDRESS(ES)
University of Akron
175 E. Mill St.
Akron OH 44325

8. PERFORMING ORGANIZATION REPORT NUMBER

9. SPONSORING/MONITORING AGENCY NAME(S) AND ADDRESS(ES)
Air Force Office of Scientific Research
875 N. Randolph St
Arlington, VA 22203

10. SPONSOR/MONITOR'S ACRONYM(S)
AFOSR

11. SPONSOR/MONITOR'S REPORT NUMBER(S)
AFRL-OSR-VA-TR-2012-1001

12. DISTRIBUTION/AVAILABILITY STATEMENT
Distribution A: Approved for Public Release

13. SUPPLEMENTARY NOTES

14. ABSTRACT
Our research had two main goals: to identify and characterize 1) novel color-producing nanostructures and 2) patterns of development of these nanostructures for biomimetic applications including coatings, fiber optics and color-changing sensors. We identified 10 novel color-producing nanostructures and gained valuable insights into the factors affecting self-assembly of optical nanostructures. These findings resulted in 20 publications, many in top-tier journals like Science, advancement of two Ph.D. students, additional funding from NSF and tenure of the PI.

15. SUBJECT TERMS
structural color, photonic crystals, self-assembly

16. SECURITY CLASSIFICATION OF:			17. LIMITATION OF ABSTRACT	18. NUMBER OF PAGES	19a. NAME OF RESPONSIBLE PERSON
a. REPORT	b. ABSTRACT	c. THIS PAGE			Matthew Shawkey
U	U	U			19b. TELEPHONE NUMBER *(Include area code)* 3309728192

Final Report 2012
AFOSR FA9550-09-1-0159 (YIP-09)
AVIAN NANOSTRUCTURED TISSUES AS MODELS FOR NEW COATINGS AND PHOTONIC CRYSTAL FIBERS

Dr. Matthew D. Shawkey, Department of Biology Integrated Bioscience Program,
University of Akron, OH 44325-3908 (shawkey@uakron.edu)

Table of contents

Abstract

Our research had two main goals: to identify and characterize 1) novel color-producing nanostructures and 2) patterns of development of these nanostructures for biomimetic applications including coatings, fiber optics and color-changing sensors. We focus our research on bird feathers, which contain an astonishing diversity of colors, many of them created through coherent scattering of light by highly organized nanostructures composed of two common biological materials: keratin and melanin. These nanostructures are known to range from simple thin films to complex 3D quasi-ordered matrices, but despite over a century of research, they remain largely undescribed and thus a rich source for novel biomimicry. Furthermore, the relatively simple structures of these tissues, consisting of oneto three- dimensional rows, lines or hexagonal packings of melanin granules and air in a keratin substrate, resemble patterns created by evaporative self-assembly of colloid particles. Thus, mimicry of these tissues through self-assembly processes may be relatively straightforward. For these reasons, we rigorously characterized the color, structure, and optics of a diverse set of bio-optical tissues from feathers. First, we used UV-Vis-Near IR spectrometry, electron and light microscopy, high voltage electron tomography, and optical modeling (fourier transforms, thin-film optics, photonic band-gap analysis, small angle x-ray scattering). From these data, we identified tissues with properties that are useful for electronic/optics or coating applications. We have identified several new structures, including:

including a) a non-iridescent blue color based on highly organized nanofibers (D'Alba et al. 2011),

b) a general mechanism for producing glossy colors from even rough surfaces (Maia et al. 2011),

c) a silver color based on adjacent glossy black and "super white" colors (Shawkey et al. 2011),

d) colors produced by a mixture of light scattering by amorphous 3D matrices and selective light absorption by pigments (D'Alba et al. 2012)

e) a "super white" structural color that reflects over 4 times as much light as a white standard

f) a photonic crystal/thin film combination that produces color across the uv-vis spectrum (Eliason and Shawkey 2012),

g) a structure producing glossy red colors (see within),

h) a multilayer thin film structure within mammal hairs (Snyder et al. 2012), and

i) a three dimensional nanostructure producing non-iridescent color (Shawkey et al. 2009).

Second, we are isolating and measuring properties of the materials used in these nanostructures, including charge and hydrophilicity of particles and substrates. We have found differences in shape of these particles that may explain part of their tendency to self assemble into optical nanostructures (Li et al. 2010, 2012; Clarke et al. 2010), and identified properties of the substrate that may Furthermore, we are characterizing how nanostructures grow in developing feathers to gain insight into these self-assembly processes. We have identified a scaffolding process that generates hollow micron-sized melanin tubes and a phase separation-based process that leads to hexagonal packing of these tubes, and thereby production of a photonic band gap structure, within a keratin substrate. We have also demonstrated that a simple thin film in feathers is formed through a similar process of phase separation, suggesting that this may represent a robust procedure for growing a diverse set of nanostructures (Maia et al. 2012). These data will lay the groundwork for identification of suitable methods for biomimicry and mass production of useful structures. We thank Hugh DeLong and the AFOSR for their support.

Summary of Achievements:

(1) 20 peer-reviewed papers published, including 3 in *Science*, one in *Nature Communications*, one in *Proceedings of the Royal Society of London B*, two in *Biology Letters*, one in *Optics Express*. Five are first-authored by graduate students supported by the grant (Rafael Maia and Chad Eliason*)*, five are first-authored by the post-doc supported by the grant (Liliana D'Alba). Many of these received exceptional popular press coverage, including mentions of AFOSR funding.

20. C. M. Eliason and **M.D. SHAWKEY.** *In press.* A 2D biophotonic heterostructure produces diverse iridescent colors in dabbling ducks. *Journal of the Royal Society Interface.*

19. Q. Li, K. Gao, Q. Meng, J.A. Clarke, **M.D. SHAWKEY**, L. D'Alba, R. Pei, M. Ellison, M.A. Norell, J. A. Vinther. 2012. A new specimen of *Microraptor* and the evolution of iridescent plumage color. *Science* 335:1215-1219. *corresponding author

    (Received extensive press coverage including *New York Times* (front page), *National Geographic, Nature, Associated Press*)

18. L. D'Alba, L. Briggs and **M.D. SHAWKEY.** 2012. Relative contributions of pigments and biophotonic nanostructures to natural color production: a case study in Budgerigars (*Melopsittacus undulatus). Journal of Experimental Biology* 215:1272-1277 .

17. H. K. Snyder, R. Maia, L. D'Alba, A. J. Schulz, K. Rowe, S. Rowe, and **M.D. SHAWKEY.** 2012. Iridescent colour production in hairs of blind golden moles (*Chrysochloridae). Biology Letters.* doi: 10.1098/rsbl.2011.1168

    (Press coverage in *Nature, Discover, New Scientist, MSNBC*)

16. R. Carney, J. Vinther, **M.D. SHAWKEY**, L. D'Alba, and J. Ackermann. 2012. New evidence on the color, ultrastructure and nature of the isolated *Archaeopteryx* feather. *Nature Communications* **3,** 637.

    (Extensive press coverage including *New York Times, Nature, Science, National Geographic*)

15. L. D'Alba, C. Van Hemert, C.M. Handel and **M.D. SHAWKEY.** 2011. A natural experiment on the condition-dependence of achromatic plumage coloration in black-capped chickadees. *PLoS One* 6: e25877.

14. R. Maia, R.H. Macedo and **M.D. SHAWKEY.** 2011. Self-assembly of iridescent barbules through depletion attraction of melanosomes during keratinization. *Journal of the Royal Society Interface*: doi: 10.1098/rsif.2011.0456.

13. **M.D. SHAWKEY**, L. D'Alba and R. Maia. 2011. Proximate bases of silver color in Anhinga feathers. *Journal of Morphology* doi: 10.1002/jmor.10993.

12. Eliason, C.M. and **M.D. SHAWKEY**. 2011. Decreased hydrophobicity of iridescent feathers: a potential cost to shiny plumage. *Journal of Experimental Biology* 214:2157-63.

    (Named as Editor's Choice for that issue of *JEB*, and as one of the top eight articles of the year)

11. L. D'Alba, V. Sarananthan, J.A. Clarke, J.A. Vinther, R.O. Prum and **M.D. SHAWKEY**. 2011. Colour-producing β-keratin nanofibres in blue penguin (Eudyptula minor) feathers. *Biology Letters.* doi: 10.1098/rsbl.2010.1163.

(Press coverage in *Science, Nature, Optics and Photonics Focus, CBS News, Rue89* and numerous other outlets.)

10. Maia, R., L. D'Alba, **M.D. SHAWKEY**. 2011. What makes a feather shine? A nanostructural basis for glossy black feathers. *Proceedings of the Royal Society of London B*. 278:1973-80.

9. **M.D. SHAWKEY,** L. D'Alba, J.A. Wozny, C.M. Eliason, J. Koop, and L. Jia. 2011. Structural color change following hydration and dehydration of iridescent mourning dove (*Zenaida macroura)* feathers. *Zoology* 115:59-58. (cover article).

8. L. D'Alba, A. Oborn, **M.D. SHAWKEY.** 2010 Experimental evidence that keeping eggs dry is a mechanism for the antimicrobial effects of avian incubation. *Naturwissenschaften* 97:1089-1095.

7. C.M. Eliason and **M.D. SHAWKEY,** 2010. Rapid, reversible response of iridescent feather color to ambient humidity. *Optics Express* 18, 21284-21292.

6. J.A. Clarke, D. Ksepka, R. Salas-Gismondi, A.J. Altamirano, **M.D. SHAWKEY,** L. D'Alba, J. Vinther, J. DeVries, P. Baby. 2010. Fossil evidence for evolution of the shape and color of penguin feathers. *Science* 330:954-957 (cover article).

(Received extensive international press coverage included *New York Times, National Geographic, Wired* (top 5 scientific discoveries of 2010)*, Time Magazine* (top 10 new species for 2010)

5. D'Alba, L., **M.D. SHAWKEY,** P. Korsten, J. Komdeur, and S.R. Beissinger. 2010. Differential deposition of antimicrobial proteins in blue tit (*Cyanistes caeruleus*) clutches by laying order and male attractiveness. *Behavioral Ecology and Sociobiology* 64:1037-1045.

4. Li, Q., G. Ke-Qin, J. Vinther, **M.D. SHAWKEY**, J.A. Clarke, L. D'Alba, Q. Meng, D.E.G. Briggs, R.O. Prum. 2010. Plumage color patterns of an extinct dinosaur. *Science* 327:1369-72.

(Received extensive international press coverage including *New York Times, National Geographic (*hour-long special entitled "Dinomorphosis"), and *Cleveland Plain-Dealer* (front page story)).

3. **SHAWKEY, M.D.,** E.L. Brodie, M.K. Firestone and S.R. Beissinger**.** 2009**.** Avian incubation inhibits growth and diversification of bacterial assemblages on eggs. *Public Library of Science One* 4:e4522.

2. **SHAWKEY, M.D.,** V. Saranthan, H. Palsdottir, J. Crum, M. Auer and R.O. Prum. 2009. Electron tomography, 3D Fourier analysis and color prediction of a 3D amorphous bio-photonic nanostructure. *Journal of the Royal Society Interface* 6:S213-220.

1. **SHAWKEY, M.D.,** N.I. Morehouse and P. Vukusic. 2009. A Protean palette: color materials and mixing in birds and butterflies. *Journal of the Royal Society Interface* 6:S221-231.

(2) Two Ph.D. students advanced to candidacy.

(3) Established collaborations with AFOSR-funded researchers Rajesh Naik at WPAFB (self assembly of photonic nanostructures), Dimitri Deheyn at Scripps (hyperspectral imaging of photonic nanostructures), Murugappan Muthukumar (self assembly of photonic nanostructures).

(4) Presented 18 invited seminars at academic (e.g. University of Pittsburgh, Denison University, Ohio Wesleyan University) and non-academic (e.g. Audubon Society meetings, Fossil Club meeting) settings. Presented academic talks at numerous conferences (e.g. Evolution, International Symposium on Natural Photonic Structures).

(5) Additional funding from NSF (Doctoral Dissertation Improvement Grant)

(6) Promotion to Associate Professor and tenure of PI.

Vertebrate animal disclaimer

All feather samples were obtained either from study skins of dead birds housed in museums or from collaborators. Thus, no protocol for use of vertebrate animals is needed.

A new reconstruction of *Microraptor* and the evolution of iridescent plumage.

Quanguo Li[1], Ke-Qin Gao[2], Qingjin Meng[1], Julia A. Clarke[3], Matthew D. Shawkey[4]*, Liliana D'Alba[4], Rui Pei[5], Mick Ellison[5], Mark A. Norell[5], Jakob Vinther[3,6].

[1]Beijing Museum of Natural History, 126 Tianqiao South Street, Beijing 100050, People's Republic of China
[2]School of Earth and Space Sciences, Peking University, Beijing 100871, People's Republic of China
[3]Department of Geological Sciences, University of Texas at Austin, 1 University Station C1100, Austin, TX 78712, USA
[4]Department of Biology and Integrated Bioscience Program, University of Akron, Akron, OH 44325-3908, USA
[5]Department of Paleontology, American Museum of Natural History, 79th St. @ Central Park West, New York, NY, USA
[6]Department of Geology and Geophysics, Yale University, New Haven CT 06520-8109, USA.

*To whom correspondence should be addressed: shawkey@uakron.edu

Iridescent feather colors involved in displays of many extant birds are produced by nanoscale arrays of melanin-containing organelles (melanosomes). Data relevant to the evolution of these colors and the properties of melanosomes involved in their generation have been limited. A dataset sampling variables of extant avian melanosomes reveals that those forming most iridescent arrays are distinctly narrow. Quantitative comparison of these data with melanosome imprints densely sampled from a new specimen of the Early Cretaceous feathered *Microraptor* predicts that its plumage was predominantly iridescent. The capacity for simple iridescent arrays is thus minimally inferred in paravian dinosaurs. This finding, and estimation of *Microraptor* feathering consistent with an ornamental function for the tail, suggest a centrality for signaling in early evolution of plumage and feather color.

Feather colors in extant birds (Aves) are created from pigments and a variety of nanostructural architectures (*1,2*). Iridescent colors, an integral part of the avian plumage color gamut involved in signaling and display, are produced through coherent light scattering by laminar or crystal-like arrays generated by layers of materials with different refractive indices, namely keratin, melanin and sometimes air, in feather barbules (*1,2*). Melanosomes can be arranged in single or multiple layers (*1,2*), and recent work shows that even slight organization of melanosomes can produce weakly iridescent ("glossy") colors (*3*). Iridescent nanostructures are diverse and have evolved independently numerous times in extant birds (*4*), but whether they are exclusively avian innovations or appear earlier in dinosaur evolution has been unknown.

Thus far, fossil evidence of iridescent plumage has been limited to a 47 Ma isolated avian feather from Germany (Grube Messel) (*5*). This feather preserves in fine nanostructural detail organization typical of many iridescent avian melanosome arrays. Such pristine preservation is rare, however, and so far unknown in the 150-120 Ma fossils from China that have proven critical for investigating the relative timing of innovations in coloration and plumage evolution in dinosaurs (*6-7*). Methods to investigate the presence of iridescent arrays in these, and similarly preserved fossils, have not been developed.

Here we investigate the relationship between melanosome properties and iridescent arrays in Aves prompted by the melanosome characteristics and plumage preserved in a new fossil feathered dinosaur specimen (BMNHC PH881, Beijing Museum of Natural History; Fig. 1, S3-S5) referred to *Microraptor* (*8*). *Microraptor* has consistently been recovered as part of Paraves, a clade that includes troodontid, dromaeosaurid and avialan theropod dinosaurs (*9-11*). The articulated specimen was recovered near Lamadong (Jianchang County, western Liaoning Province) and displays previously reported characteristics of this "four-winged" dinosaur (e.g. *9*) including asymmetrically-vaned hind limb feathers approximately 80% of the length of the asymmetrically-vaned primary wing feathers (Figs. 1, S4) as well as new plumage data. Feathers in BMNHC PH881 are particularly well preserved on the right forelimb, left hind limb, and the tail as dark imprints (Fig. 1). No lighter and darker banding, spangles, or patches (*6-7, 12*) were observed. Initial sampling of these feathers revealed apparent sheet-like, end-to-end orientation of elongate melanosomes (Fig. 2F) similar to the subtle organization resulting in glossy-black avian feathers (*3*).

To investigate melansome characteristics in avian iridescent arrays, we sampled melanosome morphology from a phylogenetically diverse set of iridescent feathers from extant birds (*7, 8, 12;* Table S4). While some iridescent feathers contain highly divergent morphologies (e.g., hollow and flattened melanosomes in iridescent hummingbird feathers) that would be readily recognizable in the fossil record, most (13 out of 19 array types in *2*) contain rods similar to those in matte feathers. We focused on the latter in our sampling. These samples and denser sets from matte black, brown and grey extant bird feathers were added to our existing database (*7, 12;* new n=168). Relative to those from black feathers, melanosomes from iridescent feathers were found to be significantly longer (~1160 vs 1000 nm) and narrower (~211 vs. 279 nm) providing higher aspect ratios (~5.4 vs. 3.5; Fig. 2, Table 1). Quadratic discriminant analysis (*8*), a standard method that allows classification of unknown samples from data on known samples, of these data predicted color of extant bird feathers with 82% accuracy (Fig. 2B, Table S1-S2), showing that iridescent colors could reliably be detected. Samples of the 47 Ma fossil feather previously inferred as iridescent on the basis of nanoscale melanosome organization (*5*) were also classified as iridescent with an 86% probability (Fig. 2B).

To then assess the colors and color patterns of the specimen, twenty-six ~ 1x1 mm samples were taken from throughout the feathered areas. All but six revealed numerous dense assemblages of melanosome imprints (*8*). Morphological measurements from melanosome imprints were acquired and analyzed in the same manner as the modern feathers (*8*). Melanosomes from BMNHC PH881 are within the range of extant melanosome dimensions and are predicted as either iridescent or black (Fig. 2, Table S2) with 58-100% probabilities. Six samples lacked melanosomes, but had no associated light banding of the type correlated with low melanosome density in previous specimens (*6-7, 12*). They were covered instead by an amorphous organic matrix (Fig. S1), suggesting the absence of visible melanosomes may be preservational and not representative of melanosome absence and white (or other pigmentary) coloration.

Evidence of a sheet-like, end-to-end orientation of melanosomes (Fig. 2F) was present in 10 samples from BMNHC PH881. Thickness of the keratin cortex overlaying the melanosomes in barbules determines the color (e.g., black- blue sheen) of many glossy black iridescent feathers (*3*), but the lack

of preserved keratin prevented the assignment to a particular iridescent hue. Co-presence of other pigment types like carotenoids in *Microraptor* cannot be excluded, but would be masked by the dense melanin deposition. These data allow a conservative reconstruction of *Microraptor* as black with a glossy, weakly iridescent sheen (Fig. 3). Interpretations of *Microraptor* as nocturnal, based on scleral ring morphology (*13*) contrast with its dark glossy plumage, a trait not found in extant nocturnal birds (*14*).

Generation of iridescent color by simple arrays of elongate, high aspect ratio melanosomes, shared by extant birds and *Microraptor*, may be part of the color-repertoire of a Middle Jurassic paravian ancestor. However, given known homoplasy in Aves and the phylogenetic lability of iridescence in particular (*4, 15*), multiple origins in early Paraves must be considered. Indeed, a sufficiently high density of elongate melanosomes may trigger physical processes leading to self-assembly into iridescent nanostructures during barbule development (*16*), suggesting that iridescence could evolve easily relative to other complex traits. Hypotheses concerning the function of iridescent colors have centered on intraspecific communication (*17*). Many are used in courtship displays (*17-18*), and studies have shown that female birds prefer males with brighter iridescent color (*19*) or that its expression is condition-dependent (*20-21*), a key prediction of honest advertisement models of sexual selection (*22*). Indeed, although it has only recently been studied as a distinctive color type, several extant bird species are sexually dimorphic in glossy color (*23*). Other functions like camouflage, inter-specific signaling and feather strengthening through melanosome alignment have been proposed but are largely untested (*16*). While we cannot assign a definitive function to iridescence in *Microraptor*, a role in signaling aligns with data on the plumage of BMNHC PH881.

BMNHC PH881 is the first reported specimen with a complete set of distal tail feathers preserved (Fig. 1, S5). The longest tail feathers in *Microraptor* are a midline pair that forms the most posterior part of the fan (Figs. 1, 3, S5, S6). Previously interpreted as a relatively broad, teardrop-shaped surface (*9, 24*) or as paired laterally-expanded rectangular wing-like surfaces (*25*) with a significant contribution to lift and stability (*24-25*), the fan surface area (e.g., linked to lift production) is significantly narrower. This new reconstruction is consistent with evidence from two other specimens with well-preserved tail feathering (*8, S6*). Although reassessment here of *Microraptor* feathering based on BMNHC PH881 and eight previously published specimens (Fig. 3; *8*) will provide a basis for further model-based estimation of potential aerodynamic implications, the graduated tail shape with a pair of long, midline feathers may be consistent with an ornamental or signaling function (26).

Paired single, or several, sets of elongate streamer-like tail feathers are seen in basal birds including all known Enantiornithes and *Confuciusornis* and have been interpreted as sexual ornaments (*27, 28*). A similar elongate streamer morphology (*29*) as well as patterned tails with stripes and spangles (*7*), are now known in several non-avialan maniraptorans. Tail feathering may have commonly functioned as an ornament in coelurosaurs despite considerable modification in bony tail form and presumably function. The long bony tail in Paraves is inherited from non-flying ancestors (*30*). It has been ascribed utility in basal paravian maneuvering, lift generation, and landing, but it is also lost early in the evolution of birds. Tail feather fanning musculature, or novel functional linkage with the forelimb have been inferred only later in bird evolution in short tailed taxa (*27, 30*). While tail structure and locomotor role shifted significantly, a signaling function may have been maintained. Iridescent color and the plumage in BMNHC PH881, with other recent findings (*6-7, 27, 29*), suggest feather ornaments were diverse, and that multiple cues may have been co-present (*31*). Sexual selection (e.g., as honest signals (*21*), arbitrary ornaments or congener recognition (*32-33*)) may be expected to interplay importantly with selection for aerodynamic attributes early in the evolution of birds.

References and notes

1. R. O. Prum, in *Bird Coloration, Vol.1, Mechanisms and Measurements*, G. E. Hill, K. J. McGraw, Eds. (Harvard Univ. Press, Boston, 2006), pp. 295–353.

2. H. Durrer, in *Biology of the Integument 2: Vertebrates* M. Bereiter-Hahn. A. G. Matolsky, K.S. Richards, Eds. (Springer-Verlag, Berlin. 1986) pp. 239-247.

3. R. Maia, L. D'Alba, M. D. Shawkey, *Proc. Roy. Soc. Lond. B* **278**, 1973 (2011).

4. M. C. Stoddard, R. O. Prum, *Behav. Ecol.* **25**, 1042 (2011).

5. J. Vinther, D. E. G Briggs, J. Clarke, G. Mayr, R. O. Prum, *Biol. Lett.* **6**, 128 (2010).

6. F. C. Zhang *et al.*, *Nature* **463**, 1075-1078 (2010).

7. Q. Li *et al.*, *Science* **327**, 1369 (2010).

8. Materials and methods are available as supporting material on Science Online.

9. X. Xu *et al.*, *Nature* **421**, 335–340 (2003).

10. X. Xu *et al.*, *Nature* **475,** 465-470 (2011).

11. A. H. Turner *et al.*, *Science* **317**, 1378–1381 (2007).

12. J. A. Clarke *et al.*, *Science* **330**, 954 (2010).

13. L. Schmitz, R. Motani, *Science* **332**, 705 (2011).

14. J. Del Hoyo *et al.*, Eds., *Handbook of the Birds of the World*. (Lynx Editions, Barcelona, Spain, 1992-2011).

15. M. D. Shawkey, M. E. Hauber, L. K. Estep, G. E. Hill, *J. Roy. Soc. Interface* **3,** 777 (2006).

16. R. Maia, R. H. F. Macedo, M. D. Shawkey, *J. Roy. Soc. Interface*, doi:10.1098/rsif.2011.0456.

17. S. M. Doucet, M. G. Meadows, *J. Roy. Soc. Interface* **6,** S115 (2009).

18. E. Scholes, *Auk*, **123**, 967 (2006).

19. A. T. D. Bennett, I. C. Cuthill, J. C. Partridge, K. Lunau, *Proc. Natl. Acad. Sci. USA* **94,** 8618 (1997).

20. K. J. McGraw, E. Mackillop, J. Dale, M. E. Hauber, *J. Exp. Biol.* **205,** 3747 (2002).

21. S. M. Doucet, *Condor* **104**, 30 (2002).

22. M. A. Andersson, *Sexual Selection* (Princeton Univ. Press, Princeton, NJ, 1994).

23. M. B. Toomey *et al.*, *Behav. Ecol. Sociobiol.* **64**, 1047 (2010).

24. S. Chatterjee, R. J. Templin, *Proc. Natl. Acad. Sci. USA* **104**, 1576 (2007).

25. D. E. Alexander, E. Gong, L. D. Martin, D. A. Burnham, A. R. Falk, *Proc. Natl. Acad. Sci. USA* **107,** 2972 (2010).

26. A.L.R. Thomas, *Bioscience* **47**, 215 (1997).

27. J. A. Clarke, Z. Zhou, F. Zhang, *J. Anat.* **208,** 287 (2006).

28. L.M., Chiappe, J. Marugan-Lobon, S. Ji, Z. Zhou, *Biol. Letters* **4** 719 (2008)

29. F. C. Zhang, Z. H. Zhou, X. Xu, X. L. Wang, C. Sullivan, *Nature* **455**, 1105 (2008).

30. S. M. Gatesy, K. P. Dial, *Evolution* **50**, 2037 (1996).

31. A. P. Møller and A. Pomiankowski, *Behav. Ecol. Sociobiol.* **32**, 167 (1992).

32. R. O. Prum, *Evolution*, **64**, 3085 (2010).

33. R. A. Fisher, *The Genetical Theory of Natural Selection*, (Dover Press, New York, 1958).

34. The research was funded by NSF EAR 0938199, AFOSR FA9550-09-1-0159, NSFC 40532008, Beijing Municipal Bureau of Human Resources, Beijing Academy of Science and Technology (BJAST) Innovation Team Fund, The University of Texas at Austin and the American Museum of Natural History. Copenhagen Museum of Natural History (Dr. J. Fjeldsaa), Yale University Peabody Museum

(R. O. Prum, K. Zyskowski), provided extant feather samples. The fossil specimen is accessioned to Beijing Museum of Natural History (BMNHC). Data are presented in the SOM.

Fig. 1. *Microraptor* specimen BMNHC PH881. (A) photographic image and (B) color-coded image (blue-grey, bone; orange, feathers). Numbers in (B) indicate location of samples used in assessment of preserved melanosomes. Numbers reference Table S2.
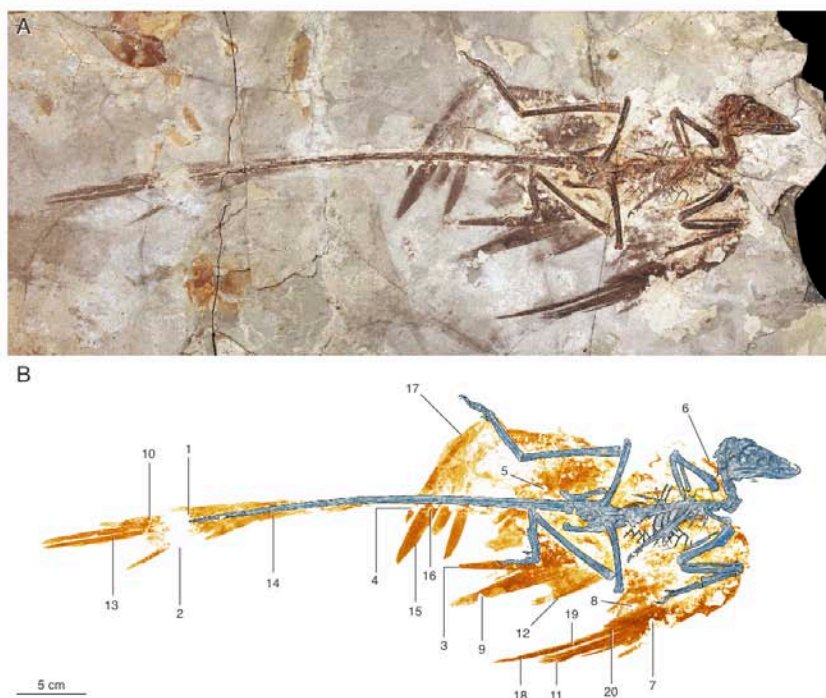
Fig. 2. **Top:** SEM images of representative melanosome samples from (a) brown, (b) "penguin-type" brown-black (a distinct melanosome morphology; see (12)), (c) grey, (d) black, (e) iridescent extant avian feathers and (f) BMNHC PH881. Insets of the sampled species are from (*14*): Tufted Titmouse *Baeolophus bicolor*, Macaroni Penguin *Eudyptes chrysolophus*, Double-crested Cormorant *Phalacrocorax auritus*, Palm Cockatoo *Probosciger aterrimus*, Brazil Duck *Amazonetta brasiliensis*; dot illustrates approximate location of sampling. **Bottom:** Quadratic discriminant analysis of measured melanosome properties (*8*) in 168 samples of black, brown, grey, extant penguin brown-black (blue dots/letters), iridescent (purple dots/letters) and BMNHC PH881 feathers. Numbers refer to BMNHC PH881 samples (Figure 2 and Table S2) and m, to a Grube Messel feather with iridescent nanostructure (*5*). For simplicity, only the first two axes (explaining 88% of the variance, see SOM) are shown. Circles indicate 95% confidence limits of means.
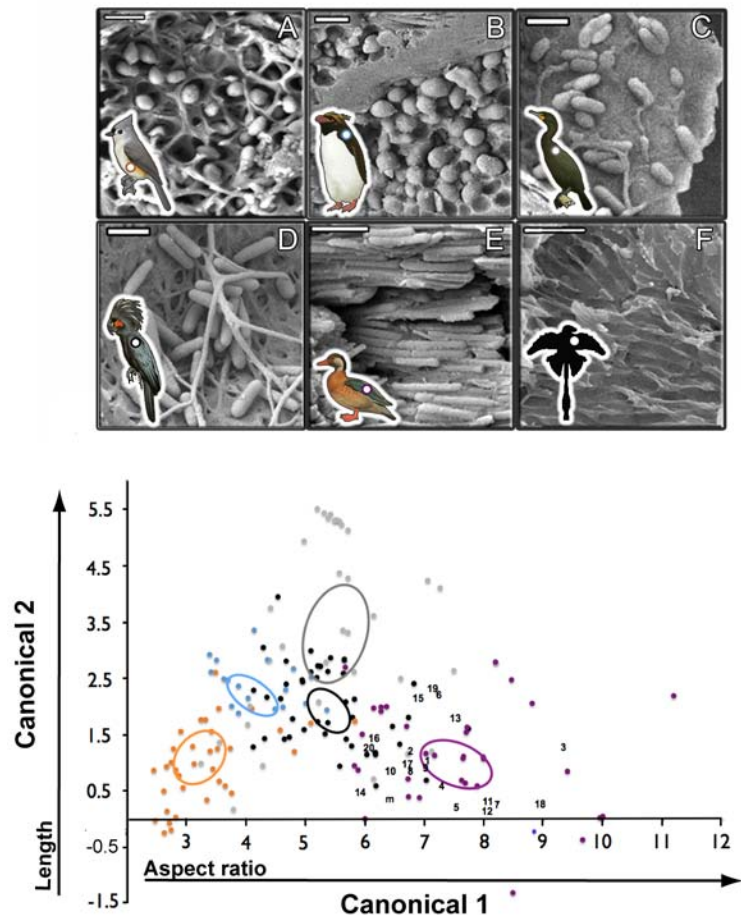
Fig. 3. Reconstruction of the Early Cretaceous paravian dinosaur, *Microraptor*: inferred color based on analysis of BMNHC PH881, while assessment of plumage also incorporated data from digital overlays of the plumage in eight previously-published specimens *(8)*.
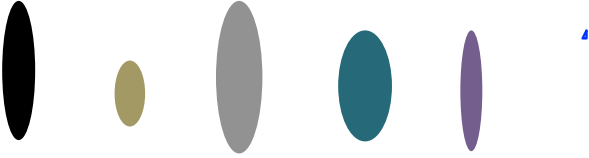
	BLACK	BROWN	GREY	PENGUINS	IRIDESCENT	FOSSIL	ANOVA F* D.F.= 5,182
Ratio	3.7 ± 0.1^b	1.8 ± 0.1^c	3.3 ± 0.2^b	2.4 ± 0.2^c	5.7 ± 0.2^a	5.6 ± 0.2^a	**67.2**
Long axis (nm)	1002.3 $\pm 22.5^c$	497.5 $\pm 31.1^d$	1248.8 $\pm 76.7^a$	920.4 $\pm 28.4^a$	1142.6 $\pm 46.9^{a,b}$	1060.1 $\pm 34.2^{b,c}$	**34.5**
Short axis (nm)	279.9 $\pm 8.7^b$	281.6 $\pm 13.7^b$	402.5 $\pm29.6^a$	421.1 $\pm 20.7^a$	208.6 $\pm 8.5^c$	195.5 $\pm 7.9^c$	**25.6**

Table 1. Melanosome characteristics of extant feather samples and BMNHC PH881. Means ± 1 s.e. and oneway ANOVA of the measurements taken from melanosomes in feathers of extant bird species, and BMNHC PH881. Values in the same row not sharing the same letter in superscript are significantly (P<0.05) different from one another (student's t test). Melanosomes in row labeled "Penguin" are sampled from crown *Sphenisciformes (Spheniscidae)*, which have a morphology (~low aspect ratio, large size) distinct from other birds (*12*).

Methods and Materials

I. Taphonomy

Quanguo Li[1], Ke-Qin Gao[2], Qingjin Meng[1], Julia A. Clarke[3], Matthew D. Shawkey[4]*, Liliana D'Alba[4], Rui Pei[5], Mick Ellison[6], Mark A. Norell[6], Jakob Vinther[3,7].

Rod-shaped micron-sized structures previously interpreted as melanosomes (*S1-5*) were found as impressions in the matrix of *Microraptor* feathers. The use of morphology and distribution to identify these structures as melanosomes has been criticized as insufficient to distinguish them from bacteria (*S6*), despite distinct correlation of their presence and density to striking color patterns (e.g., stripes) and preserved details of unique nanoscale organization seen in the production of some iridescent colors (*S4-5*). Recently, Wogelius et al. (*S7*) provided additional chemical evidence that similar structures are melanosomes and not bacteria. These authors showed that trace metals associated with eumelanin, and not bacteria, were found in association with putative melanosomes in a number of fossil species, including several feathers. Further validation that this method can reliably distinguish between trace metals from β-keratin (*S8*) (the primary component of feathers) and eumelanin is needed, but these data (*S7*) both falsify the bacterial origin and support the melanosome identity of these structures.

Melanosomes were found in 20 of 26 samples from throughout the plumage of *Microraptor*. The six samples without evidence of preserved melanosomes were found in diverse regions: i.e., select areas of the tibial feathers (2 samples), the tail feathers (2 samples), the proximal primaries and the tarsometatarsal feathers. One sample lacking preserved melanosomes was from the same feather as a sample containing dense melanosomes. All samples in which no melanosomes were detected had an amorphous organic matrix (Figure S1) that covered their entire surface. This was also seen in samples with preserved melanosomes that were observed where the organic matrix had worn away, was in cracks, or at the sample edges. No sample lacking preserved melanosomes was associated with the light color previously associated with low melanosome density (*S1, S3*). Thus, it is unclear whether the lack of melanosomes reflects the original condition or, more likely, coverage by secondary organic precipitates. We therefore do not diagnose color of these samples. Melanosomes were generally preserved as imprints in the siliciclastic (clay) matrix as well as in small quartz (SiO$_2$ confirmed with EDX analysis) crystals (Figure S2).

II. Identification of a novel class of melanosomes associated with iridescent color

Iridescent colors in birds are produced through coherent light scattering from organized arrays of melanosomes in a keratin matrix in feather barbules (*S9-10*). Light is constructively scattered by laminar or crystal-like arrays, consisting of alternating layers of materials with different refractive indexes, namely keratin, melanin and sometimes air. Although all iridescent plumage colors are produced by the same underlying processes, considerable variation exists in the structure and arrangement of the alternating layers of keratin and melanin, and, consequently, in the appearance of these different colors. Some iridescent melanosomes are entirely unique and easily recognizable (e.g. hollow disks in hummingbirds (*S11*) but in most cases they appear similar to those of black and grey feathers (*S11*). Thus, we sampled melanosomes from a diverse range of iridescent feathers (35 samples total, see Additional Data Table S1), to determine if these latter cases were distinct in a consistent way. We added these samples, as well as additional samples from black, brown and grey and black-brown penguin feathers to our existing database (*S1, S3*), for a total sample size of 168. These samples covered all avian orders except one (Phaethontidae), providing excellent phylogenetic diversity (see Additional Data Table S1).

All feather samples were taken from the University of Akron ornithological collection, the Yale Peabody Museum and the Zoological Museum of Copenhagen. We obtained data on melanosome morphology from these samples as previously described (*S1, S3*). First, feathers were embedded in Epon by trimming barbs and barbules from the central rachis, dehydrated using 100% ethanol (20 min.) twice, and infiltrated with 15, 50, 70 and 100% Epon (24 h each step). Infiltrated barbs were then placed in block molds and polymerized at 60° C for 16 hours. We then cut thick (5 μm) longitudinal sections of blocks on a Leica UC-6 ultramicrotome, mounted them on stubs with carbon tape, sputter-coated them with silver and viewed them on a JEOL JSM7401F SEM.

We used the image-processing program ImageJ (available for download at http://rsbweb.nih.gov/ij/) for analysis of SEM and TEM images. We measured maximum linear short and long axis length of melanosomes that were oriented perpendicular to line of sight. From these data we calculated mean and coefficient of variation (CV) of long and short axis, and mean aspect ratio (long:short axis). These ratios are an index of shape, and values close to 1 indicate sphericity and values farther from 1 indicate cylindricity. The distribution of melanosome morphology within feathers was frequently skewed towards one type of morphology, therefore we also calculated the skewness of long and short axis. Finally, we calculated density of melanosomes as total number of melanosomes divided by the total surface area represented in each image analyzed. We collected all data from both barbs and barbules of each extant feather.

We collected morphological data from SEM images of *Microraptor* feathers in the same manner as the extant bird feathers. Small samples of BMNHC PH881 feather impressions from the tail feather fan (sample numbers 1,2,10,13,14), hind limb (4, 15,16,17), forelimb (3, 7, 8,9, 11, 12, 18, 19, 20) and neck region (6). The samples were coated with gold (30 seconds) and studied with a Philips XL 30 environmental scanning electron microscope (situated at Yale University, Dept of Geology and Geophysics) at 10kV voltage, high vacuum and a 10 mm working distance. Morphological measurements from these imprints were assembled in the same manner as the modern feathers. These data are summarized in Table 1. All melanosomes were preserved as impressions, and hence additional analyses comparing the two previously observed preservation types (3D preservation vs. impressions (*S1*) were not performed. Melanosomes from the *Microraptor* specimen were within the range of extant melanosomes, and most similar to those from iridescent feathers (Fig. 1, Table 1). This similarity can be seen most clearly in the canonical discriminant analysis (Table S1, Fig. 1) and in Table 1.

We used a quadratic canonical discriminant analysis to estimate color of the fossil feathers. This standard method identifies the combination of variables that best separates two or more classes of objects (in this case, melanosomes from the different categories of feathers) (*S12*). Using data from training points, the classifying variables are loaded onto factors that are then used to estimate categories, and the probability of correct classification, of unknowns. We used a quadratic rather than linear discriminant analysis because some variables showed evidence of collinearity (*S12*). We used a forward stepwise method to choose variables that contributed significantly (p<0.05) to the analysis and to eliminate those that did not. The variables retained for use in the analysis were aspect ratio (p<0.001), melanosome long axis (p<0.001), melanosome short axis (p<0.001), melanosome long axis variation (p<0.001), melanosome short axis variation (p=0.001), and aspect ratio skew (p=0.001). The discriminant function as a whole was highly significant (Pillai's trace, $F_{24,640}$=15.06, p<0.001). Canonical axis 1 explained the majority of the variation in the dataset, was highly correlated with the classes and was most strongly positively associated with aspect ratio (Table S1). Canonical axis 2 explained most of the remainder of the variation, was also highly correlated with the classes and was most strongly positively associated with melanosome length. Canonical axis 3 explained the remainder

of the variation and was most strongly associated with melanosome short axis variation and aspect ratio skew.

Data from the *Microraptor* specimen clustered with modern black and iridescent feathers (Fig. 1). Accordingly, when we used the parameters from the analysis of this training set to estimate the colors of fossil feathers, *Microraptor* feathers were classified as black or iridescent with varying probabilities (Fig. 2, Table S2).

III. Identification of BMNHC PH881 as *Microraptor* and description of the specimen

Specimen BMNHC PH881 was recovered from the Early Cretaceous Jiufotang Formation of Lamadong, Jianchang County, in western Liaoning Province, PRC. It is approximately 54 cm in length from the tip of the rostrum to the terminus of the tail feathering. BMNHC PH881 is a nearly complete and articulated skeleton in a single slab with well-preserved evidence of tail, fore- and hind limb feathering (Fig. 2-4, Fig. S3-7). While most parts of the skull are also well preserved, the temporal region and braincase are shattered and provide little information. BMNHC PH881 is referred to *Microraptor* based on the following diagnostic characters (*S13*, *S26*): teeth only serrated on posterior carinae; posterior teeth with a basal constriction between crown and root, manual phalanx III-3 less than one third as thick as manual phalanx II-2; presence of a pendant accessory crest at the base of the lesser trochanter on the femur; pedal phalanges III-1 and IV-1 much more robust than the corresponding phalanges on the same digits.

Microraptor as used in the present paper refers to a single species, *Microraptor zhaoianus* pending a detailed revision of the taxon taking into account potential ontogenetic data (e.g., from histological data). The holotype specimen of *Microraptor zhaoianus* (IVPP 12330), also from the Jiufotang Formation of western Liaoning, was first reported by (*S13*). However, a second species, *Microraptor gui*, was later recognized (*S14*). More recently, this species has been proposed be a synonym of the earlier named *Microraptor zhaoianus* (*S15*), and a single *Microraptor zhaoianus* terminal has been used in most recent analyses of paravian relationships (e.g., *S16-S17*). but further revision may be undertaken in the future. More recent analyses with increased taxonomic sampling suggest *Microraptor* is one of several taxa basal within Dromaeosauridae but that it may not be the most basal part of that clade (e.g., S16-17).

We provide a description of the specimen here to support our taxonomic assessment. Comparisons were made with previously reported specimens. Xu et al. (*S13*) included a description of the *Microraptor zhaoianus* holotype, but this specimen lacks most of the skull, manus, as well as parts of the pectoral girdle. Hwang et al. (*S18*) described two other specimens of *Microraptor* (CAGS 20-7-004 and CAGS 20-8-001) giving a detailed description of the lower jaw and the postcranial skeleton. Further details of the anatomy of *Microraptor* were given at the description of the holotype of *Microraptor gui* and specimens referred to *Microraptor* sp. (*S14*). In size the new specimen (Table S3) is much closer to the *Microraptor zhaoianus* holotype (*S13*).

BMNHC PH881 has a sub-triangular skull, much like the profile of *Archaeopteryx* and basal troodontids (*S19*). The length of the skull is 5.59 cm and the height of the skull is 2.24 cm. The anterior tip of the premaxilla is blunt, where the anterior edge forms a right angle with the ventral edge, similar to *Bambiraptor* and *Sinovenator* (*S20-21*). The premaxilla bears four lancet-shaped teeth that are more closely packed than those in many other dromaeosaurids like *Sinornithosaurus* (*S22*) but are more loosely packed than in troodontids. Thirteen tooth positions are estimated on the right maxilla. The maxillary teeth are relatively large, and bear simple serrations on the posterior carina like *Sinornithosaurus* and some troodontids, but different from most other dromaeosaurids, whose teeth are

serrated on both carinae (*S22-23*). The jugal expands laterally at the base of the postorbital process, forming a small jugal boss. The postorbital process is vertically orientated, more robust than the ventral process of the lacrimal and excludes the postorbital from forming the anterior margin of the lower temporal fenestra. The posterior process of the jugal is short. Six dentary teeth are exposed on the right dentary, but more should be buried beneath the right maxilla. Estimated 12 dentary tooth positions are estimated on each side. The shape of the dentary teeth is similar to the premaxillary and the maxillary teeth. The anterior teeth are more closely packed compared with the maxillary teeth. The ventral margin of the dentary is convex, typical of dromaeosaurids such as *Sinornithosaurus* and *Velociraptor* (*S22, S24*).

Ten cervical vertebrae are present, as in other dromaeosaurids (*S24-S25*). Gastralia have been reported in both the holotype and CAGS 20-7-004 (*S13, S18*) but they are much better preserved in BMNHC PH881. Both lateral and medial segments of the gastralia are present; the medial segments are shorter than the corresponding lateral segments, as observed in *Sinornithosaurus* and *Velociraptor* (*S22, S24*).

The morphology of the pectoral and pelvic girdles and limb elements is consistent with detailed descriptions in other monographs (*S13, S14, S18, S26*) with the exception of an oval shaped foramen present in the deltopectoral crest of the humerus in BMNHC PH881. A similar structure has also been observed in one specimen referred to *Microraptor zhaoianus* CAGS 20-8-001 (e.g., *S18*: Fig. 20) but has not been previously reported to our knowledge.

IV. Description of feathering in BMNHC PH881

Primary feathers associated with the right and left forewing are preserved (Fig. S3). The left wing is extended but preserved under the thoracic elements with the left primaries extending under the right leg. The right wing is flexed, and both primaries and the secondaries are visible on this side (Fig. S3). The length and morphology of tarsometatarsal feathering associated with the left hind limb are preserved (Fig. S4). Tail feathering and the profile of the tail feather fan are also clearly exposed (Fig. 3). No information on head feathering is preserved with the exception of small tuft of feathers near the base of the skull, interpreted as part of the upper neck feathering (Fig. 2).

Approximately twelve primaries have been estimated for *Microraptor* based on other specimens (*S16*). Approximately 9 primaries are distinguishable in BMNHC PH881 (Fig. S3, left) and may support a slightly lower estimate. Preparation of the tips of the primaries of the right wing is somewhat limited making them appear slightly narrow artificially. Distal primary diameter is more accurately represented in the left distal wing exposed under the right hind limb (Fig. 2, Fig. S3). As best exposed in the right wing, however, the proximal-most two primaries are short; they are just slightly longer than the secondaries (Fig. 2, 4, S3: left). Similarly, the two leading edge primaries are also short, as seen exposed in IVPP V 13352 (Fig. S5). Five mid-series primaries are significantly more elongate and sub-equal in length as shown in both BMNHC PH881 and IVPP V 13352. At least one primary adjacent to the two short leading edge primaries that also appears slightly more abbreviate than the succeeding, or more proximal, primaries. This arrangement would confer a slight curvature to particularly the leading edge of the wing.

The secondaries are a little over half the length of the elongate, mid-series primaries and approach 60% of the most elongate of these primaries (Fig. S3). In IVPP V 13352 slight traces of several forewing covert feathers are distinguishable that are associated with the secondaries (Fig. S5). In BMNHC PH881, the tips of several apparent dorsal wing coverts also are visible associated with the primaries of the right wing.

Most of the upper leg (tibial) feathering in BMNHC PH881is obscured by preparation associated with the elements of the pelvic girdle and limb as well as feather impressions from other parts of the body. Although this feathering is partially exposed on the left side, few details can be discerned (Fig. 2). Specimen LPM-0200, however, shows that these feathers approached 1.7 times the length of the femur (Fig. S7).

No feathering is preserved associated with the pedal digits in BMNHC PH881 (Fig. 2) or other reported *Microraptor* specimens (Fig. S7). Only IVPP V 13352 preserves several short feathers associated with the posterior margin of the distal tip of the tarsometatarsus. However, none are visible associated with the pedal digits. By contrast, in *Anchiornis,* feathered digits are conspicuous in both referred specimens (*S3, S27*). Elongate pinnate tarsometatarsal feathers are associated with the left foot. On the right side they are not visible and appear to be unprepared. As in other *Microraptor* specimens (e.g., IVPP V 13352) these feathers approach the length of the forewing primaries (are approximately 80% their length) and are similarly asymmetrically vaned. The latter morphology is particularly well-exposed in BMNHC PH881(Fig. 2, Fig. S4). Shorter dorsal covert feathers are visible associated with the left tarsometatarsus of BMNHC PH881.

Although the exact number of feathers involved in the tail fan is impossible to determine in BMNHC PH881, there appear to be approximately 8-12 paired sets based on comparison of the new specimen (Figs. S5, S6), IVPP V 13352, and the illustration of TNP0096 (S14: Fig. 3). The most elongate feathers exposed in BMNHC PH881 are the last set and are approximately 114 mm in length. None of the tail feathers in BMNHC PH881 appear to be asymmetrically vaned.

V. **Reconstruction of feathering in *Microraptor:***

BMNHC PH881 was compared to the following 8 specimens preserving evidence of integument in *Microraptor*: IVPP V13352, IVPP V13477, IVPP V12330, IVPP V13476, IVPP V12727, IVPP V13320, LPM 0200 and TPN0096. Each forelimb, hind limb, and tail feather as well as their associated points of origin were traced from high resolution images acquired by one of us (M. Ellison). The tracings were scanned, resized (scaled) and positioned for overlay. Given that individual specimen overall sizes varied, each was scaled to the same size primarily using the length of the metatarsals, the most complete preserved elements among specimens; skeletal elements were similarly proportioned among specimens. The same methodology and specimen set were utilized for the forewing. Skeletal elements were also discovered to be similarly proportioned among surveyed specimens.

Figure S7 illustrates the general methodology for the hind limb feathering reconstruction. The same methodology and specimen set were utilized for the forewing. However, in this case two specimens with the best-preserved evidence of forewing feathering (IVPP V 13352 [Fig. S6] and BMNHC PH881 [Fig. S3]) in fact contributed most of the data available for the reconstruction. Limited data from additional specimens were checked against overlays from these two specimens. While there is evidence from both specimens relevant to the wing outline, feather number as well as primary and secondary feather morphology (see comments in the description of BMNHC PH881 above; Figs. S3, S8) data on the organization of covert feathers into one or several rows over the secondaries and primaries are limited (Figs. S3, S8). Reconstruction of multiple, well-organized tiers of these feathers is considered more hypothetical than other aspects of *Microraptor* feathering.

Feathers on the skull previously interpreted as indicative of a loose crest in *Microraptor* (S17) are more consistent with the slightly more elongate contour feathers typical in this region in extant Aves without a crest (Fig. S9).

In the case of the tail, tracings were made from BMNHC PH881 (Fig. S5), IVPP V 13352 as well as the illustration of the tail from TPN00996 in S17 (Fig. S6); these data agreed closely on tail feather shape, fan diameter, length along the caudal series, and organization. (See description in the main text and above).

Supplementary References

S1. J. A. Clarke *et al*. *Science* **330**, 954 (2010).
S2. F. C. Zhang *et al*. *Nature* **463**, 1075 (2010).
S3. Q. Li *et al*. *Science* **327**, 1369 (2010).
S4. J. Vinther, D. E. G. Briggs, R. O. Prum, V. Saranathan, *Biol*. *Lett*. **4**, 522 (2008).
S5. J. Vinther, D. E. G Briggs, J. Clarke, G. Mayr, R. O. Prum, *Biol*. *Lett*. **6**, 128 (2010).
S6. M. H. Schweitzer, *Ann*. *Rev*. *Earth Planet*. *Sci*. **39**, 187 (2011)
S7. R. O. Wogelius *et al*., *Science* **333,** 1622 (2011).
S8. M. Niecke, M. Heid, A. Krüger *J*. *Ornithol*. **140**, 355 (1999).
S9. R. O. Prum, in *Bird Coloration, Vol.1, Mechanisms and Measurements* G. E. Hill, K. J. McGraw, Eds. (Harvard Univ. Press, Boston, 2006) pp. 295–353.
S10. M. D. Shawkey, M. E. Hauber, L. K. Estep, G. E. Hill, *Journal of the Royal Society Interface* **3,** 777 (2006).
S11. H. Durrer, in *Biology of the Integument 2: Vertebrates* M. Bereiter-Hahn. A. G. Matolsky, K.S. Richards, Eds. (Springer-Verlag, Berlin, 1986) pp. 239-247.
S12. T. Hastie, R. Tibishirani, and J. H. Friedman, *The Elements of Statistical Learning*. (Springer, New York, 2001).
S13. X. Xu, Z. Zhou, X. Wang, *Nature* **408**, 705 (2000).
S14. X. Xu *et al*. *Nature* **421,** 335 (2003).
S15. P. Senter, R. Barsold, B. B. Britt, D. A. Burnham, *Bull*. *Gunma Mus*. *Nat*. *Hist*. **8,** 1 (2004).
S16. X. Xu *et al*. *Nature* **475,** 465 (2011)
S17. A. H. Turner *et al*. Science **317**, 1378 (2007).
S18. S. H. Hwang, M. A. Norell, Q. Ji, K. Gao, *Amer*. *Mus*. *Novitates*, 3381 (2002).
S19. P. J. Makovicky, M. A. Norell, in *The Dinosauria*. Weishampel, D.B., Dodson, P., and Osmólska, H, Eds. (University of California Press, Berkeley. 2004) pp. 184-195.
S20. D. A. Burnham, K. L. Derstler, P. J. Currie, R. T. Bakker, Z. Zhou Z., J. H. Ostrom, *Univ*. *Kansas Paleont*. *Contrib*. **13**, 1 (2000).
S21. X. Xu, M. A. Norell, X. Wang, P. J. Makovicky, X. Wu, *Nature* **415**, 780 (2002).
S22. X. Xu, X. Wang, X. Wu, *Nature* **401**, 262 (1999).
S23. M. A. Norell, P. J. Makovicky, in *The Dinosauria*. Weishampel, D.B., Dodson, P., and Osmólska, H, Eds. (University of California Press, Berkeley. 2004), pp.196-209.
S24. M. A. Norell, P. J. Makovicky. 1999. *Amer. Mus. Novitates* **3282**, 1 (1999).
S25. J. H. Ostrom, 1969. *Peabody Mus. Nat. Hist. Yale Univ. Bull.* **30**: 1 (1969).
S26. X. Xu. 2002. Phd. Dissertation of the Chinese Academy of Sciences. 1 (2002).
S27. D. Hu, L. Hou, L. Zhang, X. Xu, *Nature* **461**, 640 (2009).
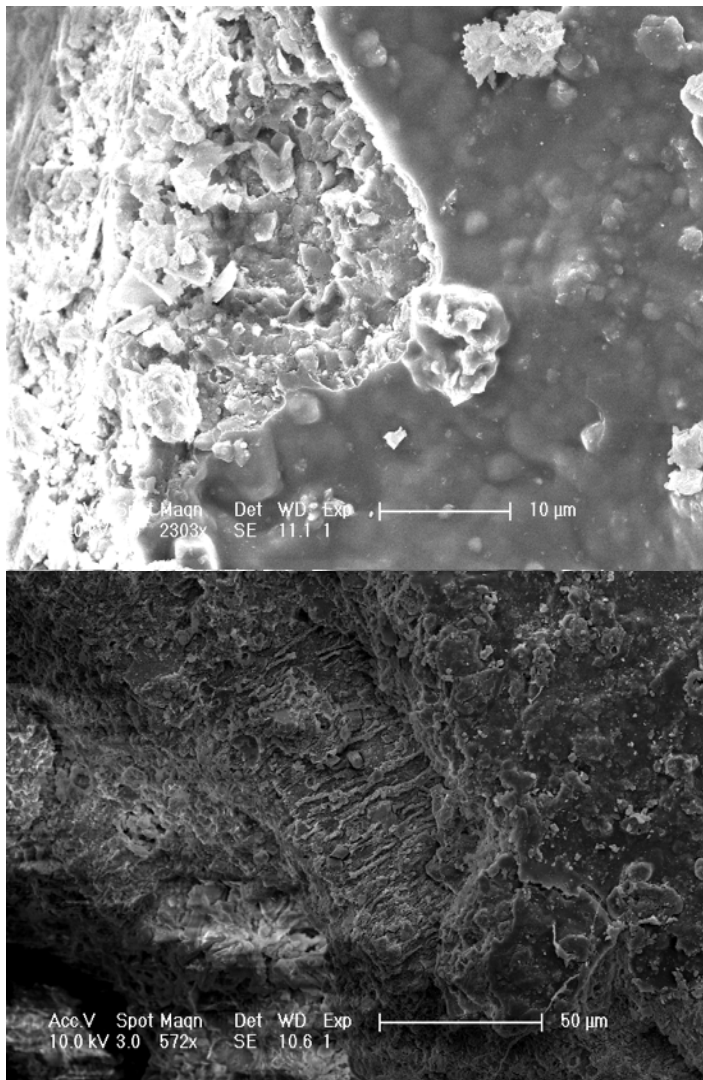S28. S.A Smith, Atlas of avian radiographic anatomy (Saunders, Philidelphia, 1992).

.

Fig. S1. SEM images of samples from BMNHC PH881 plumage in which no melanosomes were found (upper image), showing thick organic matrix covering the surface in the right side of the images. This organic matrix were also observed in samples with melanosomes preserved (lower image).
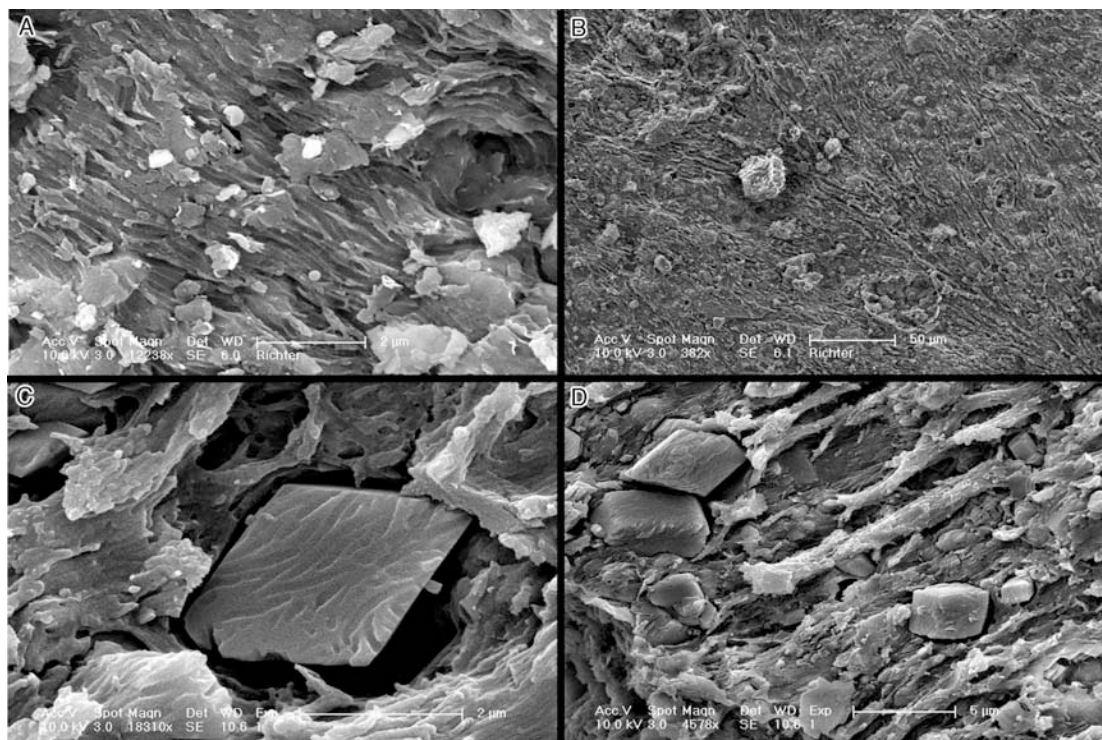
Fig. S2. Examples of the preservation of the feathers in BMNH PH881.
A) Sample 2, distal tail feather. Melanosome imprints in matrix, note the distinct   alignment of
melanosome imprints. **B**) Sample 4, tarsometatarsus feather showing   the macrostructural
preservation of the feather imprint as ridges and grooves   containing melanosome imprints. **C**)
Sample 14, anterior tail fan. Silica crystal with melanosome imprints in as well as the adjacent matrix. **D**)
Sample 14, lower
magnification showing several silica crystals in the matrix of the feather imprint or forming ridges and
grooves.
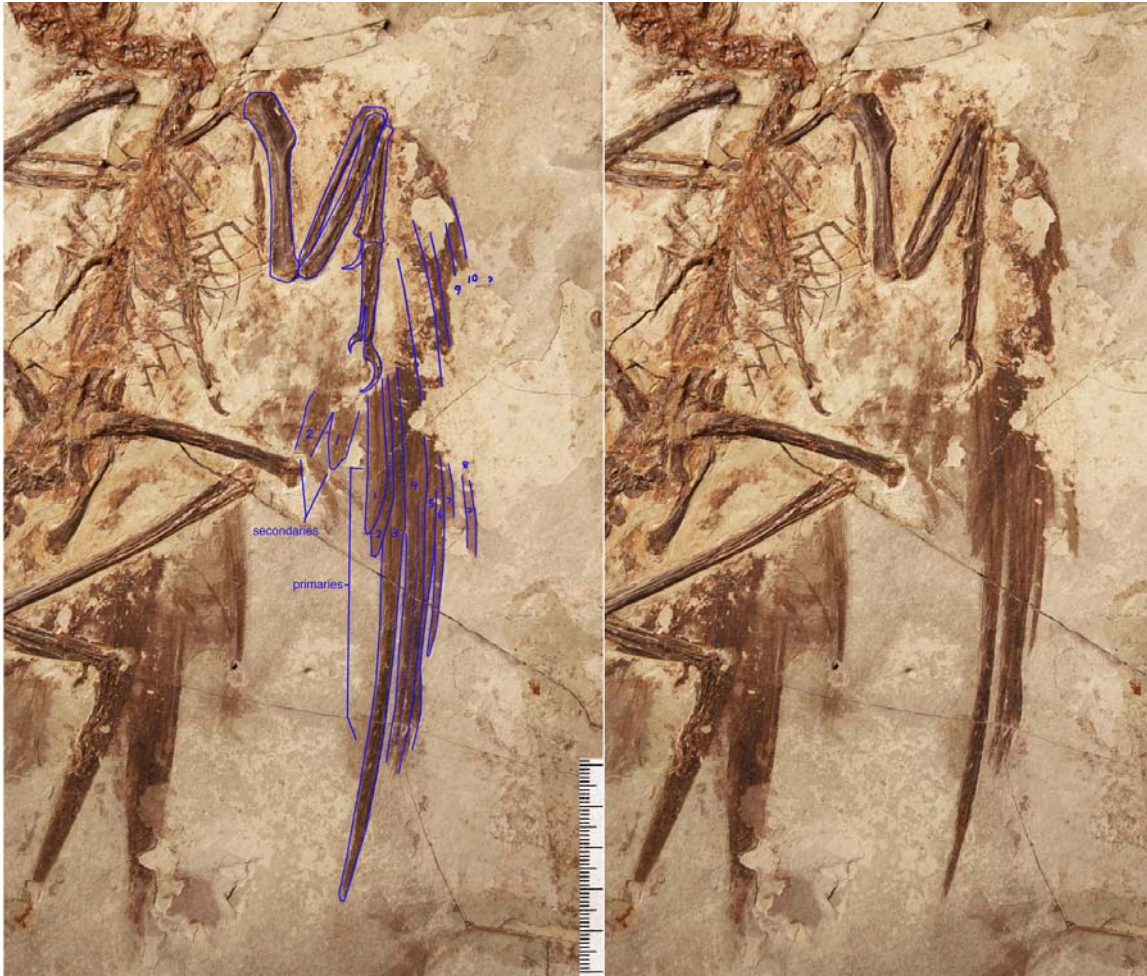
Fig. S3. Forewing feathering in BMNHC PH881 showing primary and secondary feather lengths and estimated primary feather count.

Fig. S4. Detail of the exceptionally well-preserved tips of asymmetrically-vaned tarsometatarsal feathers of the left leg passing under the tail in BMNHC PH881.

Fig. S5. The tail feathering in the BMNHC PH881 *Microraptor* specimen showing a terminal set of elongate, mid-line feathers (Fig. 2, 4). The new specimen supports distal tail feathering distinctive from all previous reconstructions.
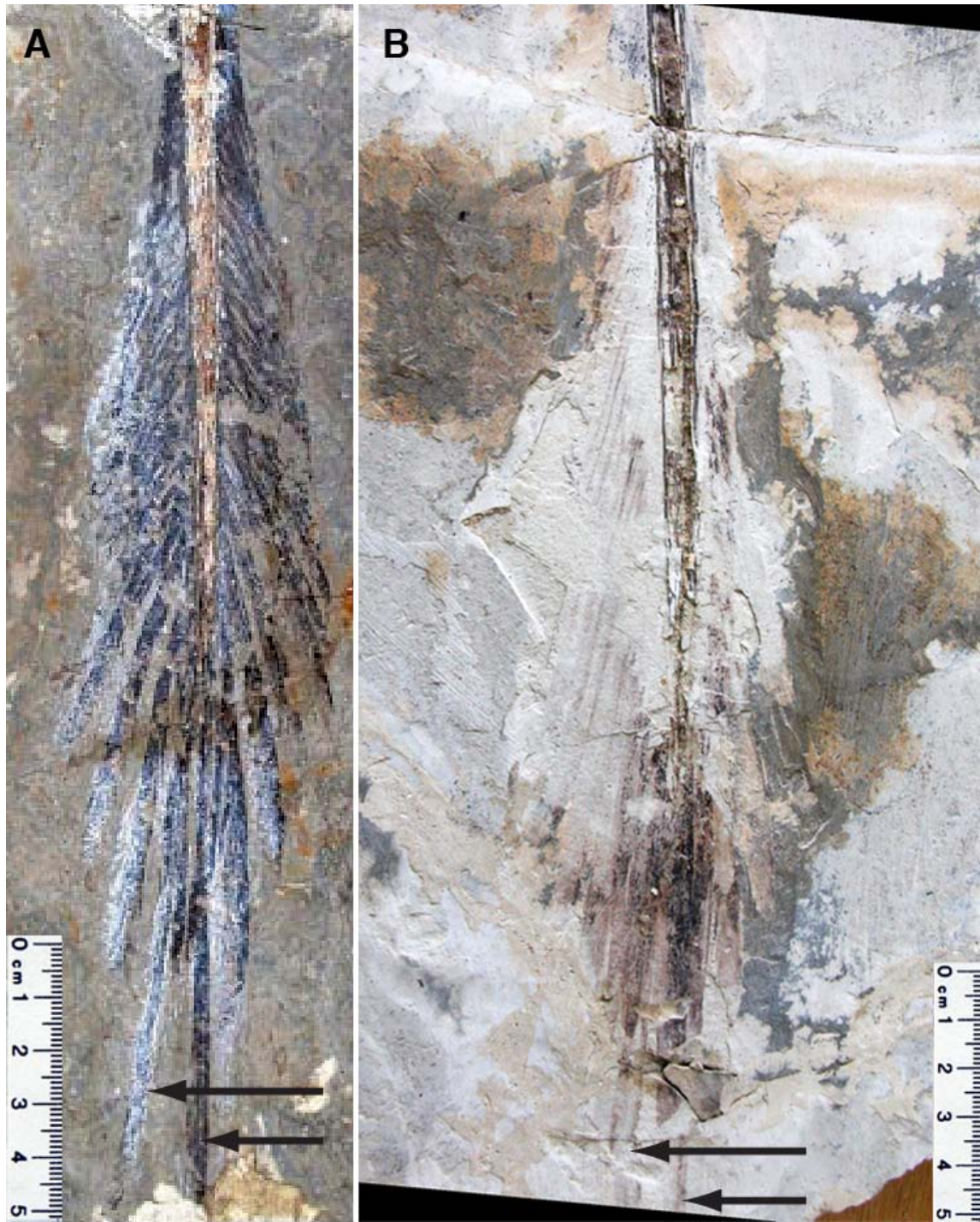
Fig. S6. Distal tail feathering in (right) IVPP V 13352 and in (left) TPN0096 (as illustrated in S14). Arrows indicate the pair of elongate feathers reported from the new specimen and subsequently recognized in these previously described specimens.
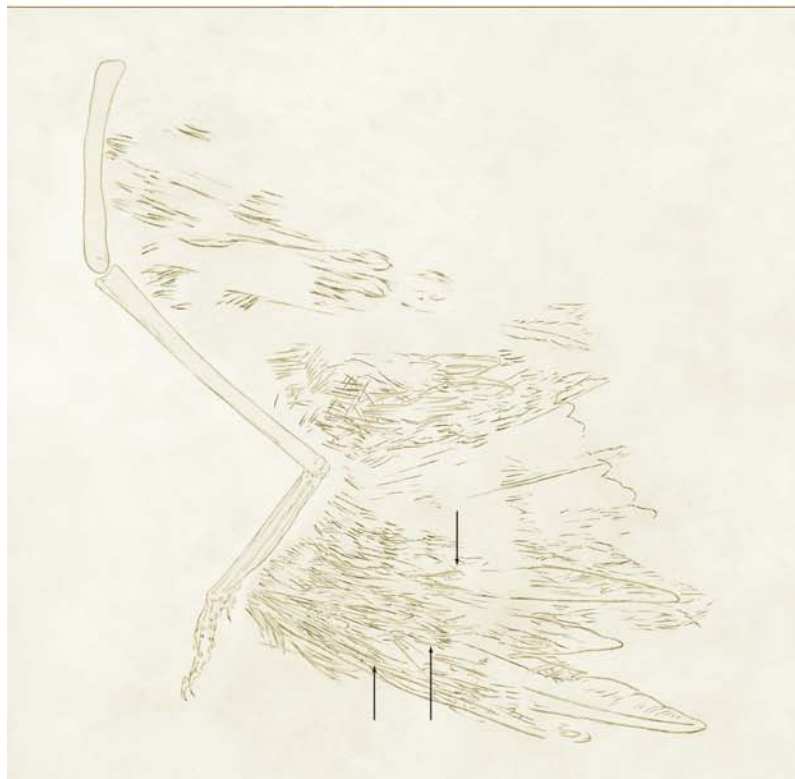
Fig. S7 (previous page). Methodology used in reconstructing *Microraptor* feathering (Fig.3). Leg feathering in A -IVPP V13476 (right leg), B – IVPP V13477 (left leg), C – IVPP V13320 (left leg), D – IVPP V13352 (left leg), E – IVPP V13352 (right leg), F –IVPP V13320 (right leg), G - LPM-0200 (left leg), H -IVPP V13476, and I - BMNHC PH881 (left leg) were traced, sized and overlain yielding the image in the bottom plate. Arrows indicate inferred covert feathers relative to elongate, asymmetrical primaries.
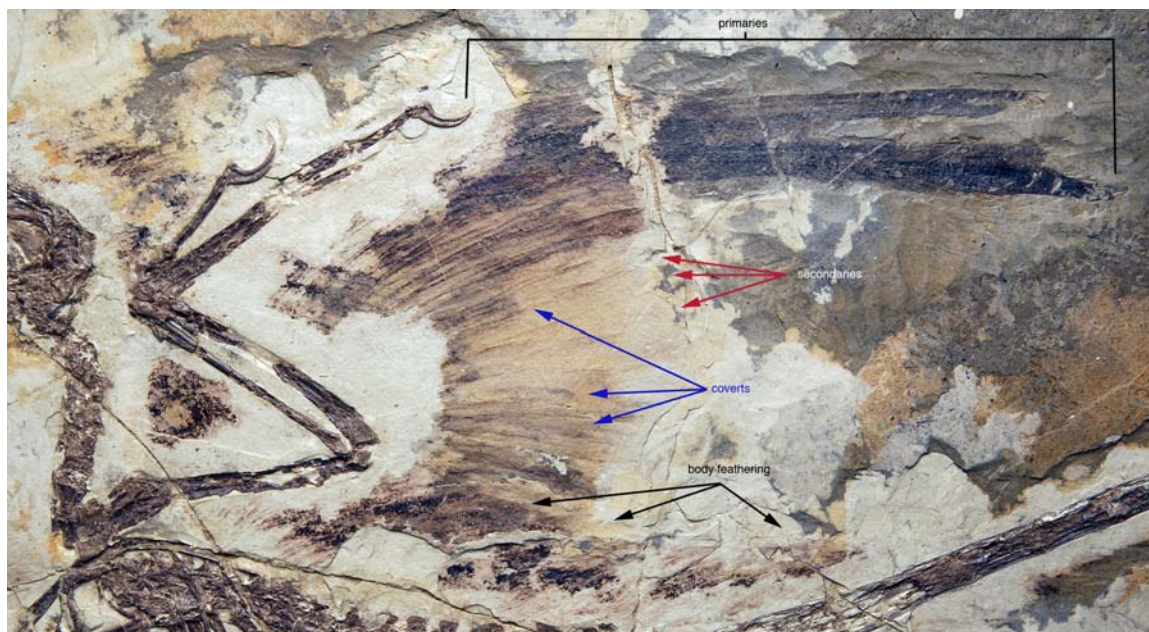
Fig. S8.Evidence of forewing and body contour feathering preserved in the *Microraptor gui* holotype specimen (IVPP V 13352). The tips of secondary feathers, position of at least one layer of dorsal coverts are indicated with red and blue arrows, respectively.
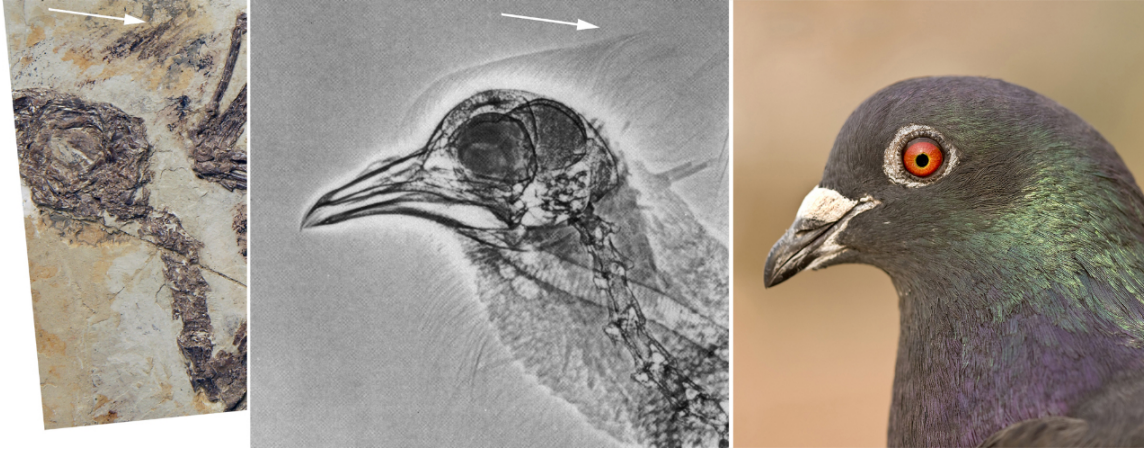
Fig. S9. Head feathering of (left) *Microraptor* specimen IVPP V 13352 compared to that of (center and right) an avian lacking a crest (*Columba livia*; Rock Dove from *S28*; Photo on right by MAD/Bigstock.com). Arrows indicate the location and relative lengths of head feathers previously interpreted as indicative of a loose crest in *Microraptor,* but a result of compression (during radiography) in the extant specimen. Feathers forming distinct crests in Aves are typically longer and more rostrally positioned.

Canonical axis #	Eigenvalue	% variation explained	Canonical correlation	Length CV	Length CV	Diameter	Diameter CV	Aspect ratio	Aspect ratio skew	**Table S1:**
1	2.09	64.23	0.82	0.04	-0.04	0.29	0.22	1.08	0.08	
2	0.76	23.33	0.66	0.84	0.52	0.06	-0.11	-0.49	-0.30	
3	0.22	6.91	0.43	0.31	-0.02	0.06	0.82	-0.19	0.82	

Eigenvalues and standardized scoring coefficients for a quadratic discriminant analysis of color (black, brown or grey) in extant birds and in samples of BMNHC PH881. The analysis identified six properties of melanosome morphology and distribution that predicted color in extant birds and then used these data to predict colors in the fossil sample.

Sample	Predicted color	P	Sample description
1	IR	0.96	Proximal portion of a posterior tail feather
2	IR (BL)	0.68 (0.31)	Posterior tail feather (proximal or distal)
3	IR	1.00	Distal portion of primary feather (left wing)
4	IR	0.93	Distal portion of elongate pinnate tarsometatarsus feather
5	IR	1.00	Not identifiable. Possibly tail, leg or left wing
6	IR	0.93	Neck region
7	IR	1.00	Distal portion of dorsal primary covert feathers (right wing)
8	IR	0.92	Distal tip of secondary feather (right wing)
9	IR (BL)	0.86 (0.13)	Distal end of primary feather (right wing)
10	IR (BL)	0.72 (0.25)	Mid-section of a posterior tail feather
11	IR	1.00	Distal tip of primary feather (right wing)
12	IR	1.00	Distal portion of primary feather (left wing)
13	IR	0.89	Proximal portion of one of the posterior-most tail feathers
14	IR (BL)	0.65 (0.28)	Anterior-most part of the tail-feather fan
15	BL (IR)	0.86 (0.11)	Distal portion of elongate pinnate tarsometatarsus feather
16	BL	0.66 (0.32)	Distal portion of elongate pinnate tarsometatarsus feather
17	IR (BL)	0.75 (0.24)	Mid-portion of shorter, distal pinnate tarsometatarsus feather
18	IR	1.00	Distal tip of primary feather (right wing)
19	IR (BL)	0.93	Mid-portion of primary feather (right wing)
20	BL (IR)	0.58 (0.41)	Proximal portion of distal primary feather (right wing)

Table S2. Predicted colors for sampled regions of BMNHC PH881. **P** = probability of group (color) membership for samples. Secondary color predictions and associated probabilities are in shown in parentheses. BL= black, IR= iridescent.

Skull length	55.9
Skull height	22.4
Humerus (right)	47.4
Ulna (right)	44.7
Metacarpal III (right)	>29.8
Manual phalange I-2 (right)	11.9
Manual phalange II-1 (right)	13.4
Manual phalange II-2 (right)	12.5
Manual phalange II-3 (right)	12.0
Manual phalange III-4 (right)	5.3
Pubis (right)	46.2
Femur (left)	51.8
Tibiotarsus (left)	70.7
Metatarsus III (left)	39.0
Metatarsus IV (left)	36.1
Pedal phalange III-1 (left)	10.4
Pedal phalange III-2 (left)	6.4
Pedal phalange III-3 (left)	6.2
Pedal phalange III-4 (left)	10.6
Pedal phalange IV-1 (left)	7.8
Pedal phalange IV-2 (left)	4.7
Pedal phalange IV-3 (left)	4.0
Pedal phalange IV-4 (left)	4.8
Pedal phalange IV-5 (left)	8.3

Table S3: Select measurements (in mm) of BMNHC PH881.

A photonic heterostructure produces diverse iridescent colours in duck wing patches

Chad M. Eliason[1]* and Matthew D. Shawkey[1]
[1]Department of Biology, The University of Akron, Akron, OH, USA
*email: cme16@zips.uakron.edu

SUMMARY

The colours of birds are diverse but limited relative to the colours they can perceive. This pattern may be partially caused by the properties of their colour production mechanisms. Aside from pigments, several classes of highly ordered nanostructures (thin films, amorphous 3D arrays) can produce a range of colours. However, the variability of any single nanostructural class has rarely been explored. Dabbling ducks are a speciose clade with substantial interspecific variation in the iridescent colouration of their wing patches (specula). Here we use electron microscopy, spectrophotometry, polarization and refractive-index matching experiments, and optical modelling to examine these colours. We show that, in all species examined, speculum colour is produced by a photonic heterostructure consisting of both a single thin-film of keratin and a 2D hexagonal lattice of melanosomes in feather barbules. Although the range of possible variations of this heterostructure is theoretically broad, only relatively close-packed, energetically stable variants producing more saturated colours were observed, suggesting that ducks are either physically constrained to these configurations or are under selection for the colours that they produce. These data thus reveal a previously undescribed biophotonic structure and suggest that both physical malleability and constraints within single nanostructural classes may help explain the broader patterns of colour across Aves.

Keywords: photonic crystal, *Anatidae*, iridescent, thin-film, polarization

1. INTRODUCTION

The display of colour for inter- and intraspecific communication has been a fundamental function of the metazoan integument since the evolution of vision in the Cambrian explosion [1]. Colours can either allow an organism to hide from potential predators or prey, or become more conspicuous for aposematism or sexual display [2-4]. The plumages of birds range from highly cryptic to highly conspicuous and indeed at the latter extreme produce some of the most vivid colours found in nature. A recent study [5] showed that, while diverse, these colours are limited relative to what birds can perceive. This pattern of unoccupied regions in colour space may be explicable at least in part by the physical constraints stemming from the mechanisms by which those colours are produced.

While selective light absorption by pigments like carotenoids and psittacofulvins can produce highly saturated colours [6], these appear to be limited to yellows and reds and are incapable of producing shorter wavelength hues (e.g., blues and violets). By contrast, structural colours resulting from coherent scattering of light by highly ordered nanostructures are capable of producing colours across most of the bird-visible spectrum [5]. For example, previously described structural colours produce near-total ultraviolet [7], blue [8], green [9], yellow [10] and red [11]. This diversity in colour is facilitated both by the diversity of morphological classes producing structural colour and also the variability of each of those classes. To illustrate this point, consider that, for all structurally-coloured materials, achieving peak reflectance in visible wavelengths depends on three general features: nanoscale organization, size of scattering structures, and refractive index (RI) contrast of its structural components. Moreover, these materials can be organized in one (e.g. multilayer reflectors [10]), two (e.g., 2D photonic crystals [8]) or three dimensions (e.g. amorphous matrices [12]), and in birds employ a rather limited set of basic materials: keratin, melanin and air [13]. Optical theory shows that slight alterations in organization, size or RI contrast can lead to dramatic changes in colour [14]. However, the theoretical and empirical malleability of any single class of nanostructure has not been thoroughly explored.

Many duck species have an iridescent wing patch known as the speculum [15] that shows a broad range of interspecific colour variation [16]. Previous studies have suggested that this colour arises through multilayer interference from organized rows of thin melanosomes and layers of keratin [17-19]. However, electron micrographs of barbule cross-sections show a two-dimensional hexagonal arrangement of melanosomes beneath a thin keratin cortex [17], suggesting that colour may in fact result from a 2D photonic crystal. Such crystals can produce a broad variety of colours, and are thus an ideal study system for examining the malleability of a structural colour class. We did so using a combination of electron microscopy, reflectance spectroscopy, and optical modelling. First, we identified the colour-producing nanostructure in six duck species. Second, using optical modelling, we compared the observed variation in this nanostructure and the colour it produces to what is theoretically possible given all potential combinations of relevant morphological parameters (radius, spacing) that are able to produce bird-visible colouration.

2. METHODS

2.1 Study system

To investigate the morphological bases of interspecific variation in speculum colour, we chose six species from the monophyletic dabbling duck clade (tribe *Anatini*) [20]. We removed a single iridescent secondary feather from the left wing of males from four of the six species using dissecting scissors for

subsequent electron microscopy (see below) and used published data for *Speculanas specularis* and *Amazonetta brasiliensis* [17] to complement these species and obtain close to the whole range of colours observed in ducks (see table 1; figure S1). We stored feathers in small envelopes in a climate-controlled room until further analysis.

2.2 Barbule nanostructure

To test the hypothesis that speculum colour results from a heterostructure consisting of a keratin thin-film and 2D hexagonal lattice of melanosomes in feather barbules, we examined barbule nanostructure by preparing cross-sections following Shawkey et al. [21]. Briefly, we washed feather barbs in 0.25 M NaOH and 0.1% Tween-20, dehydrated them with 100% ethanol, and infiltrated them with 15%, 50%, 70%, and 100% epoxy resin. We then cured the resin blocks in an oven at 60°C, trimmed them with a Leica S6 EM-Trim 2 (Leica Microsystems GmbH, Wetzlar, Germany), and cut 100-nm cross-sections with a Leica UC-6 ultramicrotome (Leica Microsystems GmbH, Wetzlar, Germany). Next, we viewed the cross-sections on a JEOL JEM-1230 transmission electron microscope operating at 120 kV. From the obtained TEM images, we used ImageJ [22] to measure the following nanostructural parameters from 2-3 barbules per species: keratin cortex thickness (d), taken at 10 evenly-spaced locations along the surface of each barbule; number of ordered melanosomes layers (i.e. periods, defined as a layer in which 3-4 consecutive melanosomes were in the same plane); melanosome radius (r); and melanosome spacing (distance between their centres; i.e. lattice constant a) (figure 1*a*). For the latter two variables, we used the particle analysis tool in ImageJ to determine the x and y coordinates and areas of 30-80 melanosomes per barbule (sample sizes were unequal due to variation in the number of visible melanosomes in a given cross-section). Next, we determined the area (A) and nearest neighbour distance (NND) between melanosomes and calculated the lattice constant as the mean NND and the radius as $r = \sqrt{A/\pi}$. For *S. specularis* and *A. brasiliensis*, we used published values of r and d and derived a from available TEM images [17].

2.3 Reflectance measurements

Overview of spectral analysis

With the exception of colour measurements taken from intact wing patches, we took all reflectance measurements using a lab-made goniometer [23] that allowed us to independently vary the angles of incidence (θ_i) and reflectance (θ_r). For polarization measurements, we used a Glan-Thompson polarizer (Harrick Scientific Products, Pleasantville, NY, USA) placed between the light source and sample (figure S2). We took unpolarized reflectance measurements at normal incidence for all six species (using intact plumages) and measured polarized reflectance and angle-resolved reflectance spectra for *Anas carolinensis*, *A. platyrhynchos*, *A. acuta*, and *A. clypeata*.

Normal incidence

To compare empirical reflectance with that predicted by optical modelling (see below), we measured specular reflectance of intact wing patches at normal incidence from 300 - 700 nm using a spectrophotometer and xenon light source (Avantes Inc., Broomfield, CO, USA). We took the average of 3 separate measurements per bird and smoothed reflectance values with a spline function to remove electrical noise from the spectrophotometer and increase the accuracy of colour variable measurements [24]. Next, we calculated hue (λ_{max}), brightness (peak reflectance) and saturation (full-width of main peak at half of maximum; FWHM).

Polarized reflectance

Owing to periodicity in refractive index parallel to the surface, reflectance of a 2D photonic crystal (PC) measured at normal incidence is expected to vary depending on the polarization of incident light [14]. While similar polarization effects also occur in multilayered (1D) structures, they are typically only observed only at high incident angles (e.g., see [25]). Therefore, to help distinguish between two alternative hypotheses (1D multilayer and 2D photonic heterostructure), we measured *s*- and *p*-polarized specular reflectance at near-normal incidence ($\theta_i = 10°$) for three feather samples: a hypothesized 2D photonic crystal (green-winged teal, *Anas carolinensis*); a positive control known to behave as a 2D photonic crystal (peaock, *Pavo cristatus*) [8]; and a negative control with a multilayered (1D) structure (ruby-throated hummingbird, *Archilochus colubris*) [11]. We predicted that both the peacock and duck samples would show differences in hue based on polarization, while the hummingbird sample would not.

Angle-resolved reflectance

To understand the angle-dependent reflectance behaviour of these samples, we measured specular reflectance for *s*- and *p*-polarized light at multiple incident angles ($\theta_i = 10, 20, 30, 40, 50, 60,$ and $70°$) and two azimuthal angles (Φ), perpendicular and parallel to the barbules (see figure 4). Because light scattering requires a difference in refractive index, the homogeneity of 1D layered systems in the *x* and *y* directions (parallel to surface) implies that Φ should have no effect on angle-resolved reflectance for different polarizations of light, while it should for a 2D PC. Thus, we calculated the ratio of *p*-to *s*-polarized reflectance (R_p/R_s) and plotted this ratio versus θ_i for $\Phi = 0°$ (parallel to barbules) and $90°$ (perpendicular to barbules). This ratio is suitable for small or anisotropic samples where the aperture of reflected light is expected to vary with orientation: since the aperture is the same for each polarization at a given orientation, the ratio remains unaffected [26]. Based on the band structure diagram (figure 1*c*), we predicted that the ratio R_p/R_s would be greater when the plane of incidence is parallel to the melanosomes and that the differences would diminish as θ_i approaches Brewster's angle. At this point, the reflectance would be dominated by thin-film effects (zero *p*-polarized reflectance from the top air-keratin interface at both orientations).

2.4 Refractive index-matching experiments

Light incident on a thin-film structure produces colour by interference between beams of light reflecting from the top and bottom interfaces of the film. Thus, to empirically examine the role of the keratin cortex in colour production, we removed its effects by placing wintergreen oil (Frontier Natural Products, Norway, IA, USA) on the surface of each feather. Because the refractive index of the oil is approximately equal to that of keratin (RI = 1.56), Fresnel reflectivity from the top interface is effectively eliminated. Further, to eliminate unwanted reflection of light at the air-oil interface, we mounted a bifurcated fibre-optic probe at a fixed distance from the feather surface and immersed it in the oil. We measured specular reflectance at normal incidence and compared the mean hue, saturation, and brightness before and after adding oil.

2.5 Optical modelling

Band structure calculation

The band structure of a photonic crystal gives the frequencies of light that are able to propagate through a periodic structure as a function of the light polarization and wave vector [14]. Frequencies that are unable to propagate through the structure comprise the photonic band gap (PBG) and are reflected from the PC. Thus, to investigate the physical mechanism of colour production, we used the standard plane-wave expansion method implemented in the software package MPB [27] to calculate the band structure

of an idealized hexagonal lattice based on experimental values for r/a and published values for the refractive indices of keratin (RI = 1.56) and melanin (RI = 2.00) [28, 29]. From the resulting band structure diagrams, we calculated the size of the partial PBG ($\Delta\omega$) at normal incidence and standardized this value by dividing it by the band gap position (ω), since band gap size is known to vary with position [14].

To determine the theoretical range of values for lattice constant and radius that would produce a PBG in visible wavelengths (300-700 nm), we used MPB to simulate band structures for a range of values of r/a between 0 and 0.5 and calculated the resulting position (ω) and size ($\Delta\omega$) of the partial PBG. We chose this range to cover all theoretically possible configurations up to a limiting value of r/a = 0.5, at which the melanosomes would be directly in contact with each other (hexagonal close-packing). Next, because hue depends on the lattice constant, we calculated hue for a range of lattice constants ($a = 80 - 250$ nm, in 10-nm increments) as $\lambda_{max} = a/\omega$ [14]. We then plotted the band gap size versus a and r and overlaid the plot with the calculated hues. We limited the values of λ_{max} to those in the visible spectrum of light, $300 - 700$ nm for birds.

Predicted reflectance

Dyck [19] described these structures as multilayers composed of melanin and keratin, with the thickness of layers equal to the diameter of melanosomes and space between melanosomes, respectively. However, in several of the close-packed structures we observed here there is little to no space between melanosomes, making this model unrealistic. We thus did not replicate this model here. We instead modelled them as hexagonal 2D PCs using the finite-difference time-domain (FDTD) method implemented in MEEP [30]. We chose this method because it allowed us to calculate reflectance across a range of wavelengths (i.e. $300 - 700$ nm) in a single simulation. We simulated reflectance spectra in MEEP based on measured nanomorphological values (a, r, d, and melanosome layer number) for each barbule per species. Additionally, to understand the role of the cortex in colour production, we compared predicted reflectance calculated when excluding and including the cortex with empirical results of refractive index-matching experiments (see below). In our simulations, we excluded the cortex by setting the refractive index surrounding the structure to that of keratin (RI = 1.56), thereby eliminating reflection from the air-keratin interface. For all simulations, we used an extinction coefficient for melanin of 0.01 [8, 31] and published values for the refractive indices of keratin (RI = 1.56) and melanin (RI = 2.00) [28, 29]. We then compared theoretical with empirical reflectance curves to test the accuracy of our modelling.

2.6 Statistics

We performed all statistical analyses in R [32]. All values are presented as mean ± 95% confidence limits unless otherwise noted.

3. RESULTS

3.1 Barbule morphology

In all six species examined, TEM images of barbule cross-sections revealed a 2D hexagonal array of melanosomes underlying a thin keratin cortex (figure 1a). The size of melanosomes (radius) ranged from 60 - 85 nm and their spacing (lattice constant) varied from 140 - 220 nm (table 2). The cortex thickness ranged from 90 - 370 nm, and the number of melanosome layers varied from $4 - 7$ between species (table 2).

3.2 Reflectance measurements

Normal incidence

All reflectance curves showed primary reflection peaks between 462 and 642 nm, and most curves were multi-peaked, with 1-2 secondary peaks occurring at shorter wavelengths (figure 2*a,c-f*). Of the six species examined, only *A. brasiliensis* had a single peak at 514 nm (figure 2*b*), while *Anas acuta* and *S. specularis* had additional tertiary peaks occurring at 300 and 325 nm, respectively (figure 2*e,f*). The primary peaks were highly saturated (narrow), with FWHM values ranging from 69 - 102 nm. Hue increased strongly with melanosome size (figure S3*a*) and, to a lesser extent, lattice constant (figure S3*b*) but did not appear to be related to either cortex thickness or number of melanosome layers. Peak reflectance (brightness) varied considerably between species, ranging from 10.67% (*Anas clypeata*) to 61.83% (*S. specularis*) (table 1), and increased slightly with the number of melanosome layers (periods) and decreased with melanosome density (*r/a*) (figure S3*c,d,* respectively).

Polarized light

The wavelength of peak reflectance (λ_{max}) for *p*-polarized light at near-normal incidence was shifted to slightly longer wavelengths than *s*-polarized light, and the peak reflectance increased slightly (figure S4). This observed bathochromic shift was also seen in a known 2D PC structure (peacock) but not in a negative control (hummingbird) (figure S4). Furthermore, peak reflectance did not change for the hummingbird (1D multilayer) but was higher for *s*-polarized light in the peacock.

Angle-resolved spectra

All feathers analysed showed significant changes in reflectance with increasing incident angle (figure 4*a,b*, dotted line). Furthermore, these angle-dependent reflectance changes varied with polarization. For *s*-polarized light, reflectance increased with θ_i (figure 4*a,b,* solid lines). By contrast, *p*-polarized reflectance steadily decreased until reaching a minimum at $\theta_i \sim 60°$ and then began to increase (figure 4*a,b*, dashed lines). We observed phase inversions in the reflectance spectra for all samples analysed (see e.g., figure 3*d*, inset). Furthermore, feather barbule orientation had an effect on angle-resolved reflectance for *s* and *p* polarizations, as light incident perpendicular to the barbules was in general more polarized ($R_s > R_p$) than light with parallel incidence; however, as θ_i approached ~60°, these differences diminished (figure 4*c*).

3.3 Refractive index-matching experiment
When oil was placed on the surface of feathers, hue did not change substantially (hue before: 538 ± 83 nm; after: 542 ± 97 nm; figure S5), suggesting that the structural colouration is produced in part by the underlying 2D PC structure. Feather colour, however, became less saturated (FWHM before: 82 ± 11 nm; after: 136 ± 49 nm) and less bright after treatment (brightness before: 66.5 ± 75.1; after: 18.5 ± 28.2). Additionally, all curves lacked the observed peak in the UV region (figure S5). These results were confirmed by simulated reflectance data, which showed little change in hue (hue before: 542 ± 95 nm; after: 539 ± 127 nm) but decreases in both saturation (FWHM before: 60 ± 19 nm; after: 80 ± 30 nm) and brightness (before: 26.30 ± 12.0; after: 17.4 ± 13.0).

3.4 Optical modelling
Based on barbule nanostructural parameters, the calculated band structure for a 2D hexagonal lattice indicated a partial PBG at $\omega \sim 0.3$ for both *s*- and *p*-polarizations in the direction normal to the barbule surface (Γ-M; blue arrow in figure 1*c*). The standardized range of frequencies reflected by the PC (gap-midgap ratio $\Delta\omega/\omega$) was $3.05 \pm 1.51\%$. There was an additional band gap in the M-X direction at $\omega \sim 0.6$; however, this would not contribute to the observed colour since the peak would occur outside of the

visible region of the spectrum for all lattice constants analysed here. The slight increases in both hue (3 nm) and reflectance for *p*-polarized light at near-normal incidence (figure S4) mirrors the subtle shift to lower frequencies (from $\omega = 0.313$ to 0.308) and subtle widening of the partial PBG (from $R_{max} = 4.69\%$ to 5.56%) taken from the calculated band structure (see figure 1*c*). Moreover, this behaviour is expectedly different from the change in reflectance observed in peacock feathers, as the gap for *p*-polarized light narrows slightly (see figure 3 in [8]).

The simulated reflectance spectra based on the full PC model (model including the cortex) closely matched the experimental curves (figure 2). Furthermore, in most cases, the heterostructure model performed better than the model excluding the effects of the keratin cortex and only considering the melanosome 2D lattice (figure 2). Indeed, while both PC models predicted the location of the primary peak, only the full PC model predicted the shallow peaks ('thin-film' peaks) occurring between 350 and 500 nm (figure 2*c,e-f*). For both PC models, predicted and measured hues were highly similar, differing only by between 7 and 36 nm (full PC model) or between 4 and 33 nm (reduced PC model).

Theoretical simulations of band gap size for various values of *r* and *a* showed a maximum at *r/a* = 0.3 (figure 5, solid line) and local minima at 0.05 and 0.5 (figure 5, dashed line). Most species were located near the close-packing limit (*r/a* = 0.5); however, hue spanned a range of wavelengths from blue (*Anas platyrhynchos*) to red (*S. specularis*), and no species had a partial PBG peak below 400 nm (figure 2).

4. DISCUSSION

Our results show that iridescent colours of duck specula are produced by 2D hexagonal photonic crystals of rod-shaped melanosomes embedded below a thin layer of keratin at the surface of feather barbules (figure 1*a*). Our empirical and theoretical results show that this system is potentially highly malleable, allowing for changes in colouration through slight changes in lattice constant, melanosome radius, and cortex thickness. However, the structural malleability of the biophotonic structure possessed by all six species examined herein may be limited within ducks to a relatively small portion of theoretically available configurations (i.e. close-packed hexagonal arrays; see also [33]).

Two-dimensional PCs have previously been described in peacocks [8] and magpies [34]. However, these differ from those found in ducks because they are either square rather than hexagonal lattices [8]; have air rather than keratin between melanosomes [8]; or have hexagonally-spaced air-spaces rather than filled melanosomes [34]. Hexagonal photonic crystals are ideal for achieving complete photonic band gaps due to their near-circular periodicity (see figure 1*a*, inset), thus these results may have implications for the design of novel photonic structures [35]. Furthermore, in the above cases, the keratin cortex apparently had little effect, possibly because it was too thick or discontinuous to cause marked interference at visible wavelengths. By contrast, in all duck species examined here, the cortex produced interference effects as indicated by secondary reflectance peaks at shorter wavelengths (figures 2, S5). Further, we show that the cortex increases brightness and saturation—possibly due to resonance occurring as a result of size matching between the thickness of the 1D film (cortex) and lattice constant (melanosome spacing) of the 2D PC [36]—and results in polarized iridescence (figures 3, 4). While the role of the keratin cortex in colour production has been studies in other iridescent bird species [10, 11], to our knowledge, this is the first study to show the optical properties arising from 1D and 2D periodicity, rather than a 1D multilayer. Thus, our results describe a novel, malleable biophotonic heterostructure, as well as an additional parameter (cortex thickness) that can potentially be independently tuned to achieve different colours.

Previous studies of speculum colour in ducks ascribed it to a multilayer (1D PC) [17-19]. Although the observed increase in s-polarized light and decrease in p-polarized light with incident angle (figures 3, 4) is characteristic of both multilayered (1D) structures [25] and 2D PCs (see description in [37]), the differences in depolarization with θ_i for different azimuthal angles (see figure 4) are not consistent with a 1D system because there is no periodicity in refractive index parallel to the surface to differentially scatter light incident from different directions. Interestingly, multilayer-like behaviour, namely the inversion in reflectance curves past θ_c, was observed in these samples (figure 3d, inset). Based on nanostructural data and known fundamentals of optics—specifically, that p-polarized light incident on a thin-film undergoes a 180° phase shift past Brewster's angle [37]—the observed behaviour (inverted reflectance curve) is thus the result of destructive interference occurring between light beams reflecting from the air-keratin interface and the photonic crystal. Thus, contrary to previous hypotheses [17-19], our modelling and polarization data are consistent with a photonic heterostructure and not a multilayer.

Trait evolvability is determined by the underlying mechanisms of control (e.g., genetic, physical) and the modularity between phenotypic components [38]. Malleable structures that can readily assume viable new forms, such as pharyngeal jaw structure in cichlids or beaks in Darwin's finches, have contributed to adaptive radiation [39]. Our simulations suggest that this colour-producing nanostructure is similarly malleable and that indeed it is capable of producing many variants of colours across the visible spectrum (figure 5). Moreover, our empirical results show that ducks have exploited this feature and, through slight variations in the size and spacing of their melanosomes, have produced diverse colours ranging from violet to red (figure 2). However, developmental or physical mechanisms can also constrain trait evolution [40]. In this case, physical constraints set an upper bound on the relationship between melanosome radius and spacing: because two melanosomes cannot occupy the same space, it is impossible for the melanosome radius to be more than half the distance between melanosomes (i.e. $r/a > 0.5$). However, by increasing the space between melanosomes (i.e. $r/a < 0.5$), ducks can increase the size of their partial PBG and hence range of frequencies reflected up to a maximum occurring at $r/a = 0.3$ (centre of polygon in figure 5). Thus, ducks could potentially maximize their feather brightness by moving towards this optimal band gap region. However, all six species examined lie in the duller but more saturated (small PBG) region of figure 5, near the close-packing limit. Because small band gaps are associated with short, narrow reflectance peaks (figure 5, inset), these results suggest that physical limits on nanostructural configuration (close-packing) may constrain ducks to less bright but highly saturated feather colours relative to theoretically-possible variations. Additionally, melanosome size in birds also appears to be constrained to diameters above ~100 nm [41, 42], further restricting the range of colours capable of being produced by ducks to hues greater than ~400 nm (figures 2, 5). However, whether ducks are able to perceive UV wavelengths is controversial [43-45], thus UV colours may not be advantageous, at least in an intraspecific context.

Recent evidence suggests that structurally coloured feathers develop through processes of self-assembly [46, 47]. Furthermore, a close-packed hexagonal configuration is highly energetically stable and is thus a likely end product of a self-assembly process [48, 49]. Indeed, self-assembly of rods into a 2D lattices has recently been observed in artificial colloid solutions of nanorods: as the solvent evaporated around them, the rods became highly aligned and hexagonally close-packed [50]. Other configurations with greater distance between melanosomes are not as stable and are thus less likely to form [49]. This limitation of development may therefore constrain duck colours to relatively close-packed, high-saturation configurations. Alternatively, this limited diversity may be caused by sexual selection of highly saturated colours (reviewed in [51]). We are currently using phylogenetic methods in a theoretical morphospace approach to test these hypotheses across a broader sampling of dabbling duck species.

Despite the aforementioned constraints on colour-production, the colours of mallard specula are diverse. In many duck species, males display their colourful wing patches during pre-copulatory interactions [52], suggesting that iridescent speculum colour may evolve through sexual selection [2]. However, the experimental removal of the iridescent speculum in mallards did not have any effect on pairing success in male mallards (*A. platyrhynchos*) [53]. More recently, a test for condition-dependent expression (a key prediction for the indicator mechanism of evolution by sexual selection) revealed positive correlations between colour and body condition in females, but not in males [54]. Thus, evidence for a signalling function is mixed. Colourful speculum feathers in ducks may also function in reproductive isolation and species recognition (e.g., through assortative mating [55]). Despite the ubiquity of viable and fertile hybrids in ducks [56], sympatric species remain distinct [57], suggesting the existence of pre-zygotic reproductive isolation mechanisms, like species-specific colour patches. If these hybrids are less fecund than non-hybrids, then speculum colours may be adaptations for reinforcement, potentially following secondary contact after allopatric speciation [58, 59]. If not, then the colours themselves may drive speciation through drift, similar to that seen in *Carduelis* finches [60], and could be a rare example of diversification through a non-adaptive key innovation.

Future studies should investigate the genetic and physical mechanisms of control that result in this complex photonic structure, as well as the level of modularity between components. The answers to such questions could provide clues to the potential ecological and evolutionary forces driving colour variation in birds.

ACKNOWLEDGEMENTS

REFERENCES

1.	Parker A.R. 2000 515 million years of structural colour. *J Opt A: Pure Appl Opt* **2**(6), R15-R28.
2.	Andersson M. 1994 *Sexual Selection*. Princeton, NJ, Princeton University Press.
3.	Cott H.B. 1940 *Adaptive coloration in animals*. London, Methuen Ltd.
4.	Burtt E.H. 1986 *The Behavioral Significant of Color*. New York, Garland Publishing, Inc.
5.	Stoddard M.C., Prum R.O. 2011 How colorful are birds? Evolution of the avian plumage color gamut. *Behav Ecol*. (doi:10.1093/beheco/arr088).
6.	McGraw K.J. 2006 Mechanics of uncommon colors: pterins, porphyrins, and psittacofulvins. In *Bird Coloration Vol I: Mechanisms and Measurements* (eds. Hill G.E., McGraw K.J.). Cambridge, MS, Harvard University Press.
7.	Andersson S. 1999 Morphology of UV reflectance in a whistling-thrush: implications for the study of structural colour signalling in birds. *J Avian Biol* **30**(2), 193-204.
8.	Zi J., Yu X.D., Li Y.Z., Hu X.H., Xu C., Wang X.J., Liu X.H., Fu R.T. 2003 Coloration strategies in peacock feathers. *Proc Natl Acad Sci U S A* **100**(22), 12576-12578.
9.	Yin H., Shi L., Sha J., Li Y., Qin Y., Dong B., Meyer S., Liu X., Zhao L., Zi J. 2006 Iridescence in the neck feathers of domestic pigeons. *Phys Rev E* **74**(5), 51916.
10.	Stavenga D.G., Leertouwer H.L., Marshall N.J., Osorio D. 2010 Dramatic colour changes in a bird of paradise caused by uniquely structured breast feather barbules. *Proc R Soc B* **278**(1715), 2098-2104.
11.	Greenewalt C.H., Brandt W., Friel D.D. 1960 The iridescent colors of hummingbird feathers. *Proc Am Philos Soc* **104**(3), 249-253.
12.	Prum R.O., Torres R., Williamson S., Dyck J. 1998 Coherent light scattering by blue feather barbs. *Nature* **396**, 28-29.
13.	Prum R.O. 2006 Anatomy, physics, and evolution of structural colors. In *Bird Coloration Volume I: Mechanisms and Measurements* (eds. Hill G.E., McGraw K.J.), pp. 295-353. Cambridge, MS, Harvard University Press.
14.	Joannopoulos J.D., Johnson S.G., Winn J.N., Meade R.D. 2008 *Photonic Crystals: Molding the Flow of Light*. Second ed. Princeton, NJ, Princeton University Press.
15.	Humphrey P.S., Clark Jr. G.A. 1961 Pterylosis of the Mallard Duck. *The Condor* **63**(5), 365-385.
16.	Madge S., Burn H. 1998 *Wildfowl: An Identification Guide to the Ducks, Geese and Swans of the World*. London, Christopher Helm.
17.	Rutschke E. 1966 Die submikroskopische struktur schillernder federn von entenvögeln. *Zeitschrift für Zellforschung* **73**, 432-443.
18.	Durrer H. 1977 Schillerfarben der vogelfeder als evolutionsproblem. *Denkschriften der Schweizerischen Naturforschenden Gesellschaft* **91**, 1-127.
19.	Dyck J. 1976 Structural Colours. In *Proc Int Ornithol Congr* (pp. 426-437. Canberra, Australia.
20.	Johnson K.P., Sorenson M.D. 1999 Phylogeny and Biogeography of Dabbling Ducks (Genus: Anas): A Comparison of Molecular and Morphological Evidence. *The Auk* **116**(3), 792-805.
21.	Shawkey M.D., Estes A.M., Siefferman L.M., Hill G.E. 2003 Nanostructure predicts intraspecific variation in ultraviolet-blue plumage colours. *Proc R Soc London, Ser B* **270**(1523), 1455-1460.
22.	Abramoff M.D., Magelhae P.J., Ram S.J. 2004 Image processing with ImageJ. *Biophotonics International* **11**(7), 36-42.
23.	Meadows M.G., Morehouse N.I., Rutowski R.L., Douglas J.M., McGraw K.J. 2011 Quantifying iridescent coloration in animals: a method for improving repeatability. *Behav Ecol Sociobiol* **65**(6), 1317-1327.

24.   Montgomerie R. 2006 Analyzing Colors. In *Bird Coloration Volume I: Mechanisms and Measurements* (eds. Hill G.E., McGraw K.J.), pp. 90-147. Cambridge, MS, Harvard University Press.
25.   Stavenga D.G., Wilts B.D., Leertouwer H.L., Hariyama T. 2011 Polarized iridescence of the multilayered elytra of the Japanese jewel beetle, Chrysochroa fulgidissima. *Philos Trans R Soc, B* **366**(1565), 709-723.
26.   Avery D.G. 1952 An improved method for measurements of optical constants by reflection. *Proc Phys Soc, London, Sect B* **65**(6), 425-428.
27.   Johnson S., Joannopoulos J. 2001 Block-iterative frequency-domain methods for Maxwell's equations in a planewave basis. *Opt Express* **8**(3), 173-190.
28.   Brink D., van der Berg N. 2004 Structural colours of the bird Bostrychia hagedash. *J Phys D: Appl Phys* **37**, 813-818.
29.   Land M.F. 1972 The Physics and biology of animal reflectors. *Progr Biophys Mol Biol* **24**, 75-106.
30.   Oskooi A.F., Roundy D., Ibanescu M., Bermel P., Joannopoulos J.D., Johnson S.G. 2010 MEEP: A flexible free-software package for electromagnetic simulations by the FDTD method. *Comput Phys Communi* **181**(3), 687-702.
31.   Yoshioka S., Kinoshita S. 2002 Effect of macroscopic structure in iridescent color of the peacock feathers. *Forma* **17**, 169-181.
32.   R Development Core Team. 2010 R: A Language and Environment for Statistical Computing. (Vienna, Austria.
33.   Kinoshita S. 2008 *Structural Colors in the Realm of Nature*. Singapore, World Scientific Publishing Co.
34.   Pol Vigneron J., Colomer J., Rassart M., Ingram A., Lousse V. 2006 Structural origin of the colored reflections from the black-billed magpie feathers. *Phys Rev E* **73**(2), 021914-021911-021914-021917. (doi:10.1103/PhysRevE.73.021914).
35.   Cassagne D., Jouanin C., Bertho D. 1996 Hexagonal photonic-band-gap structures. *Phys Rev B* **53**(11), 7134-7142.
36.   Bardosova M., Pemble M.E., Povey I.M., Tredgold R.H., Whitehead D.E. 2006 Enhanced Bragg reflections from size-matched heterostructure photonic crystal thin films prepared by the Langmuir-Blodgett method. *Appl Phys Lett* **89**(9), 093116.
37.   Bazhenova A.G., Sel'kin A.V., Men'shikova A.Y., Shevchenko N.N. 2007 Polarization-dependent suppression of Bragg reflections in light reflection from photonic crystals. *Phys Solid State* **49**(11), 2109-2120.
38.   Wagner G.P., Altenberg L. 1996 Perspective: Complex adaptations and the evolution of evolvability. *Evolution* **50**(3), 967-976.
39.   Schluter D. 2000 *The Ecology of Adaptive Radiation*. Oxford, Oxford University Press.
40.   Schwenk K. 1995 A utilitarian approach to evolutionary constraint. *Zoology* **98**, 251-262.
41.   Li Q., Gao K., Vinther J., Shawkey M.D., Clarke J., D L. 2010 Plumage color patterns of an extinct dinosaur. *Science* **327**(5971), 1369-1372.
42.   Clarke J.A., Ksepka D.T., Salas-Gismondi R., Altamirano A.J., Shawkey M.D., D'Alba L., Vinther J., DeVries T.J., Baby P. 2010 Fossil evidence for evolution of the shape and color of penguin feathers. *Science* **330**(6006), 954-957.
43.   Jane S., Bowmaker J.K. 1988 Tetrachromatic colour vision in the duck (Anas platyrhynchos L.): microspectrophotometry of visual pigments and oil droplets. *J Comp Physiol A Sens Neural Behav Physiol* **162**, 225-235.

44.   Parrish J., Smith R., Benjamin R., Ptacek J. 1981 Near ultraviolet light reception in Mallard and passeriformes. *Trans Kansas Acad Sci* **87**, 147.

45.   Parrish J., Benjamin R., Smith R. 1981 Near ultraviolet light reception in the Mallard. *Auk* **98**, 627-628.

46.   Dufresne E.R., Noh H., Saranathan V., Mochrie S.G.J., Cao H., Prum R.O. 2009 Self-assembly of amorphous biophotonic nanostructures by phase separation. *Soft Matter* **5**(9), 1792-1795.

47.   Maia R., Macedo R.H., Shawkey M.D. 2011 Nanostructural self-assembly of iridescent feather barbules through depletion attraction of melanosomes during keratinization. *J R Soc, Interface*. (doi:10.1098/rsif.2011.0456).

48.   Bezdek A., Kuperberg W. 1990 Maximum density space packing with congruent circular cylinders of infinite length. *Mathematika* **37**, 74-80.

49.   Marenduzzo D., Finan K., Cook P.R. 2006 The depletion attraction: an underappreciated force driving cellular organization. *J Cell Biol* **175**(5), 681-686.

50.   Baker J.L., Widmer-Cooper A., Toney M.F., Geissler P.L., Alivisatos A.P. 2010 Device-Scale Perpendicular Alignment of Colloidal Nanorods. *Nano Lett* **10**(1), 195-201.

51.   Hill G.E. 2006 Female mate choice for ornamental coloration. In *Bird Coloration Volume II: Function and Evolution* (eds. Hill G., McGraw K.), pp. 137-200. Cambridge, MS, Harvard University Press.

52.   Johnsgard P.A. 1965 *Handbook of Waterfowl Behavior*. Ithaca, NY, Cornell University Press.

53.   Omland K.E. 1996 Female mallard mating preferences for multiple male ornaments .2. Experimental variation. *Behav Ecol Sociobiol* **39**(6), 361-366.

54.   Legagneux P., Théry M., Guillemain M., Gomez D. 2010 Condition dependence of iridescent wing flash-marks in two species of dabbling ducks. *Behav Process* **83**(3), 324-330.

55.   Ritchie M.G. 2007 Sexual selection and speciation. *Annu Rev Ecol Evol Syst* **38**, 79-102.

56.   Grant P.R., Grant B.R. 1992 Hybridization of bird species. *Science* **256**(5054), 193-197.

57.   Coyne J.A., Orr H.A. 2004 Studying Speciation. In *Speciation* (pp. 1-29. Sunderland, MA, Sinauer Associates, Inc.

58.   Wallace A.R. 1912 *Darwinism: An exposition of the natural selection with some of its applications*. London, Macmillan & Co.

59.   Hoskin C.J., Higgie M., McDonald K.R., Moritz C. 2005 Reinforcement drives rapid allopatric speciation. *Nature* **437**, 1353-1356.

60.   Cardoso G.C., Mota P.G. 2008 Speciational evolution of coloration in the genus Carduelis. *Evolution* **62**(4), 753-762.
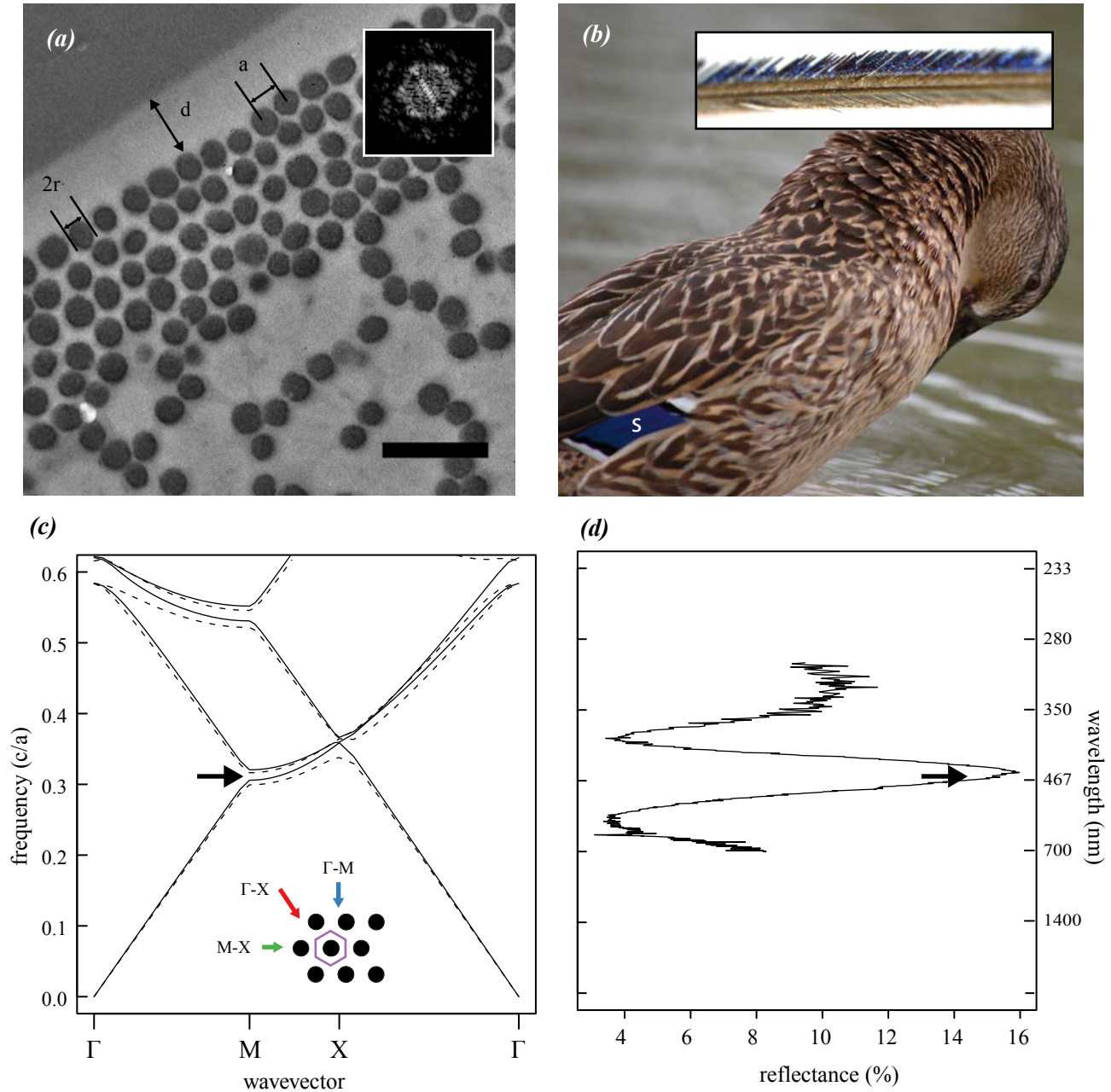
Figure 1. Feather nanostructure and colour-producing mechanism in iridescent duck feathers. (*a*) Representative cross-section of an iridescent feather barbule taken from a mallard secondary feather (*Anas platyrhynchos*) showing measured parameters *a* (lattice constant), *r* (melanosome radius) and *d* (cortex thickness); scale bar is 500 nm and inset shows Fourier transformation of region of interest, illustrating hexagonal periodicity of melanosomes. (*b*) Photograph of a female mallard showing location of speculum (s) and light microscope image of a feather barb (inset). (*c*) Band structure diagram of 2D hexagonal lattice of melanin rods (*r/a* = 0.44; RI = 2.0) embedded in keratin (RI = 1.56); lines represent modes for *s*- (E-field parallel to rods; dashed line) and *p*-polarized light (E-field perpendicular to rods; solid line), and black arrow shows location of partial photonic band gap (PBG). Inset shows schematic diagram of barbule cross-section (unit cell, purple hexagon), depicting light incident along Γ-M (blue

arrow), M-X (green arrow), and X-Γ directions (red arrow). (*d*) Plot of feather reflectance at corresponding frequencies in (*c*) with wavelength shown on secondary *y*-axis; black arrow shows location of partial PBG as in (*c*).
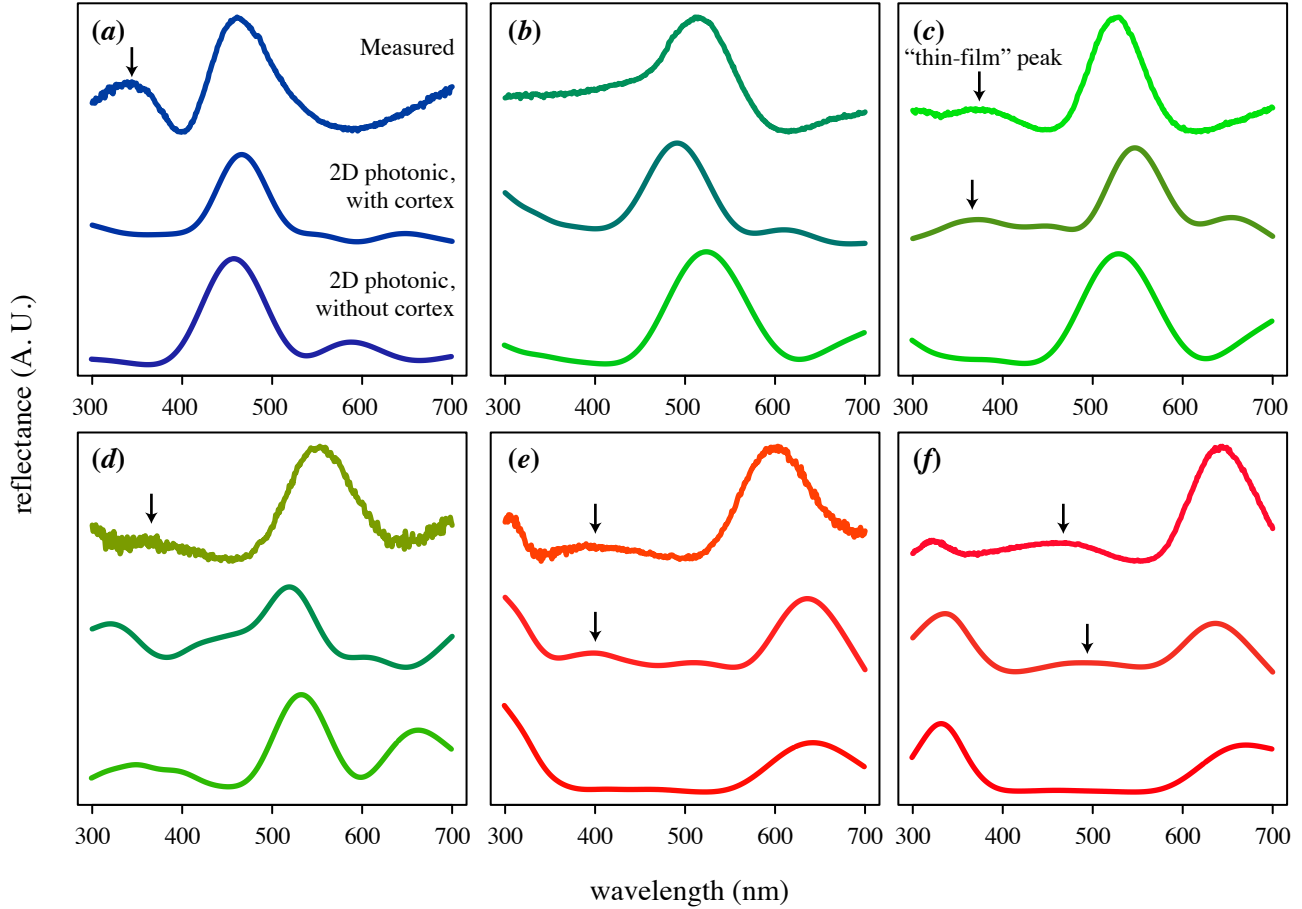

Figure 2. Agreement between measured and predicted reflectance based on 2D hexagonal photonic crystal (PC) and 2D heterostructure optical models. Panels show empirical and simulated reflectance curves (normalized to maximum of unity and based on representative nanomorphologies) for *Anas platyrhynchos* (*a*), *Amazonetta brasiliensis* (*b*), *Anas carolinensis* (*c*), *Anas clypeata* (*d*), *Anas acuta* (*e*), and *Speculanas specularis* (*f*). In each panel, top curve is empirical reflectance, the middle curve is the full PC model predictions (2D PC + cortex) and the bottom curve is the reduced PC model (excluding the cortex). To remove unwanted spectral noise, predicted spectra were smoothed using the SMOOTH.SPLINE function in R [32] (spar = 0.65). Line colours were calculated from empirical reflectance data based on human colour matching functions, thus representing the approximate colour predicted by the reflectance curves.
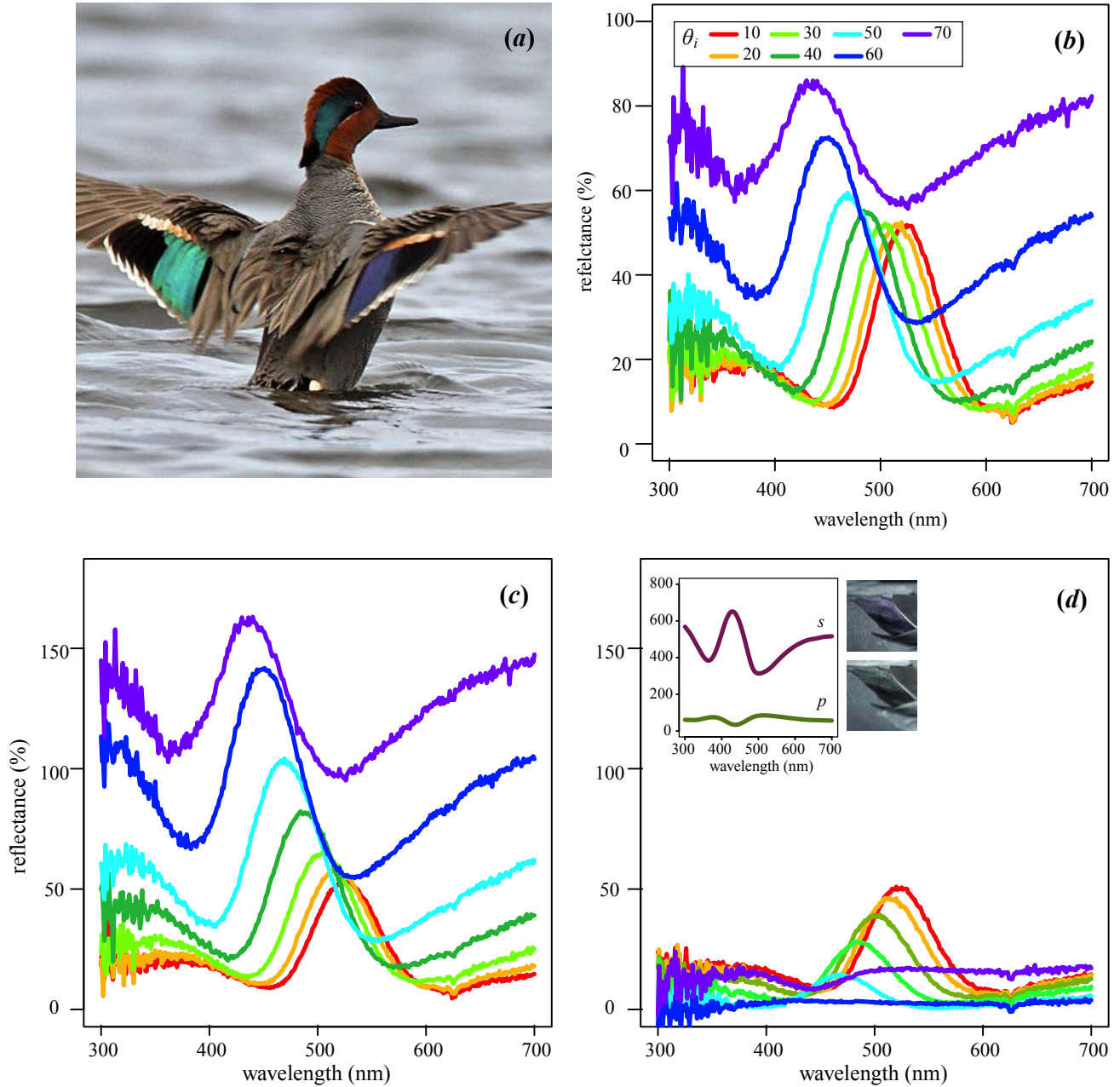
Figure 3. Effects of incident angle and light polarization on specular reflectance of green-winged teal feathers. Male green-winged teal shown to illustrate colour changes with incident angle θ_i (*a*). Reflectance spectra for unpolarized light at various incident angles (*b*). Specular reflectance of *s*- (*c*) and *p*-polarized light (*d*) at various incident angles (θ_i) with incident plane perpendicular to barbules. Inset in (*d*) shows reflectance curves at $\theta_i = 70°$ with corresponding images of same feather at each polarization (note inverted shape of curves). Image in (*a*) used with permission from M. Lamarche.
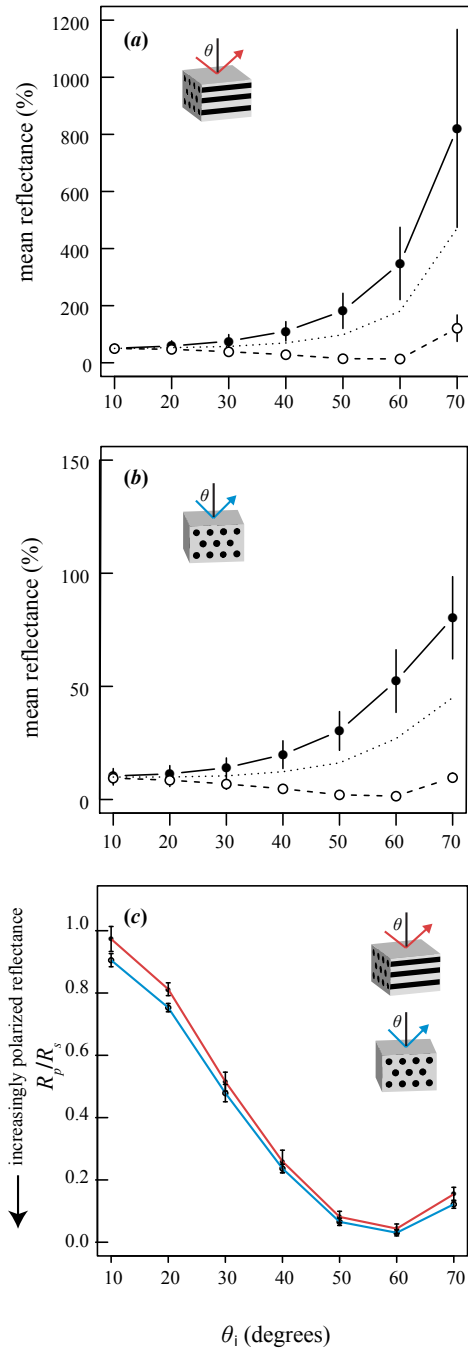
 igure 4. Effects of barbule orientation and incident angle on polarized light reflectance of iridescent duck feathers. (*a*, *b*) Mean integrated reflectance at various incident angles (θ_i) for *s*-polarized light (solid line, filled circles), *p*-polarized light (dashed line, open circles) and the average of both polarizations (dotted line) with incident plane either parallel (*a*) or perpendicular to feather barbules (*b*). Note difference in *y*-axis scale; vertical bars represent ± standard error. (*c*) Ratio of *p*- to *s*-polarized light reflectance (R_p/R_s) of iridescent feathers with incident plane parallel (red line) or perpendicular to melanosome axes (blue line).
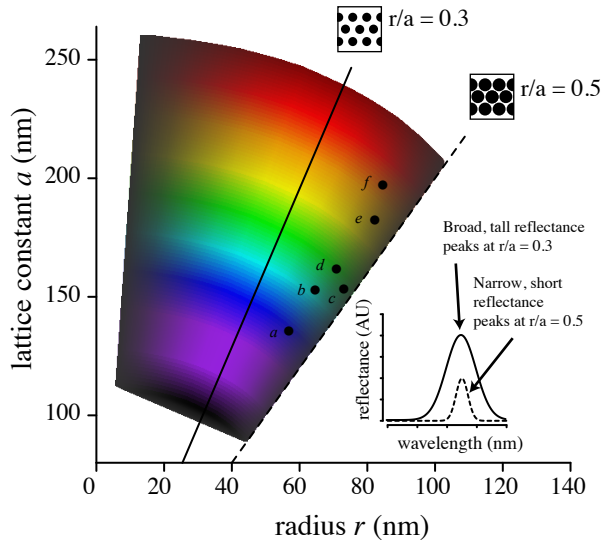
Figure 5. Theoretically possible colours of 2D photonic crystal structure in ducks compared to observed values. Coloured polygon depicts simulated band gap sizes (lightness of colour) and hues (shade of colour) for a range of possible values for melanosome radius and lattice constant, showing a maximum band gap at $r/a = 0.3$ (solid line) and a minimum at $r/a = 0.5$ (the close-packing limit; dashed line). Labelled points are observed nanostructural dimensions (same values used in figure 2) for six species of duck: *Anas platyrhynchos* (A), *Amazonetta brasiliensis* (B), *Anas carolinensis* (C), *A. clypeata* (D), *A. acuta* (E) and *Speculanas specularis* (F). Schematic drawings show melanosome configurations (black circles) at $r/a = 0.3$ and 0.5; inset shows hypothetical reflectance curves for each configuration.

Relative contributions of pigments and biophotonic nanostructures to natural color production: a case study in Budgerigar (*Melopsittacus undulatus*) feathers

Liliana D'Alba*, Leah Briggs and Matthew D. Shawkey
Department of Biology and Integrated Bioscience Program, University of Akron, Akron, OH 44325-3908, USA
*Author for corresponding (liliana@uakron.edu)

SUMMARY

Understanding the mechanistic bases of natural color diversity can provide insight into their evolution and inspiration for biomimetic optical structures. Metazoans can be colored by absorption of light from pigments or by scattering of light from biophotonic nanostructures, and these mechanisms have largely been treated as distinct. However, the interactions between them have rarely been examined. Captive breeding of budgerigars (Aves: Psittacidae, *Melopsittacus undulatus*) has produced a wide variety of color morphs spanning the majority of the spectrum visible to birds,including the ultraviolet, and thus they have been used as examples of hypothesized structure-pigment interactions. However, empirical data testing these interactions in this excellent model system are lacking. Here we used UV-vis spectrometry, light and electron microscopy, pigment extraction experiments and optical modeling to examine the physical bases of color production in seven budgerigar morphs, including grey and chromatic (purple to yellow) colors. Feathers from all morphs contained quasi-ordered air-keratin "spongy layer" matrices, but these were highly reduced and irregular in grey and yellow feathers. Similarly, all feathers but yellow and grey had a layer of melanin-containing melanosomes basal to the spongy layer. The presence of melanosomes likely increases color saturation produced by spongy layers while their absence may allow increased expression of yellow colors. Finally, extraction of yellow pigments caused some degree of color change in all feathers except purple and grey, suggesting that their presence and contribution to color production is more widespread than previously thought. These data illustrate how interactions between structures and pigments can increase the range of colors attainable in birds and potentially in synthetic systems.
Key words: structural color, psittacofulvin,

INTRODUCTION

Over evolutionary time, metazoans, and birds in particular, have occupied large portions of available color gamut, in part because of the diversity of color production mechanisms available to them (Stoddard and Prum, 2011). Coloration can result from selective light absorption by pigments deposited in feathers. Although more than 5 classes of pigments have been found in bird feathers, those most commonly present are melanins and carotenoids (McGraw 2006). Melanins, found within membrane-bound organelles (melanosomes), can produce colors ranging from black to reddish browns and pale oranges (McGraw, 2006). Carotenoid pigments are acquired by birds through their diet (Goodwin, 1984) and are responsible for most of the bright red, orange and yellow colors (Brush, 1978). A second mechanism of color production is caused by interaction between incident light and nano-scale reflective tissues (structural coloration) of feather barbs and barbules. Colors produced in this manner include the blue, violet, ultraviolet and iridescent parts of plumage (Auber, 1957; Dyck, 1976).

It has long been recognized that structural and pigment-based colors are not mutually exclusive and can interact with one another to attain colors not possible by either mechanism alone (Dyck, 1971a; Prum et al., 1999a). For example, the combination of structural blue colors with yellow colors caused by pigments is thought to give rise to most green plumage colors (Auber, 1957; Fox, 1976), but see Prum et

al., (1998). Surprisingly, however, with the exception of a few studies (Dyck, 1971a; Shawkey and Hill, 2005, 2006) the interaction between pigment and structure has not been examined in detail. Understanding these interactions is critical because different mechanisms of plumage coloration vary in, for example, their developmental cost and thus may convey different information to conspecifics. Furthermore, they may provide inspiration for new materials with novel optical properties.

As a result of over 150 years of captive-breeding, color diversity of budgerigars (Aves, Psittacidae: *Melopsittacus undulatus*) now far exceeds that of their green wild ancestors (Taylor and Warner, 1986). Color morphs include achromatic whites and greys as well as chromatic colors ranging from purple to yellow (World Budgerigar Organisation, 2004). These latter colors are thought to be produced through various combinations of both nanostructures and pigment (Simon, 1971; Parker, 2002), but as far as we are aware no data exist to support this hypothesis. Because of their diversity in color and (potentially) mechanisms, as well as rich genetic data from breeders, budgerigars may serve as a model system for understanding both physical and genetic bases of color evolution. Here, we use multiple techniques to identify the physical bases of color production in seven morphs of the Budgerigar to determine the relative contribution of pigments and structure to plumage color.

METHODS

Feather samples and microscopy

We examined contour feathers of seven different budgerigar color morphs, using samples obtained from local pet stores. We washed feathers in distilled water, dried them overnight at 60°C and prepared them for spectroscopy and microscopy.

Spectroscopy

We measured feather reflectance using UV-vis spectrometry. For all measurements, we taped overlaid stacks of three feathers of each color to black velvet. Reflectance was measured from these stacks using an Avantes AvaSpec-2048 spectrometer and AvaLight-XE pulsed xenon light source, relative to a WS-2 white reflectance standard (Avantes Inc., Boulder, CO). Spectral data was collected at coincident normal (0° incident light/0° measurement) incidence using a bifurcated micron fiber optic probe held by a probe holder (RPH-1, Avantes) with matte black interior that excluded ambient light. We took three measurements from each sample using AvaSoft software v.7.2, with the probe holder completely removed and placed at a different point on the feather surface before each measurement.

Microscopy

To characterize the micro- and nanostructures responsible for the different colors in these feathers, we used light and electron (scanning and transmission; SEM and TEM, respectively) microscopy. We prepared samples following (Shawkey et al., 2003). Briefly, we cut feather barbs, washed them in a solution of 0.1% Tween and 0.25 M NaOH, and fixed them in a 2:3 (v/v) solution of formic acid and ethanol. We then dehydrated the samples in 100% ethanol (twice for 20 minutes each time) and infiltrated them in 15, 50, 70, and 100% Epon (24 h each time). After curing the blocks at 60°C for 16 h in an oven, we trimmed them with a Leica S6 EM-Trim 2 (Leica Microsystems GmbH, Wetzlar, Germany) and cut 100-nm thin sections using a Leica UC-6 ultramicrotome (Leica Microsystems GmbH, Wetzlar, Germany). We stained these sections with uranyl acetate and lead citrate and viewed them on a Tecnai TEM (FEI, Hillsboro, OR, USA) at an operating voltage of 120 kV. For light microscopy, we cut 1 μm thick sections, transferred them with a loop to glass slides and viewed them on a Leica optical microscope.

Pigment extraction

We extracted the lipid-soluble (likely psittacofulvin; Völker, 1936) non-melanin pigments from feathers using thermochemical extraction with organic solvent transfer following (McGraw et al., 2004) Briefly,

we placed feathers in 1 mL acidified pyridine (3 drops HCl in 50 mL pyridine) and kept them at 95°C for 4 hr. The samples were then cooled to room temperature and rinsed with 1mL distilled water and 5 mL hexane:tert-butymlethylether (1:1,v/v). We included blue feathers of eastern bluebird (*Sialia sialis*) as a control for the effects of the treatment on color because a) they do not contain pigments and b) their spectral characteristics and its anatomical bases are well known (Shawkey et al., 2003; Shawkey et al., 2005; Shawkey et al., 2009). To quantify spectral changes with treatment, we measured feather reflectance again after the pigment extraction following the same spectral procedure and subtracted post- from pre-treatment reflectance values at each wavelength, creating a "treatment effect" spectral curve. We determined the absorbance spectrum (from 300 to 700 nm) of the extracted yellow pigment using an absorbance microplate spectrophotometer (Spectramax Plus 384, Molecular Devices Corp, Sunnyvale, CA). We predicted that, if pigment removal caused observed changes in feather color in an additive manner (i.e. without changing the refractive index of the substrate material), then this absorbance curve should closely match the treatment effect curve.

Quantitative analysis of barb nanostructure
Both the size and regularity of the keratin and air spaces affect aspects of reflected color (hue and saturation, respectively, (Shawkey et al., 2003; Shawkey et al., 2005). Therefore, we used ImageJ 1.36b (available for download at http://rsb.info.nih.gov/nih- image/index.html) to measure the diameter of keratin rods and air vacuoles present in barbs and to produce profile plots of barb TEM images. The profile plot shows a two-dimensional waveform representing the spatial density fluctuation in the intensity of pixels (i.e. refractive index of keratin and air) within a standardized selected area of 3.5 by 3.5 μm of the TEM image. We calculated the coefficient of variation (CV) of distance between the peaks in the waveform as a measure of nanostructural regularity.

Fourier analysis
We performed Fourier analysis on TEM images obtained for feather barbs using the Fourier tool for biological nano-optics (Prum and Torres, 2003). For all images, the largest available square portion of keratin and air (>500 pixels) uninterrupted by melanin granules, cell boundaries or keratin cortex was selected. This analysis allows the user to determine whether nanostructures are sufficiently organized at an appropriate scale to produce color by coherent light scattering alone and if variation in the organization of this tissue explained variation in hue (Prum et al., 1999a; Shawkey et al., 2003).

RESULTS
Spectroscopy
The spectral curves of yellow, green, turquoise, light blue and dark blue feathers showed two reflectance peaks, one between 330-398 nm and a larger one between 526-588 nm (Table 1, Fig. 4). Spectra of these colors fall to a minimum at ~ 440 nm. Purple feathers had a single peak at 421 nm and grey feathers had a typical achromatic spectral curve with no discrete peaks and rapid increase in reflectance at short wavelengths (~300-400 nm) (Fig. 4 A).
Microscopy
All seven colored feather barbs had some amount of spongy medullary keratin in their feather barbs (Fig. 1). The size and structure of the spongy layer varied extensively among the colored barbs examined. The diameters of keratin channels and air vacuoles were smallest in purple feathers and largest in white and grey feathers (Table 2). Moreover, the variation in spatial fluctuation was almost twice as high in grey and yellow feathers than in other colors, indicating decreased organization of the spongy layer (Table 2).

All barbs apart from yellow and grey contained a layer of melanosomes basal to the spongy layer and surrounding large central vacuoles (Fig. 1). Melanosomes were only present in barbules of grey feathers, and were absent in yellow feathers.

Pigment extraction

Yellow pigment was visible in the barbules and cortex of barbs in yellow, green and turquoise feathers (Fig. 1). After pigment removal, yellow feathers appeared white; in light and dark blue, turquoise and green feathers reflectance from 390-480 nm increased, eliminating the characteristic double peak of the spectral curves observed before the extraction (Fig. 3). The extracted pigment showed maximum absorbance between these wavelengths, and mirrored the treatment effect curve from yellow, green and turquoise feathers, indicating its central role in production of the double peaks in these colors. Weaker similarities were also seen in light and dark blue morphs, perhaps due to lower pigment concentrations (Fig. 4 a,b). By contrast, purple and grey bugderigar feathers and the control bluebird feathers showed a small change in reflectance due to the extraction and it was dissimilar to the pigment absorbance profile, (Fig. 4a,b,c), indicating a lack of pigment.

Fourier analysis

All feather barbs excluding grey and yellow showed discrete rings in the Fourier power spectra (Fig. 2), indicating high levels of nanostructural organization (Prum et al., 1998; Prum et al., 1999b; Prum et al., 1999a). The profile plots of TEM micrographs showed that in yellow and grey morphs, the spatial fluctuations in refractive index (of keratin and air) were the least regular while the plot of purple barbs showed the most regular fluctuations (Fig. 2, Table 2).

The peaks of the predicted reflectance spectra calculated from the 2D Fourier power spectra were generally congruent with the measured reflectance spectra both before and after pigment extraction (Fig. 3). The predicted and observed values deviated from one another by values ranging from 0 to 52 nm (mean = 20 nm; Tables 1, 2).

DISCUSSION

We have demonstrated that structures and pigments play more widespread roles in color production in budgerigars than previously thought. Psittacofulvin pigments, thought to be present only in yellow and green feathers (Simon, 1971; Taylor and Warner, 1986; Nemésio, 2001), affect color of blue feathers. Similarly, melanosomes are present in even light blue feathers and spongy layer is present in grey feathers barbs. Below we discuss how these components interact to produce colors.

It was proposed nearly 40 years ago that a lack of melanin in structurally colored blue barbs leads to production of light blue color (Simon, 1971) because the melanin layer served as a black background that darkens the color of the spongy layer. However, (Shawkey and Hill, 2006) showed that removal of melanin leads to almost complete loss of chromatic color. This is because the melanin serves to absorb incoherently scattered white light that would otherwise wash out the coherently scattered blue color. Our data show that all feather barbs except for yellow and grey had a basal melanin layer underlying the spongy layer, illustrating that it is critical for proper non-iridescent structural color production (although in some cases melanin may be replaced by carotenoids (Dyck, 1971b). Furthermore, our results suggest that differing shades of blue are the result of slight variations in regularity of spongy medullary nanostructures. The nanostructural regularity of light blue feathers was lower than that of dark blue barbs (Table 1), likely leading to increased incoherent scattering and thus brighter but less saturated color (Table 2).

While pigments were present in both blue feather types, their effect was more pronounced in green and turquoise feathers. Green feathers after pigment extraction appear blue to the naked eye, as would be

expected from the traditional view that blue structural color plus yellow pigment leads to a green feather (Parker, 2002). However, spectrometry revealed that the hue of the depigmented feathers remained within the green wavelengths. Moreover, the nanostructural length scale and disorder of green barbs was larger than that of dark blue barbs, and their Fourier-predicted hues were at longer wavelengths (540 nm) than those for dark blue (500 nm) feathers. The removal of pigments did not change this hue but caused enhanced reflection of blue wavelengths and hence loss of green color. Together, these results indicate that the nanostructure of green barbs is "tuned" to green color (Prum et al., 1999a), but that selective absorption of blue wavelengths by pigments is necessary to be perceived as green.

Similarly, the difference between turquoise and light blue colors appears to be attributable at least in part to pigment content. These two color morphs had similar nanostructural length scale and regularity, but hue of turquoise barbs hypsochromically shifted twice as much after pigment extraction (24 nm vs.12 nm), giving both feathers nearly identical hues. This result and the greater increase in reflectance of blue wavelengths following extraction in turquoise feathers indicate that difference in pigment concentration largely explain difference in color between these two morphs.

These results suggest that lineages utilizing both nanostructures and pigments to produce colors are uniquely capable of color diversification. Non-iridescent green color may not be possible without the use of pigments, either by themselves (e.g. turacoverdin, Dyck, 1992) or in conjunction with green-tuned spongy layers. While more extensive sampling is needed, as far as we are aware no spongy layer has been shown to produce a color outside of the ultraviolet to blue range without the use of pigments (Prum, 2006). Thus, pigments expand the capabilities of spongy layers, but, potentially, only to a certain extent. The lack of organization and thus coherent light scattering in the yellow morph suggests that the long length scales required for production of longer wavelength colors may be developmentally or physically out of reach for spongy layers. Spongy layers are thought to form through self-assembly processes (Dufresne et al., 2009; Prum et al., 2009) similar to those observed in synthetic polymers that reach stable length scales of up to several microns. However, whether spongy layers formed from beta keratin would be similarly stable is unknown. Interestingly, the disorganized layers of both the grey and yellow feathers also lack melanosomes, suggesting that their presence could potentially help stabilize spongy layers during development. These hypotheses should be tested in future work. This investigation of the anatomical and physical basis of pigmentary and structural interactions thus adds considerably to our understanding of the mechanisms of color production in birds, and sets the stage for future studies of the genetic basis of color variation and evolution.

REFERENCES

Auber, L. (1957). The structures producing "non-iridescent" blue color in bird-feathers. *Proc. Zool. Soc. London* **129**, 455-486.
Brush, A. H. (1978). Avian pigmentation. In *Chemical Zoology*, vol. 10 (ed. A. H. Brush), pp. 141-161. New York: Academic Press.

Dufresne, E. R., Noh, H., Saranathan, V., Mochrie, S. G. J., Cao, H. and Prum, R. O. (2009). Self-assembly of amorphous biophotonic nanostructures by phase separation. *Soft Matter* **5**, 1792-1795.

Dyck, J. (1971a). Structure and spectral refectance of green and blue feathers of the lovebird (Agapornis roseicollis). *Biol. Skr.* **18**, 1-67.

Dyck, J. (1971b). Structure and colour-production of the blue barbs of Agapornis roseicollis and Cotinga maynana. *Z. Zellforsch.* **115**, 17-29.

Dyck, J. (1976). Structural colors. *Proc. Internat. Ornithol. Congr.* **16**, 426-437.

Dyck, J. (1992). Reflectance Spectra of Plumage Areas Colored by Green Feather Pigments. *Auk* **109**, 293-301.

Fox, D. L. (1976). Animal Biochromes and Structural Colours. Berkeley: University of California Press.

Goodwin, T. W. (1984). The Biochemistry of the Carotenoids. New York: Chapman and Hall.

McGraw, K. J. (2006). Mechanics of melanin-based coloration. In *Bird Coloration*, vol. 1 eds. G. E. Hill and K. J. McGraw), pp. 243-294. Cambridge: Harvard University Press.

McGraw, K. J., Wakamatsu, K., Ito, S., Nolan, P. M., Jouventin, P., Dobson, F. S., Austic, R. E., Safran, R. J., Siefferman, L. M., Hill, G. E. et al. (2004). You can't judge a pigment by its color: Carotenoid and melanin content of yellow and brown feathers in swallows, bluebirds, penguins, and domestic chickens. *Condor* **106**, 390-395.

Nemésio, A. (2001). Colour production and evolution in parrots. *Int. J. Ornithol.* **4**, 75-102.

Parker, A. R. (2002). Fluorescence of yellow budgerigars. *Science* **296**, 655-655.

Prum, R. O. (2006). Anatomy, physics, and evolution of avian structural colors. In *Bird coloration*, vol. 1 eds. G. E. Hill and K. J. McGraw), pp. 295-353. Cambridge: Harvard University Press.

Prum, R. O., Torres, R. H., Williamson, S. and Dyck, J. (1998). Coherent light scattering by blue feather barbs. *Nature* **396**, 28-29.

Prum, R. O., Torres, R., Williamson, S. and Dyck, J. (1999a). Two-dimensional Fourier analysis of the spongy medullary keratin of structurally coloured feather barbs. *Proc. R. Soc. Lond. B* **266**, 13-22.

Prum, R. O., Dufresne, E. R., Quinn, T. and Waters, K. (2009). Development of colour-producing beta-keratin nanostructures in avian feather barbs. *J. R. Soc. Interface* **6**, S253-S265.

Prum, R. O., Torres, R., Kovach, C., Williamson, S. and Goodman, S. M. (1999b). Coherent light scattering by nanostructured collagen arrays in the caruncles of the Malagasy asities (Eurylaimidae : Aves). *J. Exp. Biol.* **202**, 3507-3522.

Shawkey, M. D. and Hill, G. E. (2005). Carotenoids need structural colours to shine. *Biol. Lett.* **1**, 121-124.

Shawkey, M. D. and Hill, G. E. (2006). Significance of a basal melanin layer to production of non-iridescent structural plumage color: evidence from an amelanotic Steller's jay (Cyanocitta stelleri). *J. Exp. Biol.* **209**, 1245-1250.

Shawkey, M. D., Estes, A. M., Siefferman, L. M. and Hill, G. E. (2003). Nanostructure predicts intraspecific variation in ultraviolet-blue plumage colour. *Proc. Biol. Sci.* **270**, 1455-1460.

Shawkey, M. D., Estes, A. M., Siefferman, L. and Hill, G. E. (2005). The anatomical basis of sexual dichromatism in non-iridescent ultraviolet-blue structural coloration of feathers. *Biol. J. Linn. Soc.* **84**, 259-271.

Shawkey, M. D., Saranathan, V., Palsdottir, H., Crum, J., Ellisman, M. H., Auer, M. and Prum, R. O. (2009). Electron tomography, three-dimensional Fourier analysis and colour prediction of a three-dimensional amorphous biophotonic nanostructure. *J. R. Soc. Interface* **6**, S213-S220.

Simon, H. (1971). The splendor of iridescence: structural the animal world. New York: Dodd, Mead & Company.

Stoddard, M. C. and Prum, R. O. (2011). How colorful are birds? Evolution of the avian plumage color gamut. *Behav. Ecol.* doi: 10.1093/beheco/arr088

Taylor, M. A. and Warner, C. (1986). Genetics for Budgerigar Breeders. Northampton: The Budgerigar Society.

Völker, O. (1936). Ueber den gelben Federfarbstoff des Wellensittichs (Melanopsittacus undulatus (Shaw)). *J. Ornithol.* **84**, 618-630.

World Budgerigar Organisation. (2004). Budgerigar Colour Guide, Retrieved August 9, 2011, from http://www.world-budgerigar.org/

Table 1

Color	Brightness before (%)	Brightness after (%)	Hue before (nm)	Hue after (nm)	Spectral saturation before (%)	Spectral saturation after (%)	UV chroma before (%)	UV chroma after (%)
Grey	29	31	--	--	--	--	22	16
Yellow	22	52	588	--	16	--	24	15
Turquoise	28	38	554	530	19	20	26	18
Light blue	44	31	543	531	17	15	22	21
Green	27	28	558	560	23	18	25	21
Blue	31	29	486	485	19	15	24	26
Purple	29	24	421	418	23	23	31	35

Table 2

Color	Air vacuole diameter (nm)	Keratin channel diameter (nm)	Spongy layer width (nm)	Predicted Hue (nm)	Mean Inter peak distance (nm)	CV Inter peak distance (%)
Grey	247± 11	150 ± 4	3088 ± 428	--	290	42
Yellow	218 ± 11	137 ± 5	4401 ± 448	--	332	40
Turquoise	117 ± 2	109 ± 3	5995 ± 599	540	201	23
Light blue	115 ± 3	104 ± 3	5641 ± 708	531	229	27
Green	126 ± 3	117± 4	6346 ± 386	540	222	25
Dark Blue	121 ± 3	103 ± 2	4980 ± 230	500	226	21
Purple	87 ± 3	80 ± 2	7204 ± 370	470	175	16

TABLE LEGENDS

Table 1. Means of spectral variables before and after the pigment extraction of budgerigar feathers.

Table 2. Means and s.e. of nanostructural elements of feather barbs. Predicted hue values calculated from the 2D Fourier power spectra. Means and coefficient of variation of distance between peaks obtained from profile plots of electron micrographs indicating regularity of spatial density fluctuations in refractive index of barbs spongy layer.
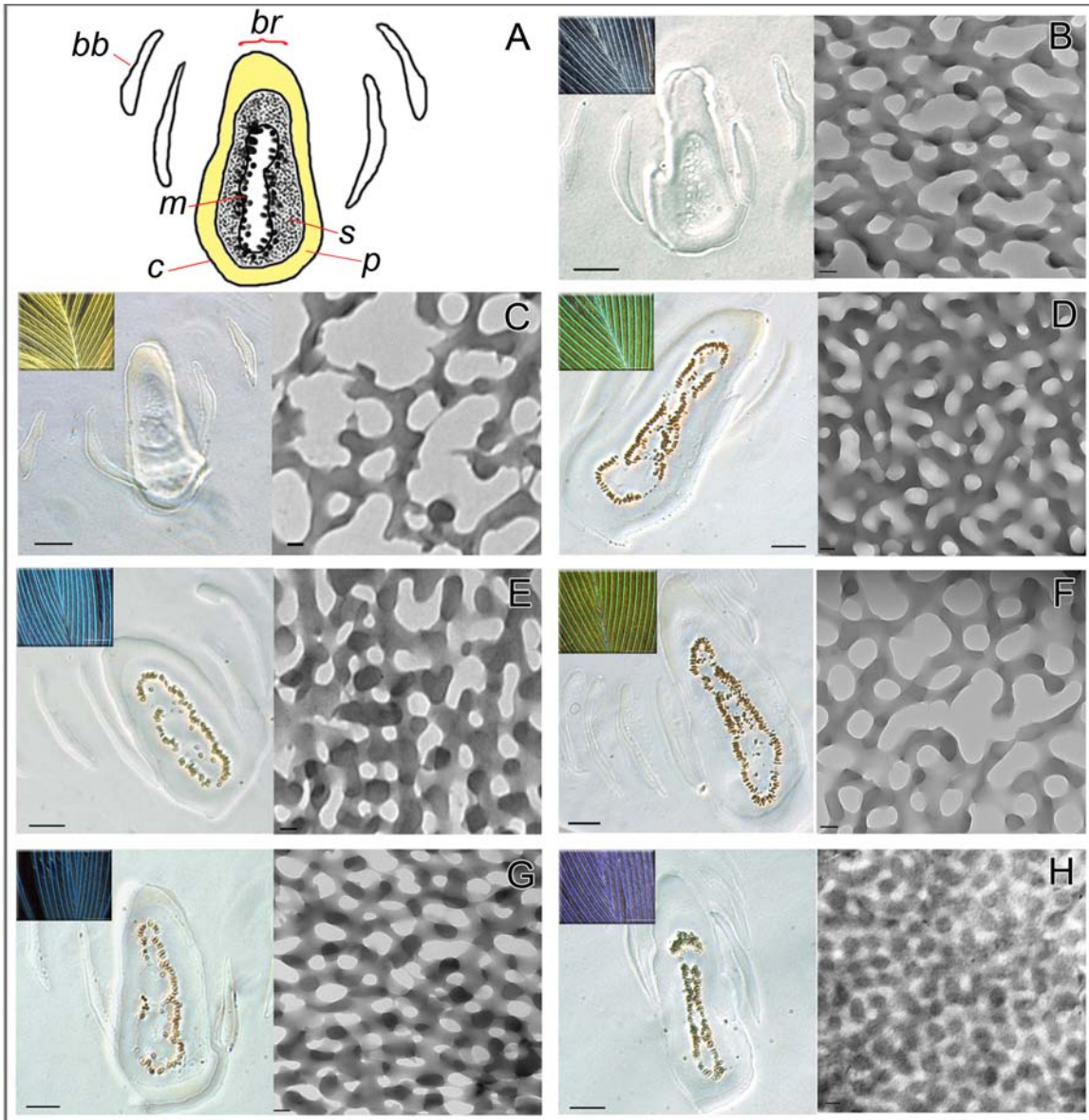
Fig. 1

Figure 1. A) Budgerigar (*Melopsittacus undulatus*), Photo credit: Corey Hochachka/Design Pics/Corbis. Panels show colored feathers of B) grey, C) yellow, D) turquoise, E) light blue, F) green, G) dark blue and H) purple morphs and their measured spectra before (solid line) and after (dashed line) pigment extraction. Line colors used correspond to perceived feather hue. Scale bars are 1 mm.

Fig. 2
Figure 2. A) Schematic drawing of a barb (br) indicating the location of barbules (bb), barb cortex (c), layer of melanosomes (m), spongy layer (s) and yellow pigment (p). Panels show light microscope and TEM images of spongy layer of B) grey, C) yellow, D) turquoise, E) light blue, F) green, G) dark blue and H) purple morphs. Scale bars for light microscope images are 10 μm, and 100 nm for TEM micrographs.
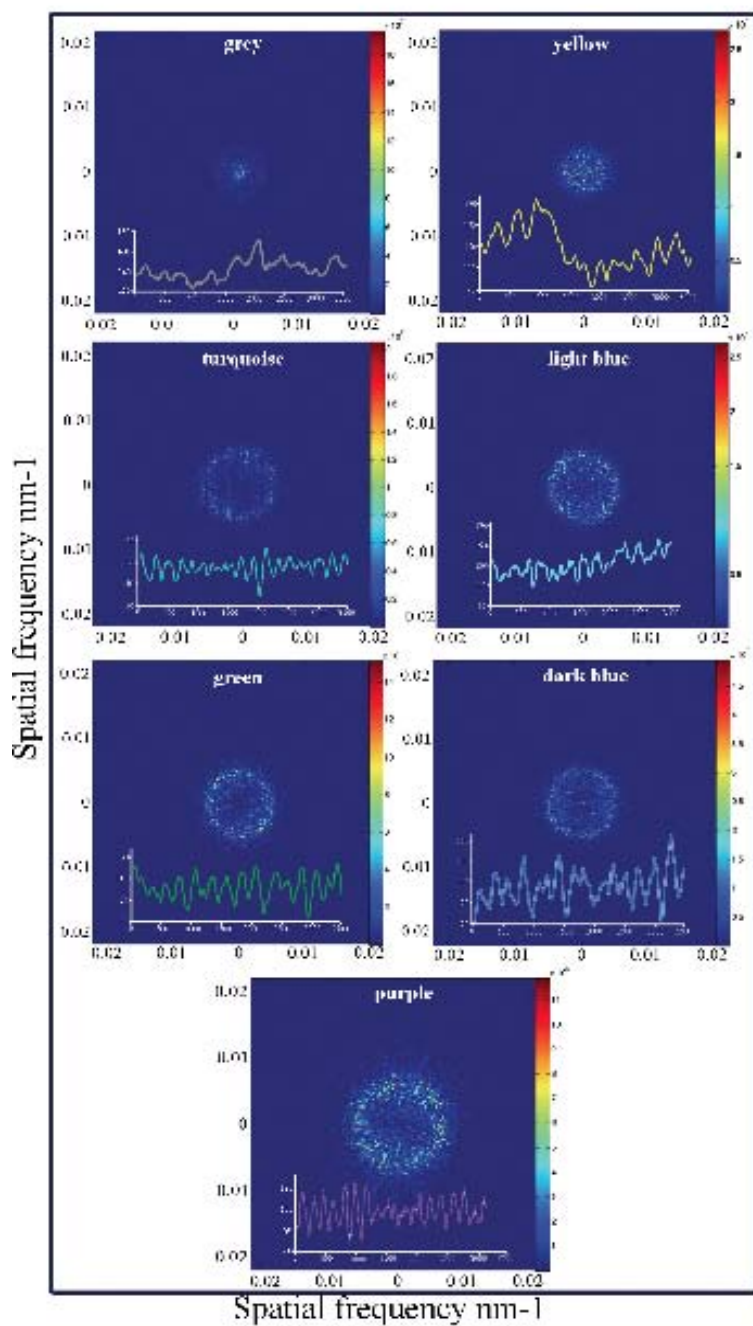
Fig. 3

Figure 3. 2D Fourier power spectra of TEM of spongy layers in Budgerigar feather barbs. The waveforms above each power spectrum obtained from TEM profile plots represent spatial fluctuations in refractive index of keratin and air (Y axis) within an area of 3500nm x 3500 nm (X axis denotes distance). Variation in spacing between wave peaks indicate irregularity of spatial fluctuations. Line colors used correspond to perceived feather hue.
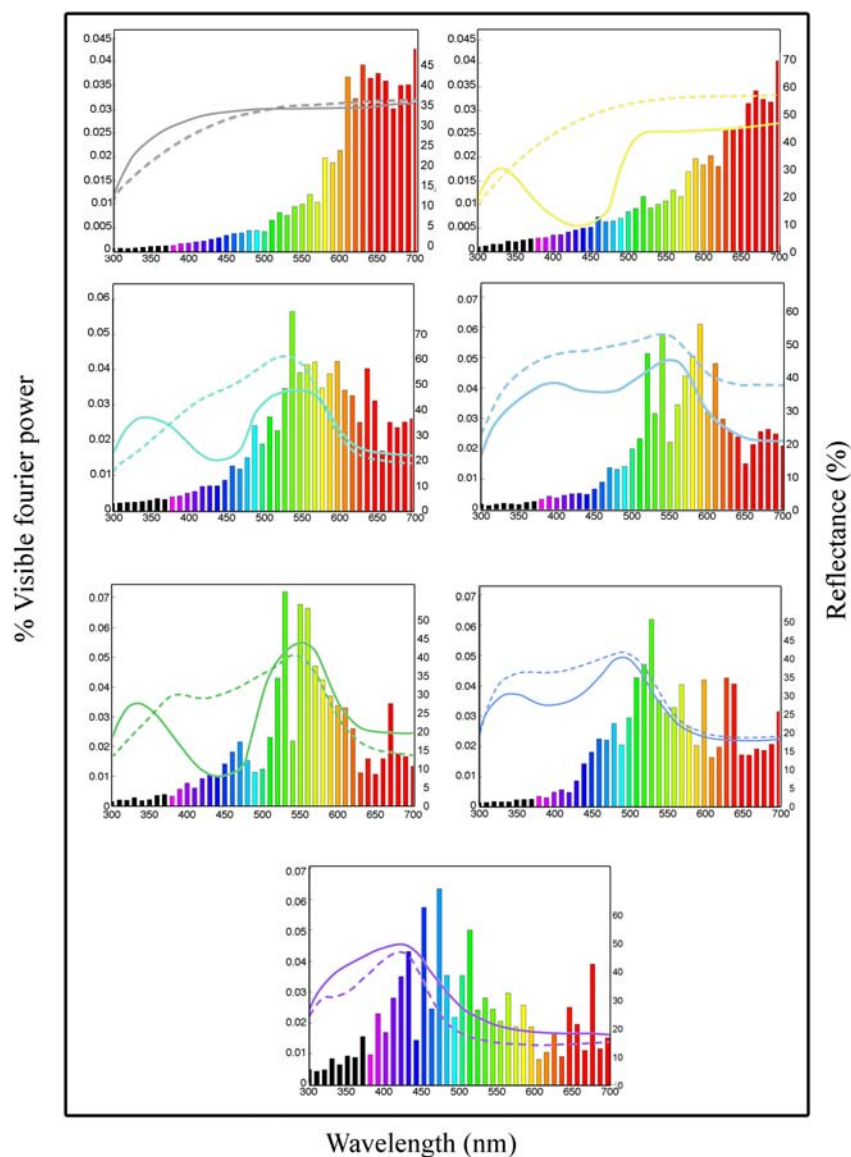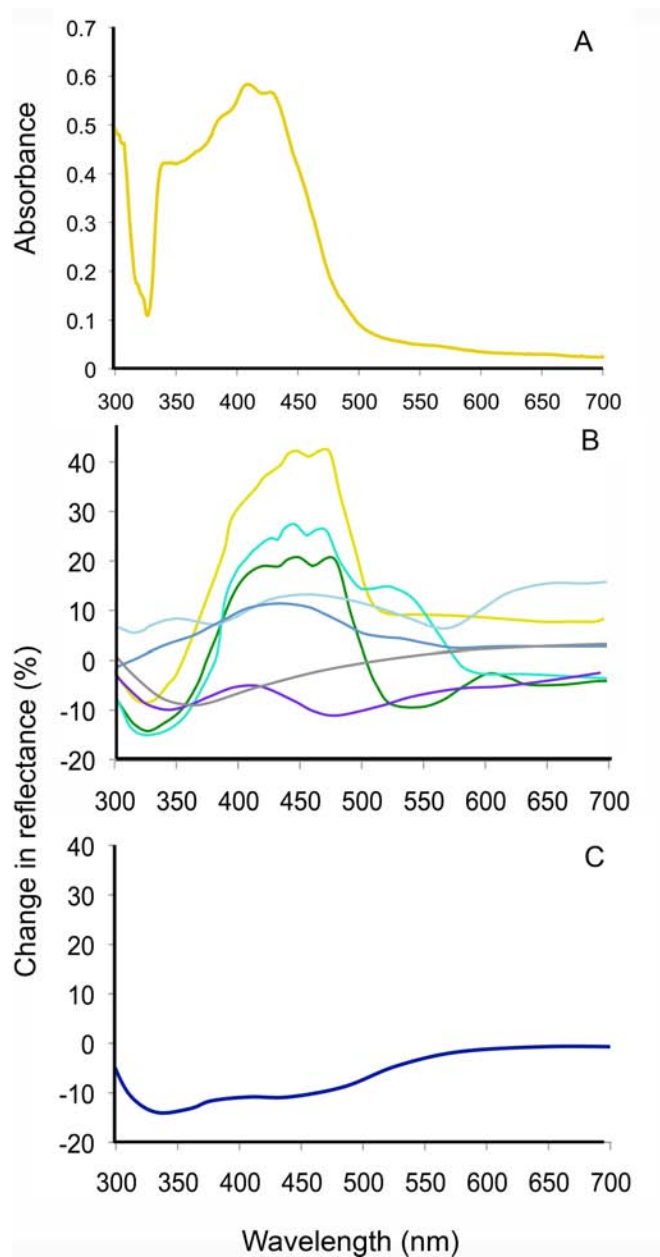
Fig. 4

Figure 4. A) Absorbance curve of extracted pigment from yellow budgerigar feathers. B) Difference in reflectance before and after the pigment extraction in all seven budgerigar color morphs and C) eastern bluebird blue feathers.

Iridescent hair color in golden moles (Mammalia:Chrysochloridea): Morphology and mechanisms

Holly K. Snyder[1], Rafael Maia[1], Liliana D'Alba[1], Allison J. Shultz[2], Karen Rowe[3], Matthew D. Shawkey[1]*

[1]Department of Biology and Integrated Bioscience Program, University of Akron, Akron OH 44325-3908
[2]
[3]

*corresponding author: shawkey@uakron.edu

ABSTRACT

Relative to other metazoans, the colors of the mammalian integument are thought to be limited in both color and mechanistic diversity. In particular, while iridescence is widespread among birds and arthropods, it has not previously been reported in mammals. Here we examine the color, morphology and optical mechanisms in hairs from four species of golden mole (Mammalia: Chrysochloridae) that are characterized by sheens ranging from purple to green. Microspectrometry revealed that this color was extremely weak (peaking at 3-5% reflectance) and variable, even within single hairs. Iridescent hairs were flattened and had highly reduced cuticular scales, providing a broad and smooth surface for light reflection. Light and electron microscopy revealed that these scales formed multiple layers of regularly sized light and dark materials, strikingly similar to that in the cuticle of iridescent beetles. Below this was a more amorphous layer surrounding small numbers of melanosomes and a hollow core. Thin-film optical modeling suggested that the multilayers produced color through thin film interference, and that the sensitivity of this mechanism to slight changes in layer thickness and number explained the variability of the color. Furthermore, the weakness of the color appears to be a result of slight differences in refractive index between the light and dark layers. While colored integumentary structures are typically thought to evolve as sexual ornaments, the blindness of moles suggests the color may be an epiphenomenon resulting from evolution via other selective factors, potentially including thermoregulation and ability to move and keep clean in dirt and sand.

INTRODUCTION

Iridescent coloration, in which color changes as a function of angle of observation or light incidence (Newton 1704), is a characteristic feature of some metazoan clades, particularly butterflies (Insecta:Lepidoptera), beetles (Insecta:Coleoptera) and birds (Aves) (Meadows et al. 2009; Shawkey et

al. 2009). While several different functions have been hypothesized for these colors, most have focused on sexual display (Doucet and Meadows 2009) and indeed some studies have shown that female birds and butterflies prefer males with brighter iridescent color (Kemp 2007, 2008, Bennett et al. 1997) or that its expression is condition-dependent (McGraw et al. 2002, Costa and Macedo 2005; Doucet 2002, Kemp et al. 2006), a key prediction of honest advertisement models of sexual selection (Andersson 1994). In contrast to pigment-based colors like carotenoids, iridescent colors are produced by coherent scattering of light (including Bragg diffraction, thin-film interference and other mechanisms) from highly ordered nanostructures (reviewed in Srinavasarao 1999, Kinoshita 2008). The simplest such nanostructures are single or multiple nanometer-scale layers of materials with different refractive indices (RI; a measurement of the change in the speed of light as it moves through a given material) that act as thin film reflectors. These have been identified in species as diverse as beetles (reviewed in Seago et al. 2009), flies (Shevtsova et al. 2011), birds (Doucet et al. 2006), ray-finned fish (Actinopterygii; Yoshioka et al 2010) and plants like spikemosses (Isoetopsida: Selaginellaceae; Glover and Whitney 2010).

By contrast, the colors of Mammalia are largely thought to be limited to relatively drab melanin-based colors (black, brown and grey), and unpigmented white (Wilson et al. 2005). Although non-iridescent blue skin colors produced by organized collagen fibers have been described (Prum and Torres 2004), as far as we are aware iridescent or other structural colors have never been examined in mammal hairs. Golden moles are small, blind insectivorous burrowing animals endemic to sub-Saharan Africa that are only distantly related to the true moles (Talpidae) (Meester 1976). Unique among mammals, their thick fur has a sheen that can feature green, blue, and violet highlights (Gorman 1990; Kuyper 1985). Their guard hairs are at least 8mm in length and like most mammal hairs contain a medulla, cortex, pigment granules, and cuticle (Williams 1938; Hausman 1920). However, the morphology and mechanism(s) producing iridescent color in these hairs has not been described. Thus, we combined microspectrometry, light microscopy, transmission and scanning electron microscopy, and thin film optical modeling to examine the color, macro- and nanostructure, and physical basis of color in four species of golden mole.

METHODS AND MATERIALS

We pulled iridescent guard hairs from the dorsum of specimens of four golden mole species (*Amblysomus hottentotus*, *Amblysomus septentrionals*, *Chrysochloris asiatica*, and *Eremitalpa granti*) in the Museum of Vertebrate Zoology at the University of California, Berkeley. We initially examined their color and overall morphology using a dissecting scope (Leica S8APO). We then quantitatively measured their reflectance using a microspectrometer (xx, range 400-700 nm) at normal incidence. All measurements were taken relative to a diffuse white standard (WS-2, Avantes Inc., Boulder, CO), and at least five measurements, each from a different one micron-sized point, were collected from each hair.

To more closely examine the external morphology of the hairs, we used scanning electron microscopy (SEM). We mounted whole hairs with the dorsal side up on stubs with carbon tape, sputter-coated them with silver, and viewed them on a JEOL JSM7401F scanning electron microscope.

To examine the ultrastructure of hairs, we used transmission electron microscopy (TEM). We prepared hairs for microscopy following the methods of Shawkey et al. (2003). Briefly, we dehydrated the samples in 100% ethanol (twice for 20 minutes each time) and infiltrated them in 15, 50, 70, and 100% Epon (24 h each time). After curing the blocks at 60°C for 16 h in an oven, we trimmed them with a Leica S6 EM-Trim 2 (Leica Microsystems GmbH, Wetzlar, Germany) and cut thick (1μm) and thin (70 nm) sections using a Leica UC-6 ultramicrotome (Leica Microsystems GmbH, Wetzlar, Germany). 1μm cross sections were placed on slides and viewed on a Leica DM2500 light microscope at 100x

magnification using transmitted light. Thin sections were placed on a 200 mesh formvar copper grid and viewed on either a Tecnai 12 (Tecnai Company, OR, USA) or JEOL JEM-1230 transmission electron microscope operating at 120 kV.

Using Image J (available for download at http://rsbweb.nih.gov/ij/), we measured the thickness of light and dark layers in the outer cortex from TEM micrographs at five evenly spaced points. We also counted the number of layers per image, and calculated the mean thickness and number of the light and dark layers from each species.

To identify the optical basis of iridescent color production, we used standard thin-film optical modeling (Jellison 1993). These models predict how light changes as it moves through materials of different RI and thereby generates predictive reflectance curves based on multilayer inference. We simulated light interacting with stacks of sequential light and dark layers, with the number of layers and their thickness equal to the average values measured from electron micrographs, to predict the theoretical reflective curves produced by the structures. We modeled the interference processes using the transfer matrix method (Jellison 1993) as implemented in the *multilayer* function (Maia et al 2009, electronic supplementary material) in the statistical program R (R development core team). Hair keratin has a reported estimated refractive index of 1.55 (XXX), which was used as a first approximation in all models. However, because the material constituting the dark layers and the extinction coefficient (k; a measurement of how much light a given material absorbs) of hair keratin is unknown, several parameters of the model (the RI of the dark material and the k of both the dark material and of the light material) were allowed to vary in the models under an optimization procedure. Optimization was performed by minimizing the sum of squared variance between normalized values of measured and estimated reflectance at each wavelength (Brink et al. 2004; Stavenga et al. 2011). We compared measured and predicted reflectance curves to determine the accuracy of modeling.

RESULTS

Golden mole hairs are straight and broad at their distal end and come to a point at their distal tip (Figure 1a). At their ventral end they are considerably thinner, more tubular and curled. This general
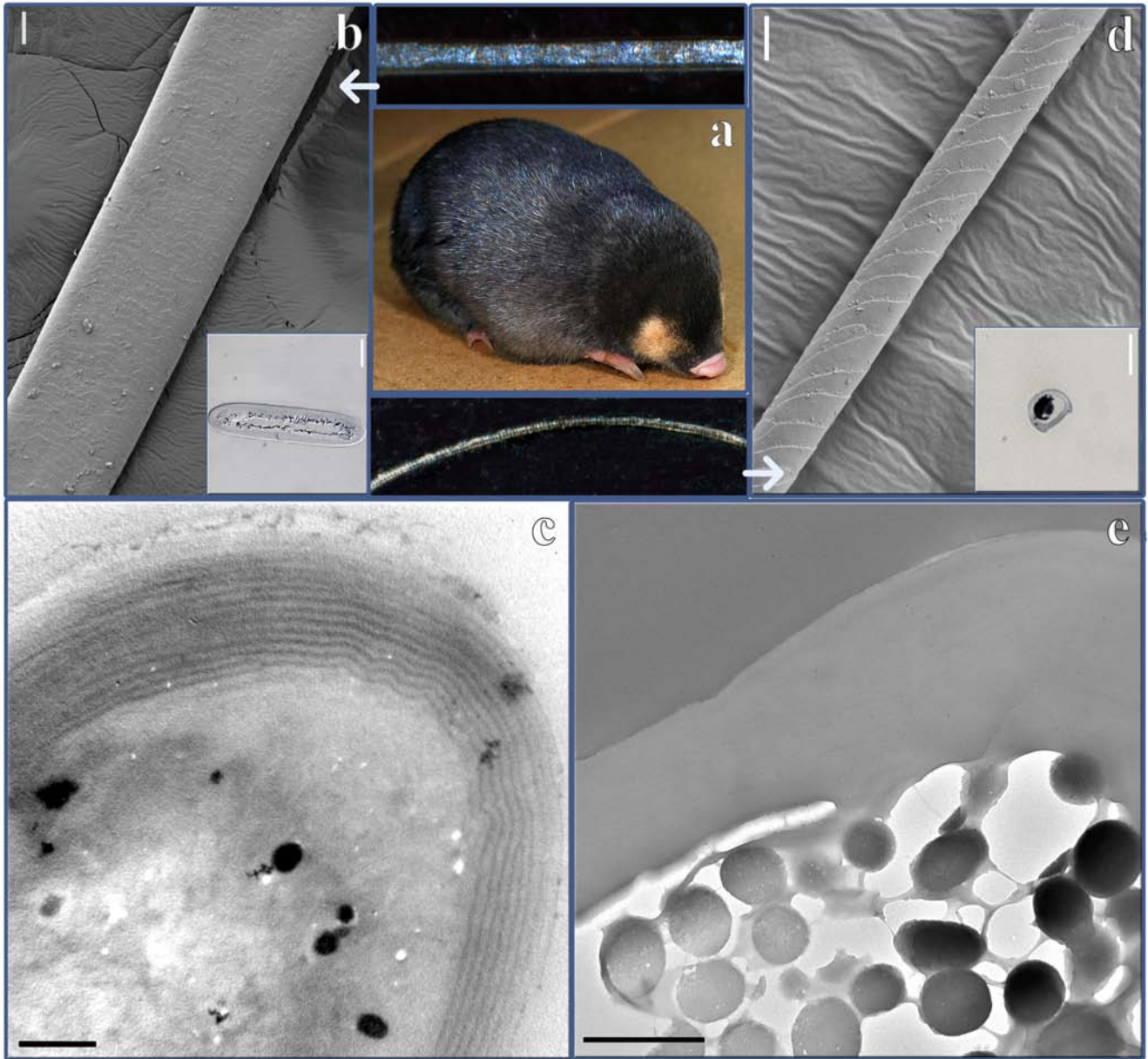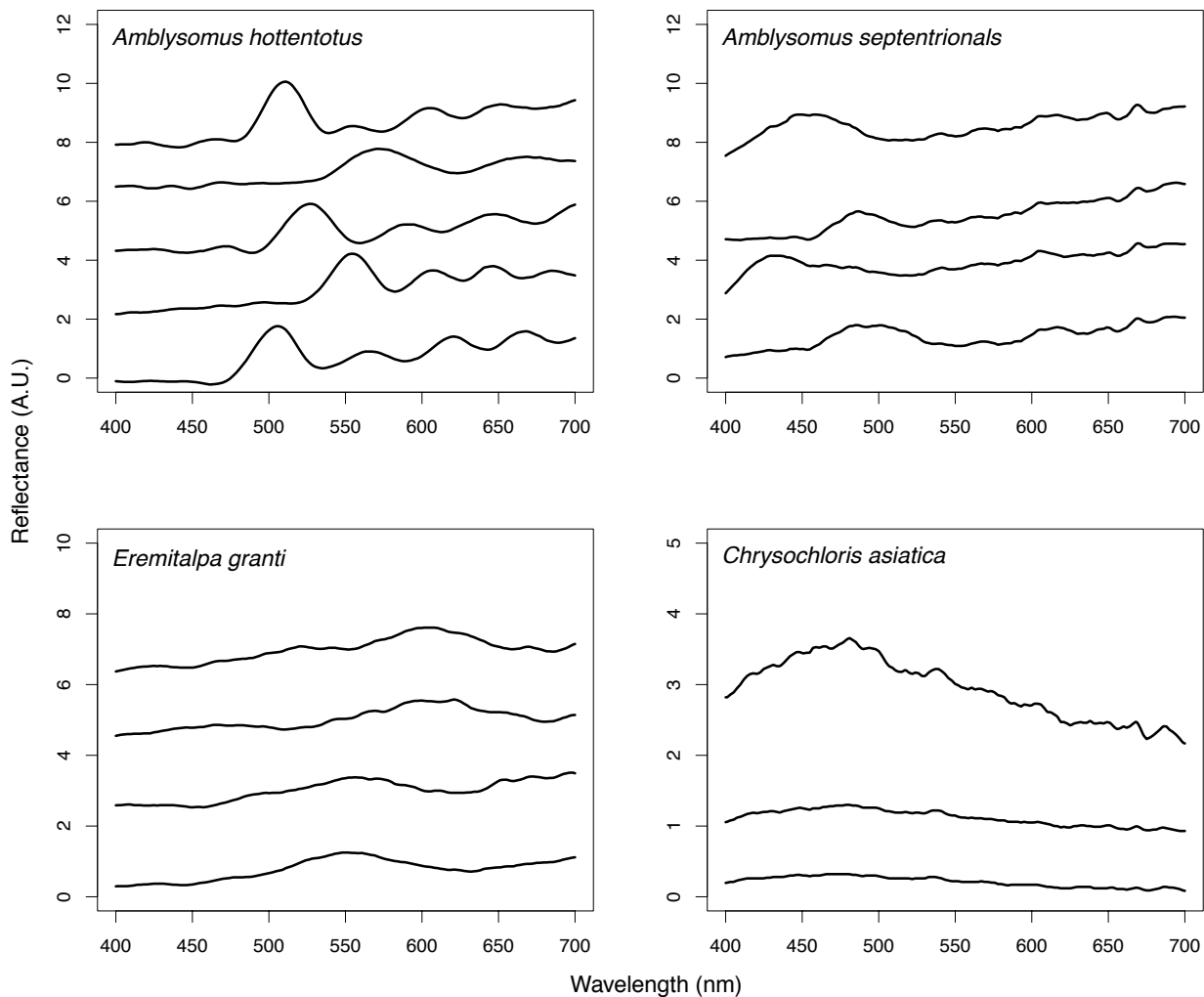
morphology is also characteristic of true moles (Williams 1938). The flattened distal ends have sheens with faintly vi sible colors (Figure 1b). These colors vary along the length of the hair (Figure 1b). SEM revealed that the surfaces of the hairs are flattened and have numerous small and flattened cuticular scales producing a relatively smooth surface (Figure 1c). Light microscopy of cross sections revealed

that the iridescent hairs   are flattened dorsoventrally and composed, as in all hairs, of three distinctive layers, moving inward from the outer surface: a darkly stained cuticle, a more lightly stained cortex containing low densities of melanosomes, and an air-filled medulla (Figure 1d).

TEM revealed the presence of discrete, alternating thin layers of dark (electron dense) and light (electron lucent) material in the outermost layer of iridescent hairs (Figure 1e). The light layers were several times thicker (ranging from means of 109-234 nm) than the dark layers (ranging from means of 21-34 nm; see Table 1). Both the sizes and numbers (from 3-19) of layers varied between species (Table 1).

Reflectance curves of hairs were uniformly low, but considerably variable between species (Figure 2). Spectral patterns from individual measurements of single hairs were relatively similar to one another, but varied in the position of those patterns on the wavelength axis. *A. hottentotus* curves had a single reflectance peak, between 500 and 550nm, and between one and four secondary oscillating peaks towards longer wavelength. *C. asiatica* had a single shallow peak typically positioned at ~550 or ~600 nm. *A. septentrionals* had a single peak positioned at either ~450 or 500 nm. Curves of all three of these species had multiple additional weak reflectance peaks. *E. granti* had the simplest and most consistent curve, with a single peak at ~450 followed by gradually decreasing reflectance.

Figure 2: Some reflectance curves for iridescent hairs from four species of golden mole, illustrating variation.

The optimization procedure estimated a value for the refractive index of this layer to be between 1.51 and 1.54, and thus a value of 1.53 was used in all models. Both materials were also estimated to have very low absorbance, with values between 0.02 and 0.05 for the light layers and 0.01 and 0.03 for the dark layer. Low extinction coefficients are also predicted because multiple oscillating secondary peaks can be observed in the measured spectra (figure 2), which commonly result from light resonating within the interfaces of the layers (Fabry-Pérot interference; Zi et al 2003, Li et al 2005). For the models, we therefore used values of 0.04 and 0.02 for the light and dark layers, respectively.

High variation in measured spectral curves (Figure 2) complicated comparison (also seen in Stavenga et al. 2011), but in all cases at least one matched reasonably well in shape and peak reflectance with the predicted curve (figure 3). Mismatches were typically between placement of patterns on the wavelength axis, and not the spectral patterns themselves. However, the predicted pattern for *C. asiatica* had a steeper reflectance slope than the measured curve.

Species	Light Layer (nm)	Dark Layer (nm)	Number of layers
Amblysomus hottentotus	121.7 (15.3)	27.8 (6.7)	8
Amblysomus septentrionals	237.4 (31.7)	34.3 (8.7)	3
Chrysochloris asiatica	108.6 (15.2)	30.7 (2.4)	19
Eremitalpa granti	145.8 (21.52)	20.9 (3.9)	6

Table 1. Mean (and standard deviation) values of layer thickness from measurements of TEM images of each species.

Figure 3: TEM images (left) and measured (dark line) and predicted (dashed line) reflectance curves for hairs of four species of golden mole. The TEM images show dark and light layers in the cuticle of each species. The predicted reflectance curves were calculated using a model of light interacting with a
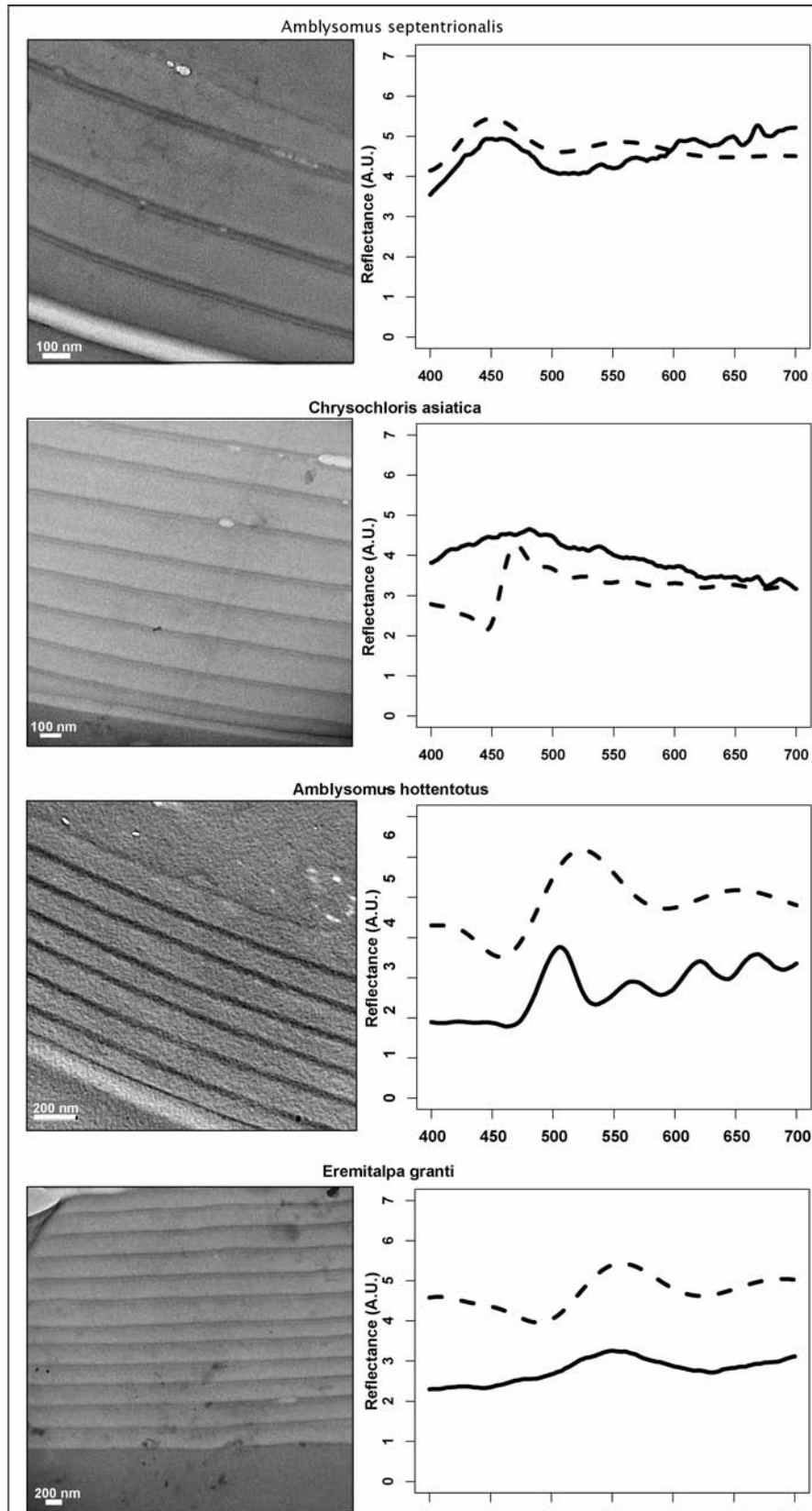
DISCUSSION

As far as we are aware, this is the first report of structural color in a mammal hair. Several key morphological features produce the iridescent coloration of golden mole hairs. First, their flattened paddle-like shape increases the surface area available for reflection. Second, the greatly reduced cuticular scales provide a smooth reflective surface that enhances specular reflectance. Third, the layers of light and dark materials in the cuticle act as multilayer reflectors that produce color through thin film interference. Typical non-iridescent hairs are circular to ovoid in cross section and have large and protruding cuticular scales, but may have multilayered cuticles of varying sizes (e.g. Hausman 1920). Those in human hairs, the most well-studied example, are in some cases of comparable size and regularity to those of golden moles (Khumalo et al. 2005; Wei et al. 2005), suggesting their presence is a necessary, but not sufficient condition for iridescent color. The additional surface area provided by flattening, and the flat surface itself that acts as a plane reflector, contribute to the enhanced reflection from iridescent hairs. Analogously, in all cases thus far studied barbules containing single or multilayer reflectors in iridescent feathers are extensively flattened relative to non-iridescent feathers (Prum 2006, Shawkey et al. 2006; Doucet et al. 2006, Eliason et al. 2011), as is the elytral surface of the Japanese jewel beetle *Chrysochroa fulgidissima* (Stavenga et al. 2011). Thus, this appears to be a common feature of natural iridescent structures.

Smooth surfaces are much more conducive to iridescent color production than rough surfaces (WIlmouth 1986). The enhancement of hair gloss through smoothing of scales is a well studied phenomenon and is in fact one of the primary mechanisms of many hair care products (Nagase et al. 2002; Stamm et al. 1977). High specular, or mirror-like, reflectance relative to diffuse reflectance, leading to high gloss, occurs when light hits a flat and smooth surface (Wilmouth 1986). When bumps larger than the wavelengths of visible light (400 nm) are present on the surface, diffuse reflectance becomes more prominent and gloss decreases. As iridescent colors are characterized by high specular reflectance it is therefore not surprising that scales of mole hairs are small and largely level with the hair surface. This arrangement enhances, while the large protruding scales on most other mammal species (Hausman 1920), decrease specular reflectance and thereby the expression of color from the multilayers.

These scales form the layers of the multilayer structure, and thus their size is critical to color production in golden moles in two ways. First, their thickness is correct to produce the observed iridescent colors through thin-film interference. Slight changes in the thickness of layers can cause noticeable shifts in reflected color (Jellison 1993; Stavenga et al. 2011). Second, their small longitudinal size likely leads to high local variability in the number of layers at any given point on the hair. The low reflectance of these colors is apparently caused by the small differences in refractive index between the light and dark layers. Strikingly convergent multilayer reflectors seen in several beetle species produce extremely bright colors through the same physical mechanisms (Seago et al. 2009), and the differences in refractive index between the layers in these reflectors has been estimated to be much higher (e.g. Parker et al. 1998; Schultz and Rankin 1985). However, the chemical composition of these layers is unknown in both moles and beetles. As in humans, the layers of mole hairs may be composed of α keratin that varies slightly in its sulfur content (Khumalo et al. 2005). By contrast, the possible chemical composition of the light and dark layers in beetles is more open-ended because of the promiscuous binding capacity of chitin, the chemical backbone of the arthropod cuticle (Kumar 2000). This polysaccharide binds many proteins and other compounds like uric acid (Caveny 1971, Neville 1977) well, allowing extensive variation in its material properties like stiffness as well as its optical properties. The greater refractive index contrast between light and dark layers afforded by chitin may allow Arthropoda to attain brighter and more

diverse colors. In feathers, layers of beta keratin are alternated with the high RI material melanin or the low RI material air to generate bright colors (Prum 2006). Why similar arrangements have apparently not evolved in mammal hairs is an interesting and multi-faceted question for future research.

While iridescent and other bright colors are typically thought to evolve through sexual selection, the lack of sight in moles makes this hypothesis unlikely here. The multilayer structures formed by scales are common in hairs of other species, but their color production may be inhibited by either a too-great thickness or protrusion of scales, or the shape of the hair itself. Flattening of scales and hairs may both streamline the profile of moles and prevent dirt from lodging in the scales. This would allow more fluid movement through dirt and sand and reduce time spent cleaning, respectively. However, although their short and dense fur is similarly thought to reduce friction in all directions, hairs of true moles vary in their cross sectional shape and only a few approach the level of flattening seen in golden moles (Williams 1938). These data also suggest that the scales of the common mole are not reduced in size, but a more thorough survey with modern microscopy techniques is needed. Interestingly, highly flattened hairs have been reported in a blue wildebeest (Moyo 2005), also noted for its bluish sheen, suggesting that this morphology is not limited to fossorial animals. Experimental approaches will help to test these functional hypotheses for hair modification. In any case, colored mole hairs demonstrate that in some cases colors produced by highly ordered structures may evolve simply as a byproduct of selection, or perhaps even drift, and thus sexual selection need not be the default explanation. These results illustrate the ubiquity of iridescent coloration in nature, provide testable hypotheses on its evolution and may find applications in new coatings and hair-care products or procedures.

REFERENCES

Andersson, M. 1994. Sexual Selection. Princeton University Press, New Jersey, NJ.

Bennett ATD, Cuthill IC, Partridge JC, Lunau K. 1997 Ultraviolet plumage colors predict mate preferences in starlings. Proc Natl Acad Sci USA 94, 8618-21.

Berthier, S. Charron, E. & Da Silva, A. 2003.Determination of the cuticle index of the scales of theiridescent butterfly *Morphomenelaus*. Optics Communications.228, 349-356.

Brink, D. J. & van der Berg, N. G. 2004.Structural colors from the feather of the bird *Bostrychiahagedash*. J. Journal of Physics D: Applied Physics. 37, 813–818.

Bronner, G.N. & P.D. Jenkins. 2005. Order Afrosoricida. Pp. 70-81. Mammal Species of the World, 3rd edition.Wilson, D. E. and D.M. Reeder (eds.). Johns Hopkins University Press, Baltimore. 2142.

Bronner, G.N. 2000.New species and subspecies of golden mole (Chrysochloridae: *Amblysomus*) from Mpumalanga, South Africa. Mammalia.64, 41-54.

Chernova, O.F. 2002.Architectonic and diagnostic significance of hair cuticle. Biology Bulletin. 29, 238-247.

Costa, F., and R. H. Macedo. 2005. Coccidian oocyst parasitism in the blue-black grassquit: influence on secondary sex ornaments and body condition. Animal Behaviour 70:1401-1409.

Doucet, S. M., Shawkey, M. D., Hill, G. E. &Montgomerie, R.2005. Iridescent plumage in satin bowerbirds: structure,mechanisms and nanostructural predictors of individualvariation in color. Journal of Experimental Biology. 209, 380–390.

Fox, D.L. 1976. Animal biochromes and structural colours: physical, chemical &distributional, and physiological features of coloured bodies in the animal world. University of California Press.41-46.

Glover, BJ and H.M. Whitney 2010. Structural color and iridescence in plants: the poorly studied relations of pigment color. Annals of Botany 105: 505-511

Gorman, G. & Stone, R.D. 1990 The natural history of moles. Cornell University Press, 1-7.

Greenwalt, C. H., Brandt, W. &Friel, D. D. 1960. Iridescent colors of hummingbird feathers. Journal of the Optical Society of America. 50,1005–1013.

Hausman, L.G. 1920.Structural characteristics of the hair of mammals.The American Naturalist.54, 496-523.

Jackson, C.R. Setsaas, T.H. Robertson, M.P. Scantlebury, & M. Bennett, N.C. 2009. Insights into torpor and behavioral thermoregulation of the endangered Juliana's golden mole. Journal of Zoology. 278, 299-307.

Jellison G, Jr. 1993. Data analysis for spectroscopic ellipsometry. Thin Solid Films 234:416-422.

Kemp DJ (2007) Female butterflies prefer males bearing bright iridescent ornamentation. Proceedings of the Royal Society of London (B) 274:1043-1047

Kemp DJ (2008) Female mating biases for bright ultraviolet iridescence in the butterfly Eurema hecabe (Pieridae). Behavioral Ecology 19:1-9.

Kemp DJ, Vukusic P, Rutowski RL (2006) Stress-mediated covariance between nano-structural architecture and ultraviolet butterfly iridescence. Functional Ecology 20:282-289

Khumalo, N.P. Dawber, R.P.R. Ferguson, D.J.P. 2005. Apparent fragility of African hair is unrelated to the cystine-rich protein distribution: A cytochemical electron microscopic study. Experimental Dermatology. 14, 311–314.

Land, M. F. 1972.The physics and biology of animal reflectors. Progress in Biophysics and Molecular Biology. 24, 77–106.

Li, Y., Lu, Z., Yin, H., Yu, X., Liu, X., & Zi, J. (2005). Structural origin of the brown color of barbules in male peacock tail feathers. Physical Review E, 72(1), 010902. doi:10.1103/PhysRevE.72.010902

Loyau, A. Gomez, D. Moureau, B. The´ry, M. Hart, N. Jalme, M. Bennett, A.&Sorci, G. 2007.Iridescent structurally based coloration of eyespots correlates with mating success in the peacock. Behavorial Ecology.

Lythgoe, J.N. 1975.The structure and function of iridescent corneas in teleost fishes. Proceedings of the Royal Society of London.Series B. 188, 437-457.

Maia,R. Caetano, J. Ba´o, S. Macedo, R. 2009 Iridescent structural colour production in male blue-black grassquit feather barbules: the role of keratin and melanin.J. R. Society Interface.6, S203-S211.

McGraw, K. J., E. Mackillop, J. Dale, and M. E. Hauber. 2002. Different colors reveal different information: how nutritional stress affects the expression of melanin- and structurally based ornamental plumage. Journal of Experimental Biology 205:3747-3755.

McMichael, A. Hordinsky, M. 2008. Hair and scalp Diseases: Medical, Surgical, and Cosmotic Treatments. Informa Healthcare. 8.

Meester, J. 1976. South African Red Data Book-Small Mammals. National Scientific Programmes Unit: CSI. 9-16
Moyo, T. 2005. The identification of mammalian species through the classification of hair patterns using image pattern recognition. Honors thesis, penn state.

Newton, I. 1704 *Opticks*. Mineola, NY: Dover Publications.

Noyes, J.A. Vukusic, P. & Hooper, I.R. 2007.Experimental method for reliably establishing the refractive index of buprestid beetle exocuticle Optics Express.Vol. 15, 4352.

Prum, R. O., Torres, R. H., Kovach, C., Williamson, S. &Goodman, S. M. 1999*b* Coherent light scattering by nanostructured collagen arrays in the caruncles of *Malagasy aities*. Journal of Experimental Biology 202, 3507–3522.

R Development Core Team See http://r-project.org/.

Schultz, T. Hadley, N. 1987 Structural colors of tiger beetles and their role in heat transfer through the integument. Physiological Zoology.60, 737-745.

Seago A, Brady P, Vigneron JP, Schultz T. 2008. Gold bugs and beyond:a review of iridescence and structural colour mechanisms in beetles (Coleoptera). J Roy Soc Interface 6:S165-S184.

Shawkey, M. D., Hauber, M. E., Estep, L. K. & Hill, G. E.2006. Evolutionary transitions and structural mechanisms of avian plumage coloration in grackles and allies (Icteridae). Journal of The Royal Society Interface. 3, 777–783.

Shawkey, M.D., A.M. Estes, L.M. Siefferman and G.E. Hill. 2003. Nanostructure predicts intraspecific variation in ultraviolet-blue plumage colour. Proceedings of the Royal Society of London B. 270, 1455-60.

Shawkey MD, Morehouse NI, Vukusic PR. 2009. A protean palette: color materials and mixing in birds and butterflies. J Roy Soc Interface 6:S221-S231.

Shevtsova, E, C. Hansson, D.H. Janzen, J. Kaerandsen. 2011. Stable structural color patterns displayed on transparent wings. PNAS 108:668-673.

Springer, M.Cleven, G. Madsen, O. Jong, W. Waddell, V.Amrine, H. &Stanhope, M. 1997.EndemicAfricanmammals shake the phylogenetic tree. Nature.388, 61-64.

Wilson, Don E.; Reeder, DeeAnn M., eds (2005). "Preface and introductory material". *Mammal Species of the World* (3rd ed.). Baltimore: Johns Hopkins University Press, 2 vols. (2142 pp.). p. xxvi. ISBN 978-0-8018-8221-0. OCLC 62265494.

Williams, C. 1938.Aids to the identification of mole and shrew hairs with general comments on hair structure and hair determination. The Journal of Wildlife Management. 2, 239-250.

Yoshioka, S., Matsuhana, B., Tanaka, S., Inouye, Y., Oshima, N., & Kinoshita, S. (2010). Mechanism of variable structural colour in the neon tetra: quantitative evaluation of the Venetian blind model. Journal of the Royal Society, Interface / the Royal Society. doi:10.1098/rsif.2010.0253

Zi, J., Yu, X., Li, Y., Hu, X., Xu, C., Wang, X., Liu, X., et al. (2003). Coloration strategies in peacock feathers. Proceedings Of The National Academy Of Sciences Of The United States Of America, 100(22), 12576-12578. doi:10.1073/pnas.2133313100

Future Directions

We are now beginning to mimic some of these nanostructures we have described using both natural materials and synthetic polymers. Such biomimetic structures could be particularly attractive for this inspiration because in birds they appear to be formed through energetically inexpensive processes of self-assembly. Recent work from our lab [17] and others [18] suggests that active cellular processes play very little, if any, role in organizing the components of structurally colored materials. Rather, self assembly process like depletion-attraction (for iridescent colors ;[17]) and spinodal decomposition/nucleation and growth (3D matrices; [18]) may be sufficient to do so.

In a grant to be submitted this summer, we willpropose to mimic previously characterized 1) iridescent and 2) non-iridescent nanostructures using both synthetic and natural materials.

1) Biomimicry of iridescent nanostructures

Iridescent nanostructures are characterized by organized arrays of melanosomes surrounded by thin films of keratin within feather barbules [Figure 1; 11]. These act as simple thin films, multilayers or 2D photonic crystals. Although they are complex, they may form through relatively simple self-assembly processes as the keratin polymerizes in the barbules. Though the emergence of organized systems through increasing entropy may seem paradoxical, the Asakura-Oosawa model of attraction forces resulting from osmotic depletion have been extensively documented in colloidal mixtures [17], and have been shown or suggested to play critical roles in many biological processes. In mixtures of hard ("noninteracting") particles and polymers (in this case, melanosomes and keratin), the center of mass of the polymer cannot occupy an area of the particle's surface equal to its own radius, creating an area of excluded volume surrounding the particle. As the large particles approach one another, these areas of excluded volume overlap, resulting in a larger volume that can be occupied by the polymer and therefore a loss of free energy. This overlap leads to the depletion of the polymer in the gaps between particles, creating an osmotic gradient that attracts particles to one another (Figure 2).
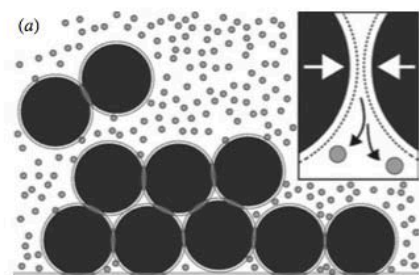

Figure 2. Schematic of depletion attraction forces during keratinization of iridescent feather barbules. (a) keratin units (grey circles) cannot occupy the excluded volume (dashed lines) around melanosomes (black circles). When they are close to one another or to the barbule edge, these exclusion areas overlap (grey areas), resulting in a greater total volume that can be occupied by keratin, and therefore in less free energy in the system. Because difference in size between melanosomes and keratin units is very large, keratin can occupy gaps between melanosomes and the barbule edge.

The range of these interactions is proportional to the size of the polymer and their magnitude is proportional to its concentration; therefore, as polymerization proceeds, the effect of depletion interactions on particle arrangement constantly increases (Figure 2). Furthermore, at vesicle walls the overlap of particle and wall-excluded volumes results in a free energy loss approximately twice that between two particles. As a consequence, the concentration of dilute polymers necessary for attraction depletion forces is much lower, potentially leading to the coexistence of an organized, particle-rich phase near the walls, and a polymer-rich phase in the bulk [17].

We propose to test the hypothesis that ontogeny of the nanostructural organization of iridescent barbules proceeds through self-assembly via depletion attraction forces. Specifically, these forces pin melanosomes to the cell wall and to each other, forming a stable homogenous layer around the outer edge of male barbule cells. Data

collected under my previous AFOSR grant suggest that melanosomes have an inherent tendency to self-assemble, regardless of their shape, size or concentration. Indeed, melanosomes with aspect ratios ranging from 1-6 and at concentrations formed coffee rings following dewetting from a DI water solution on glass. This is in contrast to a recent report that polystyrene particles only self assemble at ARs > 5 [19], suggesting that some feature of melanosomes increases their propensity for self-assembly. A series of experiments varying surface tension, pH, etc revealed that only non-iridescent melanosomes in a high pH solution did not form coffee rings. However, these experiments, while informative, were highly simplified and did not test the potential interactions of melanosomes a) with a drying polymer (β-keratin), b) in a confined space the size of a single cell, nor their ability to self-assemble into more ordered configurations like the square lattices found in peacocks (Zi et al.). These latter cases are potentially even more interesting because, while coffee rings and hexagonal lattices represent energetically stable states, square lattices do not. Moreover, a thin layer of β keratin encircling the ordered melanosome structure is needed to produce many of the iridescent structural color effects [6]. Thus, we propose to undertake a new set of experiments to refine our understanding of how self-assembly proceeds. These experiments are designed to enable us to closely mimic the development of self-organizing optical nanostructures using both natural and synthetic polymers.

We have isolated melanosomes from diverse iridescent and non-iridescent feathers, and will use these in all experiments. We will test whether interactions with drying keratin affect self-assembly of melanosomes by mixing them together, drop-coating the mixture, allowing it to dry and observing the resulting structures, using coffee ring formation as a proxy for self-assembly. The simplicity of this basic methodology allows experimental variables to be easily changed to test their effects. All experiments will be performed with both melanosomes and keratin isolated from both iridescent and non-iridescent feathers.

Experiment 1: Varying concentrations of melanosomes and keratin. We will vary the proportions of melanin and keratin from 90:10 to 10:90 in separate experiments and identify the points of strongest and weakest coffee ring formation. One of the fundamental predictions of depletion attraction is that the strength of interactions between hard particles and polymers scales positively with concentration of the particles relative to the polymer. We therefore predict that relatively higher concentrations of melanosomes will lead to greater self-assembly. *Preliminary data:* Using chicken keratin and melanosomes isolated from non-iridescent red-winged blackbird feathers, we showed that, as predicted, melanosomes formed coffee rings at high concentrations, but not at low concentrations. This is in contrast to the results we obtained using melanosomes suspended in water, in which coffee rings were formed even at extremely low concentrations.

Experiment 2: As feathers develop and keratin polymerizes, depletion-attraction interactions will initially increase in response to increasing keratin fiber size, followed by a decrease as a result of the reduced contrast between bundled keratin fibers and melanosome size. Our hypothesis further predicts that drying speed will affect likelihood of coffee ring formation, as rapid polymerization will allow insufficient time for depletion attraction forces to build up. We will test this hypothesis by increasing and decreasing polymerization time using a temperature gradient. Cool temperatures will slow down the reaction process while warm temperatures will speed it up.
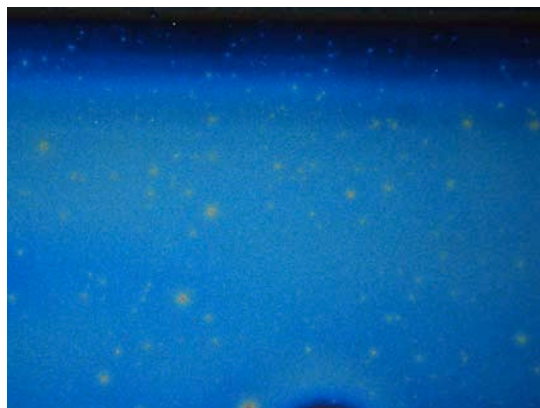
2) *Biomimicry of non-iridescent nanostructures*

Non-iridescent structural colors in birds are produced by coherent light scattering from one of two nanostructural classes: either a torturous array of anastomosing keratin channels or regularly sized air spheres in a keratin matrix [6]. It has recently been hypothesized that these nanostructures form through passive processes of self-assembly (Dufresne et al. 2009), specifically phase separation, but this

hypothesis has not been tested experimentally. We propose to test it with both natural (β -keratin) and synthetic polymers.

a)Natural polymers. The primary component of non-iridescent nanostructures is β keratin, and our working hypothesis is that the β keratin from nanostructured feathers is chemically distinct to that from non-nanostructured feathers. We propose that its chemical properties at least in part cause it to self-assemble. We have thus isolated β keratin from non-nanostructured white chicken feathers and nanostructured blue eastern bluebird (*Sialia sialis*) in two ways. First, we dissolve it in a sulfur solution following the methods [6], who demonstrated that reassembled keratin films produced using this method are structurally and chemically similar to the native material. Second, in collaboration with Rajesh Naik and Patrick Dennis at the AFRL, we have extracted and purified it using standard techniques. Feathers are approximately 90% β -keratin, with the remainder composed of trace metals, fat, hormones and other impurities. While the simple dissolution method preserves these components, the latter purification method does not, allowing us to test their effect on self-assembly. We propose to address the following questions about these polymers as follows

1) **Does nanostructured tissue re-assemble after dissolution?** If self-assembly is important to development of nanostructures, then we predict that they would retain some capacity for self-assembly after dissolution. To test this, we flow-coat solutions of the two keratin types at varying speeds onto silica and allow them to dry. Following visual inspection, we measure their reflectance using a UV-vis spectrometer (Avantes, Inc.) at varying degrees of incidence and observation, and examine their structure using atomic force microscopy (AFM), and small-angle x-ray scattering (SAXS). Our preliminary data show that, when dissolved in a sulfur solution, the keratin from the blue feathers creates a blue film, while that from the chicken feathers does not (Fig. 3). These data suggest that the nanostructured keratin self-assembles after dissolution, but further structural data are needed to confirm this. Interestingly, keratin dissolved in HFIP, a solvent that quickly evaporates, does not form blue films, suggesting that speed of drying

Figure 3: Flow-coated thin films of keratin from blue nanostructured feathers (a) and unstructured white feathers (b) dissolved in a 1% sodium sulfide solution

or water content may contribute to its self-assembly. We will further test this hypothesis by adding incrementally increasing amounts of water to HFIP-keratin solutions.

2) **Do the amino acid composition and phosphorylation state of nanostructured and unstructured keratin differ?** Self-assembly may be triggered by the interactions among keratin monomers during polymerization. We therefore predict that nanostructured keratin will have a different primary sequence than unstructured keratin, and will test this prediction using standard techniques (mass

spectrometry and direct protein sequencing). Our preliminary data show different banding patterns in protein gels for the two types of keratin, suggesting that their sequences are different. Interestingly, nanostructured keratin stained much more strongly for phosphorylation, indicating that it may also differ in phosphorylation state. We will verify this observation with more extensive testing and will also perform direct experimental tests on the effects of phosphoprylation on keratin. Specifically, we will de-phosphorylate nanostructured keratin and phosphorylate unstructured keratin. We predict that these treatments will lead to loss of color production by films cast from nanostructured keratin and gain of color function by films cast from unstructured keratin.

b) Synthetic polymers- Our collaborator Dr. Muthukumar at the University of Massachusetts has developed a quantitative theoretical model about the chemical structure of materials that would undergo phase separation at the size scales needed for structural color production. He has proposed that block co-plymers are the best candidates, and we will work with him to identify the molecular sizes of the two components that are most likely to lead to these types of nanostructures. We will then obtain these plymers and allow them to undergo phase separation, examining them afterwards using the same tools listed for natural polymers (spectrometry, AFM, SAXS). While this approach will entail some trial and error, the solid theoretical background of our tests should allow for efficient use of materials and time, and yield some new insights into the fundamental processes at work.
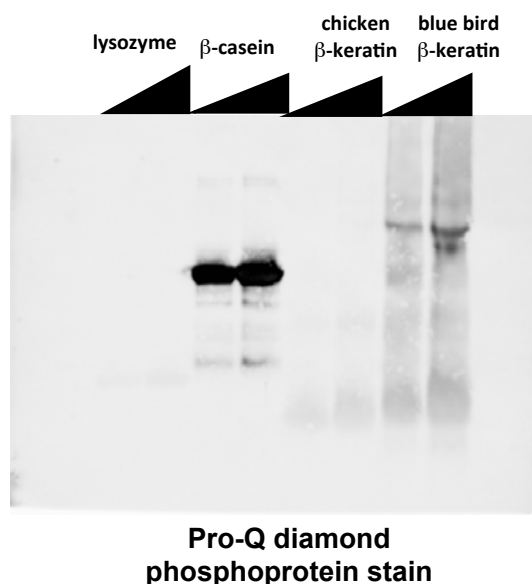

Pro-Q diamond phosphoprotein stain

Figure 4: Gel showing higher phosphorylation of nanostructured bluebird keratin than in unstructured chicken keratin. Lysozyme and β-casein are negative and positive controls, respectively.

References

1. Parker A.R. 2000 515 million years of structural colour. *J Opt A: Pure Appl Opt* **2**(6), R15-R28.
2. Andersson M. 1994 *Sexual Selection*. Princeton, NJ, Princeton University Press.
3. Cott H.B. 1940 *Adaptive coloration in animals*. London, Methuen Ltd.
4. Burtt E.H. 1986 *The Behavioral Significant of Color*. New York, Garland Publishing, Inc.
5. McGraw K.J. 2006 Mechanics of uncommon colors: pterins, porphyrins, and psittacofulvins. In *Bird Coloration Vol I: Mechanisms and Measurements* (eds. Hill G.E., McGraw K.J.). Cambridge, MS, Harvard University Press.
6. Andersson S. 1999 Morphology of UV reflectance in a whistling-thrush: implications for the study of structural colour signalling in birds. *J Avian Biol* **30**(2), 193-204.
7. Zi J., Yu X.D., Li Y.Z., Hu X.H., Xu C., Wang X.J., Liu X.H., Fu R.T. 2003 Coloration strategies in peacock feathers. *Proc Natl Acad Sci U S A* **100**(22), 12576-12578.
8. Yin H., Shi L., Sha J., Li Y., Qin Y., Dong B., Meyer S., Liu X., Zhao L., Zi J. 2006 Iridescence in the neck feathers of domestic pigeons. *Phys Rev E* **74**(5), 51916.
9. Stavenga D.G., Leertouwer H.L., Marshall N.J., Osorio D. 2010 Dramatic colour

changes in a bird of paradise caused by uniquely structured breast feather barbules. *Proc R Soc B* **278**(1715), 2098-2104.

10. Greenewalt C.H., Brandt W., Friel D.D. 1960 The iridescent colors of hummingbird feathers. *Proc Am Philos Soc* **104**(3), 249-253.

11. Prum R.O. 2006 Anatomy, physics, and evolution of structural colors. In *Bird Coloration Volume I: Mechanisms and Measurements* (eds. Hill G.E., McGraw K.J.), pp. 295-353. Cambridge, MS, Harvard University Press.

12. Parker A.R., Townley, H.E. 2007. Biomimetics of photonic nanostructures. *Nature Nanotech* **2,** 347-353.

13. D'Alba L., et al. 2011. Colour-producing β -keratin nanofibers in blue penguin feathers. *Biol Lett* doi: 10.1098/rsbl.2010.1163.

14. Maia, R., D'Alba, L., Shawkey, M.D**.** 2011. What makes a feather shine? A nanostructural basis for glossy black feathers. *Proceedings of the Royal Society of London B*. 278:1973-80.

15. Shawkey, M.D., D'Alba, L., Maia, R. 2011. Proximate bases of silver color in Anhinga feathers. *Journal of Morphology* doi: 10.1002/jmor.10993

16. D'Alba, L., Briggs, L., Shawkey, M.D**.** *In press*. Relative contributions of pigments and biophotonic nanostructures to natural color production: a case study in Budgerigars (*Melopsittacus undulatus*). *Journal of Experimental Biology*.

17. Maia, R., Macedo, R.H., Shawkey, M.D. 2011. Self-assembly of iridescent barbules through depletion attraction of melanosomes during keratinization. *Journal of the Royal Society Interface*: doi: 10.1098/rsif.2011.0456.

18. Dufresne, E. R., Noh, H., Saranathan, V., Mochrie, S. G. J., Cao, H. and Prum, R. O. (2009). Self-assembly of amorphous biophotonic nanostructures by phase separation. *Soft Matter* **5**, 1792-1795.

19. Yunker, P.J. et al. 2011. Suppression of the coffe ring effect by shape-dependent capillary interactions. *Nature* 476:308-310.